A Hybrid, Half-Bridge, Modular Multilevel Converter Circulating Current Controller for Use in Inertia Deficient Power Systems

written by

Jessie Lapsley

A thesis submitted to the Faculty of Graduate Studies of

The University of Manitoba

in partial fulfillment of the requirements for the degree of

Master of Science

Department of Electrical and Computer Engineering

University of Manitoba

Winnipeg, Manitoba, Canada

Abstract

Within modern power systems, conventional synchronous generation (powered by fossil fuels) is increasingly being replaced by inverter-based renewable generation. As the penetration of renewable generation grows, there is an overall decrease in the inertia that exists within the power system. The regulation of frequency historically relied on high levels of inertia that existed within the network. Therefore, there is a growing need to supplement the missing inertia, ensuring the modern power system remains secure and stable. This thesis presents a controller for a modular multilevel converter (MMC) that quickly injects active power into an inertia deficient system and also supports various active power/load imbalances. Circulating currents in the MMC, which are traditionally eliminated, are injected into the arms of the MMC to manipulate the peaks of the arm currents. The maximum power controller flattens these peaks, allowing the MMC to be overloaded (by 27.5% in this work) without damaging its components. A linear relationship is established between the peak arm current (when the MMC is delivering 27.5% over its rated power) and the magnitude of the injected 2^{nd} harmonic current (keeping the phase of the 2^{nd} harmonic current constant). This property is used to develop the proportional-droop controller. The proposed method is validated in the PSCAD/EMTDC environment using both a simple test system and the IEEE 9-bus system. This thesis shows that circulating current can be used to manipulate the arm currents of the MMC such that MMCs can be used to deliver over-rated active power to the inertia deficient power systems.

Acknowledgements

I would like to thank all of the individuals who aided me on this path of learning:

I would like to express my humble and sincere gratitude to my academic advisor, Dr. Shaahin Filizadeh, for his unwavering support, optimism, philosophical outlook and depth of knowledge.

This endeavor would not have been possible without the financial support provided by Mitacs Accelerate, RTDS Technologies Inc. , UMGF and the University of Manitoba. Thank you.

A special thank you goes to my friend and former instructor, Mr. Steven Howell, whose advice set me on this path.

Thank you to all the professors in the ECE department and colleagues I took courses with for their openness and willingness to share their knowledge. I would also like to thank Shrimal Koruwage for all of his IT help.

I'd like to acknowledge all of the friends I made on while on this research team. Your conversations ignited many ideas and thoughts. I appreciate you all.

Many thanks to goes to my good friend, Mr. Ted Brajczuk, our morning conversations motivated me. Your attention to detail is like no other.

Last, but not least, words cannot express my gratitude to my wife, Samantha, thank you for supporting me through this entire journey.

Contents

List of Figures

List of Tables

List of Acronyms

AC alternating current

APOD Alternative phase opposition disposition

BESS battery energy storage systems

BJTs bipolar junction transistors

CCSC circulating current suppression controller

CPS Carrier phase shifted

DC direct current

DFIGs doubly fed induction generators

DSP digital signal processing

FB-SM full bridge submodule

FCAS frequency controlled ancillary services

FFR fast frequency response

FSIGs fixed speed inductions generators

GTOs gate turn-off thyristors

HB-SM half bridge submodule

HVAC high voltage alternating current

HVDC High voltage direct current

IGBT insulated gate bipolar transistor

LCCs line commutated converters

MPPT maximum power point tracking

NLC Nearest level control

PD Phase disposition

PI proportional-integral

POCs points of connection

POD Phase opposition disposition

PLL phase locked loop

PMU phasor measurement unit

PWM Pulse-width modulation

RoCoFs rates of change of frequency

SMs submodules

SOA safe operating area

SVPWM Space vector pulse-width modulation

THD total harmonic distortion

UFLS under frequency load shedding

VSCs voltage source converters

VWSTs variable wind speed turbines

Chapter 1

Introduction

1.1 Background

Power systems were pioneered in the late 19^{th} century and at that time were used for the sole purpose of lighting incandescent lamps in small communities [1]. Although both alternating current (AC) and direct current (DC) technologies were initially explored, AC emerged as the victor and subsequently dominated the power system structure. AC technologies offered numerous advantages over DC technologies at that time. It was known that generators and motors were simpler to implement using AC technologies than their DC counterparts. Also, with the advent of the transformer in the early 20^{th} century it was easier to create a variety of voltage levels that could be used for generation, transmission and distribution infrastructures of the power system. This granted the ability to maximize the efficiency of power transfer.

As the 20^{th} century unfolded and small communities began developing into towns, and later, large cities, the amount of power required increased. This created a demand for more generation and a need to transfer larger amounts of energy over longer distances. In the first half of the 20^{th} century this increased demand was met using overhead high voltage alternating current (HVAC) transmission. This was largely due

to the historical use of AC. Since AC technologies dominated power systems, much more research went into them, leading to a more mature technology as compared to DC technologies. By the middle of the 20^{th} century, two situations emerged that were not suited for HVAC transmission: long transmission coming from the sea (or ocean) and the interconnection of un-synchronized grids. High voltage direct current (HVDC) transmission was better suited for those situations. In order to connect DC systems to the AC power grid, conversion from DC to AC is required. The mercury arc valve, the result of a decade of research, became the base of the first HVDC converter. This began the commercial use of HVDC transmission.

Mercury valve HVDC converters were the main converters used for the next two decades, but reliability, the high cost of valves and the poisonous nature of mercury limited the mercury valve's expansion. Technology continued to improve and saw the thyristor developed. It was used extensively through the 1970s and 1980s in line commutated converters (LCCs) that served to expand HVDC transmission. LCCs are still prevalent in today's power system as the research on them is extensive and they are reliable. However, as the needs of society continued to change the short comings of the technology became more obvious. The shortcomings thyristor-based LCCs have are: (i) they have limited controllablility (as only the firing angle of the thyristor is controllable), (ii) they are poorly suited for a system black start, (iii) they have to be connected to a relatively strong system, and (iv) they operate with low power factors, therefore, requiring large reactive power compensation [2].

The 1990s ushered in the fully-controlled semiconductor devices of adequate ratings for use in high-power applications. This became the main choice for switches in the next generation of converters. These semiconductor devices offered a wider range of control as compared to the thyristor. The low gate-power requirements and the fast switching of the insulated gate bipolar transistor (IGBT) meant easily attained voltages to trigger the switch and reduced switching losses (or use of a higher switching

frequency). These attributes were not shared by the other technologies, such as gate turn-off thyristors (GTOs) and bipolar junction transistors (BJTs). Through the use of the IGBT, the door was opened for research into voltage source converters (VSCs) for HVDC. At the beginning of the 21st century, Prof. Marquart introduced the modular multilevel converter (MMC) [3], which today is the VSC topology of choice. In contrast with LCCs, MMCs are capable of black start, can work with a relatively weak system and are highly controllable [4].

The benefits that the MMC has over LLCs does come with additional complexity in the controls. The MMC has a myriad of variables that have to be controlled to ensure proper operation. The controllers can generally be split into two subgroups; external controllers and internal controllers. The external controllers encompass the requirements of the outputs at the points of connection (POCs). Examples of these are the output current (or power flow), the DC link voltage and the AC voltage at the POC. The internal controllers manage the individual arm balances and include controllers for circulating currents, submodule capacitor voltages and generation of the gating signals for the switches [4].

Circulating currents remain solely in the arms of the MMC and are not seen at the output. As any circulating current adds to the overall losses in the MMC and requires larger IGBT ratings, it is common practice to eliminate them using a circulating current suppression controller (CCSC) [4]. However, a large amount of research has emerged that applies judicious amounts of circulating currents to enhance MMCs such that they can be involved in ancillary services [5, 6, 7]. For example, there is research that investigates different ways to manipulate the internal parameters of the MMC for the end purpose of inertia emulation [8]. This work focuses on using circulating currents to increase the power capability of a MMC. This additional capacity, which is activated during emergency situations, grants the MMC the ability to transfer overrated active power. Therefore, additional active power, used to counteract inertia

deficiencies, could be transferred from generation to the network without significantly increasing the ratings of the components making up the MMC. It should be kept in mind that due to the MMC's transistors sensitivity to unfavorable thermal situations (that can arise from increasing the amount of fundamental current transferred through the arm of the MMC), this benefit would be achieved at the cost overrating the transistors, implementing a thermal control system that would limit the current sent through the transistors based on a temperature limit or improvements to the cooling system for the MMC in anticipation of higher operating temperatures.

1.2 Motivation

The modern power system is evolving. The conventional power system has historically consisted of large synchronous machines equipped with large prime movers put in motion using the gravitational force of fresh water, or when fresh water sources are not readily available, nuclear energy or the burning of fossil fuels. Climate change stemming from excessive CO_2 emissions and growing concerns about the reducing amount of fossil fuel reserves have forced many countries to increase the penetration of renewable generation in their power network [9]. Existing power systems already make use of renewable resources derived from hydro and geothermal energy; therefore, the main increases of renewable generation are in the forms of wind power, photo-voltaic energy and battery storage.

In addition to power system-level renewable resources, there has been increased popularity in distributed energy generation. These take the form of photo-voltaic panels for individual houses, which could further reduce load demand. A combination of higher wind and solar penetration mixed with an increase in distributed energy generation could speed up the decommissioning of synchronous generators. As the newly added asynchronous generation assumes a larger share of the generation portfolio, a

reduced amount of inertia could be present within the system.

The high amounts of available inertia that existed in the conventional power systems were a major contributor to necessary ancillary services for power systems. Ancillary services are required for stable operation but do not explicitly contribute to the active power transfer. One of the important ancillary services, the regulation of frequency, has traditionally been provided from inertia. Large prime movers require great amounts of time and energy to deviate from their rated frequency and hence create stability. The load-generation balance disrupted through the loss of a large generator is remedied immediately through the release of kinetic energy stored in the rotors of synchronous machines within the system. As synchronous machines are decommissioned and renewable penetrations continue to increase, there grows a need for many solutions to ensure the stability and security of the modern power system.

1.3 Problem Definition

Past research in the field of inertia emulation has seen a multitude of potential solutions to address frequency control as system inertia reduces. The work in [8, 10] focuses on compensating for the deficit of inertia by operating the converter to behave like a synchronous machine. This is done by modeling the converter to provide both the electrical and mechanical dynamics that a similarly-sized synchronous machine would provide from the perspective of the grid. Simpler versions of this concept rely on using the swing equation to model basic laws of motion. The benefit arises as the system sees the renewable generation coupled to the grid through a converter as a synchronous machine. This implies all previous underlying notions for modeling and control are valid. However, the controller can be much more complicated.

Using additional storage has also been investigated. Here, the power imbalance is rectified by power delivered from a storage device as in [11]. The main drawback

when using this method is the additional storage required to meet the reserve demand. This means that either the submodule capacitors must be increased in capacity, or additional external batteries (or capacitors) are needed to meet the energy demands. Also, as the IGBTs still have a stringent current limit, the MMC would have to be run at a level such that enough capacity remains available for emergency situations. These result in design trade-offs and additional costs.

The converter remains the coupling device to the grid for both generation and HVDC transmission. Regardless of where the additional active power originates from, it is necessary to ensure that the converter possesses the ability to transfer the active power without risk of damage. Injecting circulating currents into the MMC arm for the purpose of minimizing the peak of the arm current is one way to achieve this. Using this method the MMC is able to operate in an overload region, while not significantly over-sizing the components of the MMC, specifically the IGBTs. Such an approach is presented in [5, 7]. These introduce the ability to minimize the peak of the arm current to a level that maximizes the remaining capacity for additional power transfer. [5] introduces a second type of control based on the droop control principles. Such approaches are both proven to be effective; however, only one is examined at a time. Having a controller that incorporates both maximum capacity as well as droop settings allows the MMC to react effectively while minimizing overall losses. This approach is the core idea explored in this thesis.

1.4 Thesis Structure

The remainder of this thesis is structured as follows: Chapters 2 and 3 provide the context for the remainder of this work. Chapter 2 introduces the operating principles and control strategies for MMCs, detailing topologies as well as both internal and external controls. Chapter 3 provides context as to where this research may be

applied. Here, the definitions used for frequency and inertia are presented, various inertia emulation approaches are briefly discussed and considerations of real-world implementation are outlined. Chapter 4 presents the methodology of the proposed controller. Chapter 5 presents validation results using the IEEE 9-bus system in the electromagnetic transient simulation software, PSCAD-EMTDC. Finally, chapter 6 details the contributions of this thesis, makes conclusions on the presented research, and suggests avenues for future work.

Chapter 2

Operating Principles of the MMC

This chapter introduces the main circuit of the MMC. This includes topology, operating principles and the fundamentals surrounding controls.

2.1 MMCs

The converter commonly used in modern VSC-HVDC transmission is the MMC. A 3-phase schematic diagram is presented in Figure 2.1. Modularity is achieved from individual submodules (SMs), which are the fundamental building blocks of the MMC. These SMs can be added to meet the requirements for powers or to increase voltage ratings. MMCs commonly use a large number of SMs for HVDC transmission in order to achieve the high voltages required. Using many SMs reduces the need for additional filtering and because the SMs are largely identical, the manufacturing and design aspects also see benefits.

The MMC consists of six arms. Each arm is equipped with N SMs, connected in series. The voltage across the SMs is summed to produce an upper arm voltage, v_u, and a lower arm voltage, v_l. To absorb any voltage mismatches in the DC loop, and reduce the effects caused by switching harmonics, an inductance, L, is included in each arm. A resistance, R, is also shown in each arm to model the effect of parasitic

losses in the inductance as well as those in the individual SMs.

The SM is commonly implemented in a half-bridge arrangement, composed of a capacitor and two fully-controlled power semiconductors, usually IGBTs, with anti-parallel diodes. The operation of the MMC is based on the control of the switches in each SM, either inserting or bypassing the voltage across that SM's capacitor. This action is done in such a way that the desired AC and DC voltages at the POCs of the converter are produced [4].

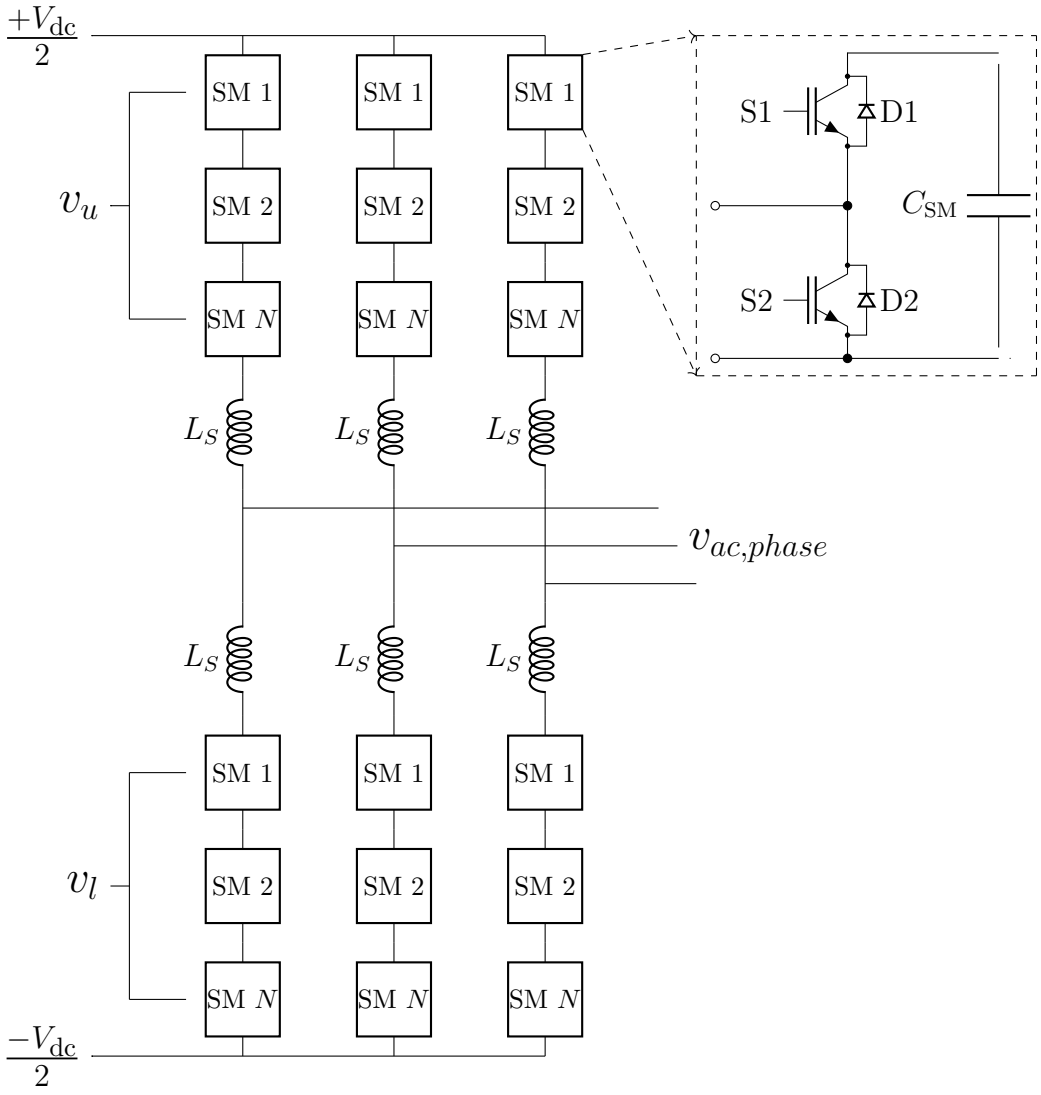

Figure 2.1: 3-Phase Representation of a MMC

2.2 Topology

There are a large array of possible MMC topologies that can be implemented. Two are shown in Figure 2.2. These topologies vary in structure and complexity. In practice, MMCs commonly use the half bridge submodule (HB-SM) topology. There has also been a fair amount of research conducted on the full bridge submodule (FB-SM) topology. FB-SMs can create positive, zero, and negative voltages. Therefore, they can be exploited for DC fault current handling capabilities. However, the fact that the FB-SM doubles the amount of switches (as compared to the HB-SM), means it introduces roughly two times the losses of the HB-SM. This increase of cost (both operational and material), using a more complex structure leads to the FB-SM's less popularity in practice [12, 13]. The current wide-spread use of HB-SM technology is the reason why the research presented in this thesis is solely based on the HB-SMs. The subsequent section will explain the basic operating states of the HB-SM.

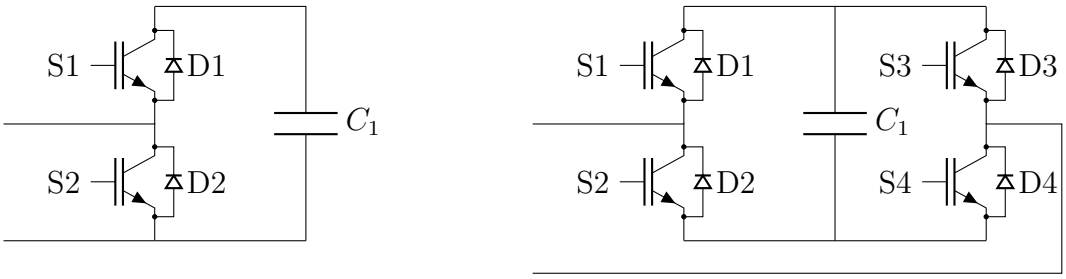

Figure 2.2: Half Bridge Topology (left) and Full Bridge Topology (right)

2.2.1 Half Bridge Topology

The HB-SM is depicted in Figure 2.3. The topology consists of two controllable semiconductor devices that are implemented as switches. Generally, an IGBT is used. Each switch is equipped with an anti-parallel-connected diode. Finally, there is a capacitor that is connected across both switches. Through control of the switches

the SM can produce two voltage levels of $V_{C\text{sm}}$ and zero, where $V_{C\text{sm}}$ is the voltage across the SM capacitor.

The SM capacitor is inserted, meaning it outputs the voltage across the capacitor ($V_{C\text{sm}}$) during the insert state [14]. The direction of the arm current determines whether the capacitor is charging or discharging. When the gate signals sent to the switches turn S1 on and S2 off and the arm current is entering the MMC, current flows through D1, inserting the SM capacitor while charging it as presented in Figure 2.3(a). If the current is exiting the MMC, the capacitor is discharged with the path going through S1 as seen in Figure 2.3(b).

The SM capacitor is bypassed, meaning it outputs a voltage of 0 during the bypass state [14]. When S1 is off and S2 is on and the arm current enters the MMC, the current flows through the lower switch S2, bypassing the capacitor and outputting a voltage of 0 (Figure 2.3(c)). When the the current exits the MMC, the path taken is through diode D2 (Figure 2.3(d)).

The SM capacitor is said to be in a blocked state when both switches S1 and S2 are off [14]. This state is only used during start up or during a fault condition. When the current enters the MMC, it flows through diode D1, charging the capacitor and outputting $V_{C\text{sm}}$ (Figure 2.3(e)). When the current is exiting the MMC, it flows though diode D2 and does not contribute to the capacitor voltage (Figure 2.3(f)).

Theoretically, a HB-SM has one additional state where the gate signals that are sent to the switches turn both S1 on and S2 on. However, as this state creates a short circuit across the SM capacitor it is never realized in practice. The various state are summarized in Table 2.1.

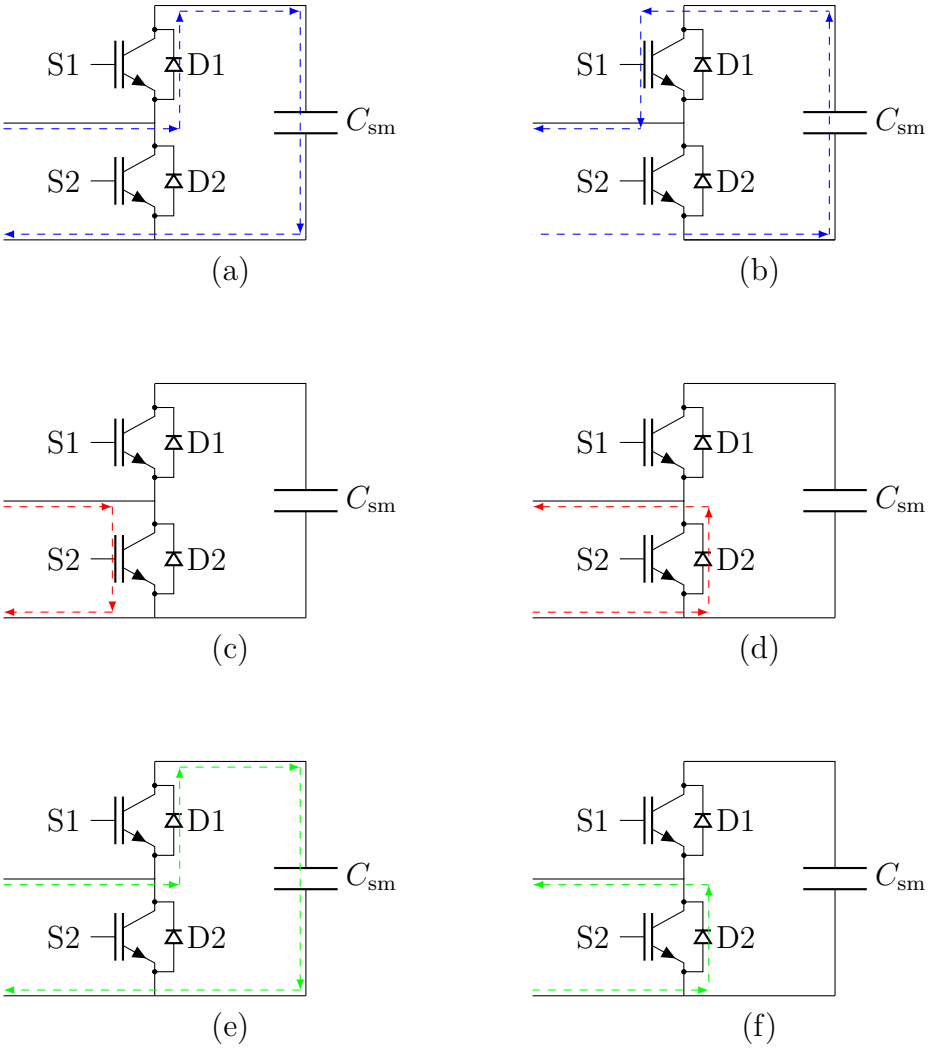

Figure 2.3: Operation of HB-SM MMC

Table 2.1: States of Operation of a HB-SM

S1	S2	Arm Current	Voltage Output	Capacitor
ON	OFF	Entering	$V_{C\text{sm}}$	Charging
ON	OFF	Exiting	$V_{C\text{sm}}$	Discharging
OFF	ON	Entering	zero	Bypassed
OFF	ON	Exiting	zero	Bypassed
OFF	OFF	Entering	$V_{C\text{sm}}$	Charging
OFF	OFF	Exiting	zero	Bypassed
ON	ON	N/A	N/A	Short Circuit

2.3 Internal Control

The benefits the MMC is equipped with come at the cost of an increased complexity of control. MMCs make use of switching in and bypassing SMs in order to approximate the reference signal provided to them. Each arm has to be controlled to achieve the desired action.

2.3.1 Circulating Current Control

In the following section the definition for circulating current used in this work is presented as well as methods for removing the circulating current from the arm current, known as CCSC.

Circulating Current

The ideal MMC is connected to a perfect DC source and is built with infinitely large ideal SM capacitors. This produces a purely DC current at the DC link and an output current that contains only the fundamental frequency. Here, the DC component of the

arm current charges/discharges the SM capacitors, and the fundamental component of the arm current exits the MMC. Keeping the circulating current as purely DC maintains minimum MMC losses. However, perfect DC sources do not exist, and MMCs are built with SM capacitors of finite size. This leads to harmonics that only appear in the arms of the MMC and do not leave the converter. This section discusses the existence of the dominant harmonic that exists in the MMC arm current.

The phase current contains two components; a DC component, I_{dc}, and a fundamental component, I_{a}. I_{a} does not flow continuously through the SM capacitors. It only flows through a SM capacitor when the SM is inserted and it ceases to flow through it when the SM is bypassed. This means the current going through each phase arm is multiplied by the desired modulation term.

Assuming identical arms, in terms of inductance and resistance values (which is a fair assumption for an MMC under normal steady state operation), I_{dc} is split evenly into three. The current through each arm is also made up of half of the fundamental phase current, I_{a} (based upon the symmetry of the circuit as viewed from the AC side). Therefore, the upper arm current can generally be defined as

$$i^u = \frac{1}{3} I_{\mathrm{dc}} + \frac{\sqrt{2}}{2} I_{\mathrm{a}} sin(\omega_0 t + \delta) \tag{2.1}$$

The modulation term for the upper arm of phase a can generally be represented as

$$m^u = \frac{1}{2}(1 - m_0 sin(\omega_0 t)) \tag{2.2}$$

With the assumption that the average behavior of the capacitors in each arm is identical, one representative capacitor can be modeled for each arm. The upper capacitor voltage, v_c^u, is based on the modulating signal, m^u, multiplied by the upper arm phase current, i^u:

$$v_{\mathrm{c}}{}^{\mathrm{u}} = \frac{1}{C_{\mathrm{sm}}} \int m^u i^u \, dt \tag{2.3}$$

Integrating equation (2.3) leads to:

$$v_c^u = \frac{1}{C_{\text{sm}}}\left(\frac{1}{6\omega_0} m_0 I_{\text{dc}} cos(\omega_0 t) - \frac{\sqrt{2}}{4\omega_0} I_a cos(\omega_0 t + \delta) + \frac{\sqrt{2}}{16\omega_0} I_a m_0 sin(2\omega_0 t + \delta)\right) \quad (2.4)$$

This introduces a 2nd harmonic current that flows through the arm, which produces a 2nd harmonic voltage component that adds to the capacitor voltage. These 2nd harmonic voltages are present in the upper and lower arms in each phase and create paths in the arms where 2nd harmonic current is able to flow. This continues to cascade and additional harmonics are created with the introduction of the 2nd harmonic current. However, the magnitudes of subsequent harmonics are small (relative to the fundamental) and as the harmonics increase in frequency, they see a higher reactance from the arm inductor, further reducing their magnitude.

The 2nd harmonic current component generally remains in the arm of the MMC. The switches within the SM are sensitive to overcurrents. Excessive overcurrent greatly increases the probability of IGBT failure. To transfer the maximum amount of fundamental current through the MMC and reduce losses, the circulating current should be kept to a minimum during steady state operation. To reduce these adverse characteristics, circulating current is generally removed from the arm current. One way of achieving this is through the use of a CCSC. The CCSC adds a small voltage to the modulating waveform that cancels out the 2nd harmonic. An alternative method for removing the 2nd harmonic current is to use a filter tuned to the 2nd harmonic. Inserting this filter in series with each of the arms will remove the 2nd harmonic current from the MMC.

Circulating current is the result of modulating current through the SMs in the arm. These issues cascade and introduce many harmonics (the 2nd harmonics are observed to be the largest); however, higher harmonics have small magnitudes and they are filtered out by the arm inductors. Therefore, this work only considers the

2^{nd} harmonic current when discussing circulating currents.

Conventional Circulating Current Suppression Control

As mentioned earlier, to minimize losses that stem from circulating currents within the arms of the converter, MMCs are commonly equipped with filters or a CCSC. This work is built on manipulating the 2^{nd} harmonic current in the arm and therefore makes use of the latter. The CCSC is implemented using the Park's transformation to transform the 3-phase circulating currents into two dc currents, consisting of the d and q components. The circulating current in the arms of the MMC can be calculated using,

$$I_{circ,j} = \frac{I_{pj} + I_{nj}}{2} \tag{2.5}$$

where I_{pj} and I_{nj} are the upper and lower 3-phase arm currents respectively. Once the 3-phase circulating current ($I_{circ,j}$) is transformed into the dq frame of reference, controllers (e.g., proportional-integral (PI)) drive the d and q components to the set reference values ($I_{cir,dref}$ and $I_{cir,qref}$), which are zero in the case of common CCSC [15]. An example of a CCSC controller is presented in Figure 2.4.

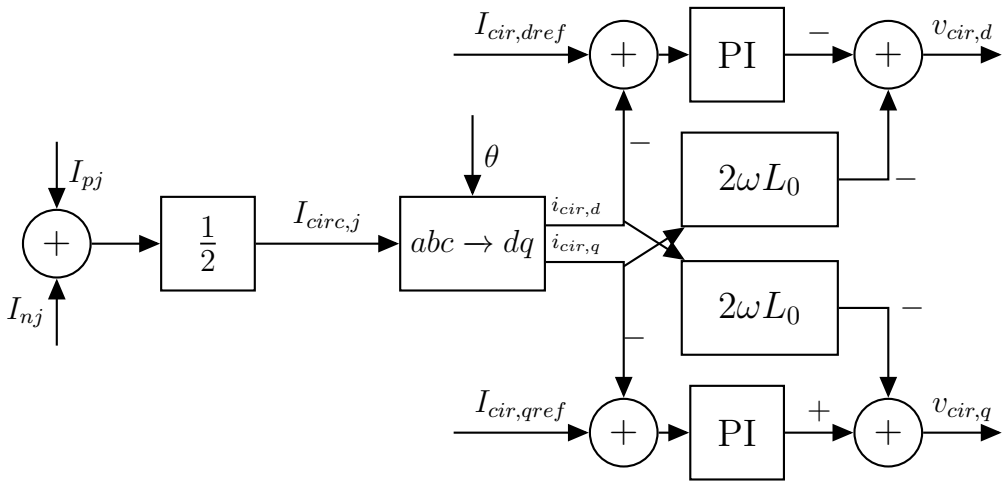

Figure 2.4: Block diagram of a CCSC controller

2.3.2 Waveform Synthesis Techniques

Waveform synthesis methods are employed in order to generate waveforms at the output of the converter with the desired frequency, amplitude, and phase shift. This section reviews a number of the methods that are commonly used in MMCs.

Pulse-Width Modulation

Pulse-width modulation (PWM) refers to a method used to control the duty cycle of converter switches at high frequencies for the purpose of generating a low-frequency output that generally matches a target reference waveform. This is achieved through comparisons of a low-frequency target waveform with high-frequency carrier waveforms. Popular choices for carrier waveforms include single-edged waveforms (saw-tooth) and triangular waveforms. However, the use of triangular carriers in three-phase applications provides the added benefit of harmonic cancellations that are not present when using saw-tooth carriers. Therefore, only triangular waveform carriers will be discussed [16].

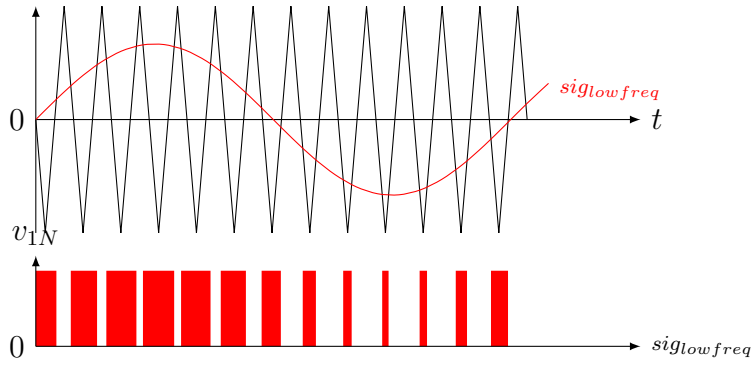

Figure 2.5: Single-Phase Pulse-Width Modulation Concept.

Single Modulating Wave, Single Carrier Wave

A modulating wave (sine wave for demonstration) is compared with a high-frequency triangular carrier signal (Figure 2.5). When the modulating signal is greater than the

carrier signal, a high level is produced; a low level is produced when the modulating signal is lower than the carrier signal. These levels are fed to the gate of a switch and are responsible for the ON (high level) and OFF (low level) switching. The result of the switching produces an output whose rolling average resembles the modulating signal. As there are only two available levels, the output signal is marred with harmonics and generally requires filtering to recover the desired modulating wave. The higher the frequency of the carrier signal, the higher the resolution of the output wave [16].

Single Modulating Wave, Multiple Carrier Waves

The previous discussion of single modulating wave and single carrier wave can be altered to be a valid control scheme for MMCs. Similar principles are used, however, the number of carriers increases according to the number of SMs in each arm. The same philosophy applies, where if the modulating signal is greater than the carrier signal, a high level is produced and when the modulating signal is lower than the carrier signal a low level is produced. The result of the switching produces an output that resembles the modulating signal. The typically large number of SMs creates many different levels. A consequence of this is that the output signal contains low amounts of harmonics and generally filtering is not needed to recover the desired modulating wave. Again, increasing the carrier frequency produces a higher resolution for the output wave [16].

Carrier Disposition PWM

There are various ways to arrange the carrier waves. Phase disposition displaces N carrier waveforms symmetrically along the vertical axis with each carrier having an amplitude of $\frac{1}{N}$. Some of the common methods of arranging the carriers are listed below:

- Alternative phase opposition disposition (APOD): Carriers in adjacent bands are phase shifted by π rad.
- Phase opposition disposition (POD): Carriers above the zero reference line are out of phase with those below the zero reference line by π rad.
- Phase disposition (PD): All carriers are in phase across all bands.

Carrier Phase Shifted PWM

An alternative to displacing the carrier along the vertical axis is to displace the carriers evenly by phase. Carrier phase shifted (CPS) PWM is accomplished by distributing $2N$ carrier waveforms symmetrically with a relative phase shift of $\frac{2\pi}{2N}$ with respect to each carrier. Each carrier has an amplitude of 1 pu [16].

Space Vector Pulse-Width Modulation

Space vector pulse-width modulation (SVPWM) was introduced as other forms of PWM were being explored [9]. It uses switching states, which are often times stored in memory, to create a space vector. The advantages of using SVPWM is its suitability for digital signal processing (DSP) implementation and its additional degree of freedom in which the switching states can be optimized, which reduces switching losses. Disadvantages arise in the complexity of implementation. A n-level inverter has n^3 switching states and uses $6(n-1)^2$ triangles to create the space vector [17]. As n grows the required computation also grows exponentially, which makes it unattractive for use in MMCs. However, [18] introduces improvements on SVPWM including not requiring a look up table and suitability for overmodulation, while significantly reducing its computational complexity. This method was verified on a 101-level MMC.

Nearest Level Control

Nearest level control (NLC) presents an alternative method for the control of the SMs of an MMC. The nature of NLC requires no triangular carrier waves and thus reduces the switching frequency. Therefore, NLC has the benefit of reducing switching losses when compared to PWM [19]. A consequence of the reduced switching frequency implies that a large number of SMs are required in order to keep harmonics that arise from low-frequency switching. A large number of SMs are generally used in high voltage applications in order to create the voltage levels required. Therefore, NLC is a valid switching control method for this particular application.

In addition to the reduction in switching losses, the implementation of NLC is simple. The reference voltage waveform is normalized and sampled regularly. To minimize the total harmonic distortion (THD) it is recommended to use a high sampling frequency [9]. Each sampled value is multiplied by the number of SMs, N, and this determines the number of SMs that are to be inserted. The output is a discrete voltage wave that resembles a staircase, approximating the reference voltage.

2.3.3 Submodule Energy Balancing

SM energy balancing is accomplished by keeping the individual SM capacitor voltages close to the average value. The decision regarding which SMs should be inserted (or bypassed) is made using instantaneous voltage measurements from the SM capacitors. Extreme values of capacitor voltages are switched in (or out) for the purpose of bringing them closer to the average value. From this, four cases can be defined [4].

- SM inserted and arm current is positive. A bypassed SM with the lowest capacitor voltage is inserted. This will cause the capacitor to charge and approach the average.

- SM inserted and arm current is negative. A bypassed SM with the highest

capacitor voltage is inserted. This will cause the capacitor to discharge and approach the average.

- SM bypassed and arm current is positive. An inserted SM with the highest capacitor voltage is bypassed. This will cause the capacitor voltage to remain constant (no further charging) and not deviate further from the average.

- SM bypassed and arm current is negative. An inserted SM with the lowest capacitor voltage is bypassed. This will cause the capacitor voltage to remain constant (no further discharging) and not deviate further from the average.

This can be implemented through the use of a decision tree.

2.4 External Control

The complexity of the internal control of the MMC creates the additional benefit for the MMC to have total control over the amplitude and phase of the output voltage or the output current. This implies that the converter has the ability to control the active and reactive powers separately.

The converter is able to operate under four individual control modes:

- Active power control.

- DC voltage control.

- DC current control.

- AC voltage control (or reactive power control).

These four modes are selected based on the desired application for the MMC. MMC-HVDC systems are implemented in tandem, separated by a DC link. With this knowledge in mind the rectifier (AC to DC) and the inverter (DC to AC) are

responsible for any two of the four control modes previously discussed [20]. Implementation of this control is generally accomplished through the direct control method or the decoupled control method. This work uses the decoupled method, due to its compatibility with the decoupled CCSC. In the next sections both methods are briefly discussed.

2.4.1 Direct Method

The MMC's connection to the system is represented in Figure 2.6 as a single-phase circuit diagram. In this figure the system voltage is V_s, the voltage at the converter terminal is V_c, and X_L represents the combined reactance of the converter transformer and converter reactor. Note that δ is the phase difference between the system voltage (V_s) and the converter voltage (V_c). Since the network voltage is the reference, its phase is denoted as zero.

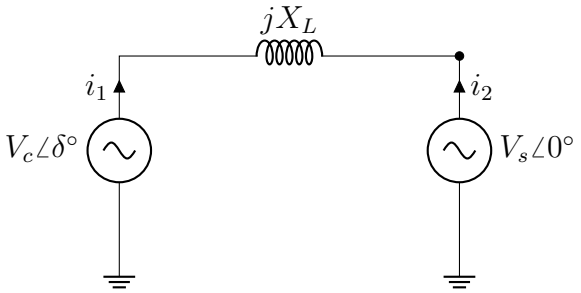

Figure 2.6: Single Phase Equivalent Circuit of an MMC Connected to a Grid.

The apparent power the converter is injecting into the system is:

$$S = V_s\angle 0° i_1^* = P + jQ \tag{2.6}$$

where S is the apparent power, P is the active power, and Q is the reactive power.

Expanding the terms yields P and Q as follows:

$$P = \frac{|V_s|\,|V_c|}{X_L}\sin\delta \tag{2.7}$$

$$Q = \frac{|V_s|\,|V_c|}{X_L}\cos\delta - \frac{|V_s|^2}{X_L} \tag{2.8}$$

It is seen in (2.7) that the active power is achieved through controlling δ. This is done through shifting the phase of the fundamental component of V_c with respect to V_s, which is accessed via a phase locked loop (PLL). Reactive power control, as seen in (2.8), is done by controlling V_c. This is done by altering the modulation index, m, in one of the PWM methods explained previously in this chapter [20].

While using direct control it is clear from (2.7) and (2.8) that variations in δ or $|V_c|$ affect both the active and reactive power. This leads to the conclusion that any change in δ (or $|V_c|$) must occur with an additional change in $|V_c|$ (or δ) to ensure the accuracy of the desired active and reactive power.

2.4.2 Decoupled Method

AC variables in a power system oscillate at the fundamental frequency. Transforming these oscillating variables to a synchronously rotating frame produces DC values that are much simpler to manipulate for control purposes. The Park's transformation [21] is used to transform the variables from an abc coordinate frame to a $dq0$ coordinate frame. This is represented as:

$$\begin{bmatrix} X_q \\ X_d \\ X_0 \end{bmatrix} = \mathbf{T} \begin{bmatrix} X_a \\ X_b \\ X_c \end{bmatrix} \tag{2.9}$$

where $\mathbf{T}$ is the following transformation matrix,

$$\mathbf{T} = \frac{2}{3}\begin{bmatrix} \cos(\omega t) & \cos(\omega t - \frac{2\pi}{3}) & \cos(\omega t + \frac{2\pi}{3}) \\ \sin(\omega t) & \sin(\omega t - \frac{2\pi}{3}) & \sin(\omega t + \frac{2\pi}{3}) \\ \frac{1}{2} & \frac{1}{2} & \frac{1}{2} \end{bmatrix} \tag{2.10}$$

The resulting variables are static and exist in a frame rotating at ω, which is the system frequency. The system frequency is obtained through the use of a PLL, which is locked to the system voltage.

Taking the inverse of the transformation of $\mathbf{T}$ produces $\mathbf{T^{-1}}$:

$$\mathbf{T^{-1}} = \begin{bmatrix} \cos(\omega t) & \sin(\omega t) & 1 \\ \cos(\omega t - \frac{2\pi}{3}) & \sin(\omega t - \frac{2\pi}{3}) & 1 \\ \cos(\omega t + \frac{2\pi}{3}) & \sin(\omega t + \frac{2\pi}{3}) & 1 \end{bmatrix} \tag{2.11}$$

Active power in the *abc* reference frame is:

$$P_{(abc)} = V_a I_a + V_b I_b + V_c I_c \tag{2.12}$$

Using the given transformation to define the active power in the rotating $dq0$ reference frame yields,

$$P_{(dq0)} = \frac{3}{2}(V_q I_q + V_d I_d + 2V_0 I_0) \tag{2.13}$$

Balanced operation leads to constant values for the d and q components and zero for the 0 component. Assuming balanced operation, this can be written as,

$$P_{(dq0)} = \frac{3}{2}(V_q I_q + V_d I_d) \tag{2.14}$$

Similarly, reactive power can be defined in the $dq0$ frame as (see [22] for mathematical

details),

$$Q_{(dq0)} = \frac{3}{2}(V_q I_d - V_d I_q) \tag{2.15}$$

Applying the transformation to a set of balanced three-phase voltages at the nominal frequency yields,

$$V_q = V_m \tag{2.16}$$

$$V_d = 0 \tag{2.17}$$

where V_m is the magnitude of the voltage waveform. Substituting these values simplifies the active and reactive power to

$$P_{(dq0)} = \frac{3}{2} V_m I_q \tag{2.18}$$

$$Q_{(dq0)} = \frac{3}{2} V_q I_d \tag{2.19}$$

The circuit in figure 2.6 can be altered to include the inductance contributed by the MMC arm, the transmission line, the converter transformer and the converter reactor, in an updated term labelled $L_{(TOT)}$. The currents in figure 2.6 can be replaced by the current injected into the system, I. The updated image is presented in figure 2.7.

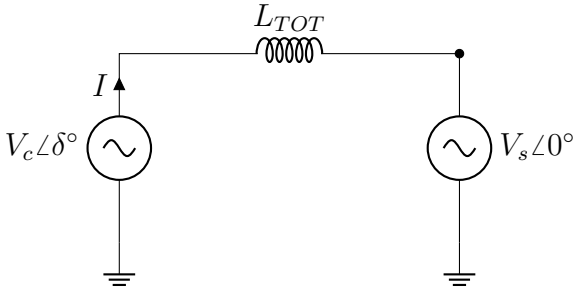

Figure 2.7: Single Phase Equivalent Circuit of an MMC Connected to a Grid.

Applying KVL to the circuit of figure 2.7 yields

$$V_{c(abc)} = V_{s(abc)} + L_{(TOT)} \frac{dI_{(abc)}}{dt} \tag{2.20}$$

Using the $\mathbf{T}$ transformation to transform $V_{c(abc)}$ to $V_{c(qd0)}$ yields,

$$V_{c(qd0)} = V_{s(qd0)} + \mathbf{T}L_{(TOT)}\frac{d}{dt}(\mathbf{T^{-1}}I_{(qd0)}) \tag{2.21}$$

As detailed in [23] the last term of equation (2.21) can be written as

$$\mathbf{T}L_{(TOT)}\frac{d}{dt}(\mathbf{T^{-1}}I_{(qd0)}) = \mathbf{T}L_{(TOT)}\frac{d}{dt}(\mathbf{T^{-1}}I_{(qd0)}) + \mathbf{T}\mathbf{T^{-1}}\frac{d}{dt}(I_{(qd0)}) \tag{2.22}$$

It can be shown (for details see [23]) that

$$\frac{d\mathbf{T^{-1}}}{dt} = \omega \begin{bmatrix} -\sin(\omega t) & \cos(\omega t) & 0 \\ -\sin(\omega t - \frac{2\pi}{3}) & \cos(\omega t - \frac{2\pi}{3}) & 0 \\ -\sin(\omega t + \frac{2\pi}{3}) & \cos(\omega t + \frac{2\pi}{3}) & 0 \end{bmatrix} \tag{2.23}$$

which leads to

$$\mathbf{T}\frac{d\mathbf{T^{-1}}}{dt} = \omega \begin{bmatrix} 0 & 1 & 0 \\ -1 & 0 & 0 \\ 0 & 0 & 0 \end{bmatrix} \tag{2.24}$$

Making use of these allows (2.21) to be written as

$$V_{c(qd0)} = V_{s(qd0)} + \omega L_{(TOT)}I_d - \omega L_{(TOT)}I_q + L_{(TOT)}\frac{dI_{qd0}}{dt} \tag{2.25}$$

Separating the d and q components yields the following two equations that can be used to implement decoupled control. Here, the decoupling terms ($\omega L_{(TOT)}I_d$ in 2.26 and $\omega L_{(TOT)}I_q$ in 2.27) are necessary to counteract the cross-coupling effects that are known to occur between the d and the q axes [24].

$$V_{c(q)} = V_{s(q)} + \omega L_{(TOT)}I_d + L_{(TOT)}\frac{dI_q}{dt} \tag{2.26}$$

$$V_{c(d)} = V_{s(d)} - \omega L_{(TOT)} I_q + L_{(TOT)} \frac{dI_d}{dt} \tag{2.27}$$

2.5 Summary

This chapter presented the basic operation of the MMC, touching on both internal and external controls. A high level discussion of MMC operation was presented. A detailed explanation of the operation of the HB-SM topology was provided. Several modulation techniques were detailed, showing the flexibility of options. A basic capacitor voltage balancing scheme was given. Lastly, external control of the MMC through the direct method and decoupled method was explained.

Chapter 3

Review of Existing Methods for Frequency Control

In this chapter, background and past research on emulated inertia are provided. The concepts of frequency stability and inertia are defined, approaches for effectively reducing the peak arm current in an MMC are presented, an overview of past research on methods for emulating inertia is summarized, and considerations for real-world implementation are briefly covered.

3.1 Frequency Stability

The growth of power systems created a larger focus on a power system's ability to operate at equilibrium under steady state conditions and also return to a level of equilibrium following a disturbance [25], commonly known as power system stability. Power system stability has been a major topic for research since the 1920s [26]. A power system is required to operate satisfactorily amidst a wide range of disturbances, both small and large. Small disturbances, often the results of continual load changes happening at the customer end, require the power system to continually adjust to changes. Large disturbances, often resulting from faulted lines, loss of a large load

or loss of generation, normally require specialized control schemes that react to the structural changes within the power system. Both small and large disturbances cause changes to happen to the power system, such as, rotor angle deviations, power flow variations and voltage variations. Stability is reached if the system is able to find a new operating point where equilibrium is possible [27].

For ease of classification, the problem of power system stability can be generally separated into three categories; rotor angle stability, voltage stability and frequency stability (Figure 3.1). Although these three categories are defined as separate entities, the equipment used to resolve disturbances can cause variations in bus voltages, rotor angles and power flows. Therefore, all three classifications are interconnected. The effect of reducing inertia within the power system presents, most significantly, in the frequency stability of the system [28]. Therefore, frequency stability will be the type of stability focused on in this thesis.

Frequency stability has been described in [27] as the system's ability to reach and maintain a steady frequency following a large generation and (or) load imbalance. It revolves around a system's ability to correct the load generation imbalance while minimizing any unintentional loss of loads.

Within the power system it is paramount that the system frequency is held to a nearly constant value. Large drops in the frequency within the network contribute to high magnetizing currents in induction machines and transformers, and also can interfere with the timing controls within synchronous machines [25]. Pertaining to renewable generation, large rates of change of frequency (RoCoFs) ($>2\frac{Hz}{s}$) contribute to incorrect tracking of the PLLs, resulting in erroneous controller actions. Also, due to time delays introduced, renewable generation may have inadequate under frequency load shedding (UFLS) schemes [29].

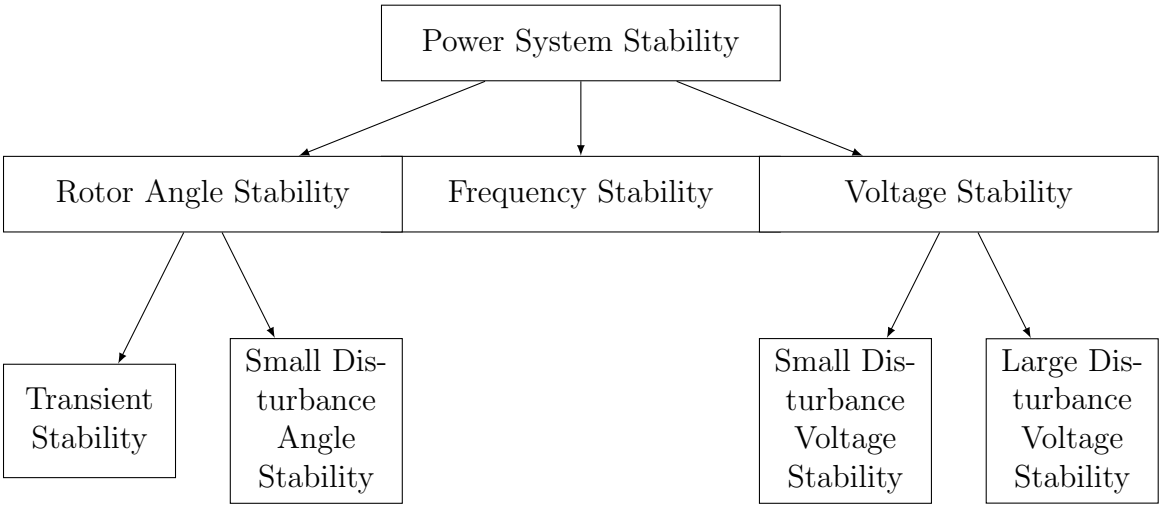

Figure 3.1: Summary of Power System Stability Classes

3.1.1 Definition of Inertia

The dynamics resulting from an imbalance between mechanical and electrical torques during a frequency event in a synchronous machine may be represented with the swing equation [25]:

$$J\omega_m \frac{d\omega_m}{dt} = P_{gen} - P_{load} \tag{3.1}$$

where J is the combined moment of inertia of the generator and turbine in kg.m^2, ω_m is the angular velocity of the rotor in rad/s, P_{gen} is the generated power dictated by the mechanical torque and P_{load} is the power demand dictated by the electromagnetic torque.

The swing equation can be normalized by making use of the per unit inertia constant, H, which is defined as the kinetic energy in W/s at rated speed, normalized to the nominal VA rating of the generator. The H constant indicates how long, in seconds, a generator is able to provide its rated power at the rated frequency.

$$H = \frac{1}{2} \frac{J\omega_{0m}^2}{VA_{base}} \tag{3.2}$$

Rearranging this equation and substituting it into (3.1) yields,

$$2H\frac{d\omega_{g,pu}}{dt} = P_{gen,pu} - P_{load,pu} \tag{3.3}$$

where the subscript pu denotes per unit. As the angular velocity is in per unit, (3.3) can be rewritten in terms of frequency as,

$$\frac{2H}{f}\frac{df}{dt} = P_{gen,pu} - P_{load,pu} \tag{3.4}$$

where f is the rated system frequency and $\frac{df}{dt}$ is the RoCoF. As renewable generation is added and synchronous machines are decommissioned, the inertia of the power system decreases, which in turn increases the RoCoF within the same time frame. Large RoCoFs are undesirable as they interfere with the synchronization abilities of synchronous generation [30] and PLLs in renewable generation [29]. This can lead to the incorrect operation of protection and in the worst-case scenarios, cascading blackouts. Therefore, the power system requires an additional source of inertia. In this paper a specific control scheme for this purpose is implemented within the converter.

Inertia is directly linked to a power system's ability to resist change. The larger the inertia the more difficult it is to change the frequency of a power system. Since synchronous machines are coupled to the power system, the delivery of inertia during a frequency event is executed instantaneously and without the need of a control system. Renewable generation, in the form of wind and photo-voltaics, is decoupled from the power system and hence has a reduced amount or complete absence of inertia.

The virtual inertia implemented in the hybrid controller of this thesis is of the fast frequency response (FFR) type [31], meaning additional active power can be either injected or reduced quickly. This research works under the assumption that additional active power is readily available to be transferred to the network via the MMC, replicating the effect of rotational inertia. The renewable generation(s) in

question must not be operating at peak rated active power, or some sort of storage item (battery storage for example) must be connected to the grid via a MMC. The inertia is not implemented instantaneously, as it is in synchronous machines, because the detection time of the frequency event needs to be taken into consideration. Also, the decoupled nature of renewable generation means there is no stored kinetic energy. Adding this term into (3.4) yields,

$$\frac{2H}{f}\frac{df}{dt} = P_{gen,pu} - P_{load,pu} + P_{RES,virtual} \tag{3.5}$$

In (3.5), $P_{RES,virtual}$ is the additional active power delivered from renewable generation for the purposes of limiting the frequency nadir, reducing the RoCoF, and ensuring that the system is able to reach a new stable operating point.

3.2 Inertia Emulation Approaches

Many approaches have been explored in search of solutions for the diminishing inertia of future power systems. The approaches presented in the following sections are some variations of control that can be implemented. Section 3.2.1 outlines methods of providing inertia from onshore wind farms. Section 3.2.2 discusses the use of capacitors (either SM or DC link capacitors) to provide energy for inertia emulation. Section 3.2.3 expands the wind farm discussion to include offshore wind farms. Storage elements' participation in virtual inertia is summarized in section 3.2.4. Section 3.2.5 introduces a method for controlling a MMC so it appears, from the system perspective, to operate as a synchronous machine. Finally, in the case of FFR, the method of this work, additional active power is requested to the network and transferred via the MMC. Generally speaking, sending additional active power through the MMC requires the MMC to be over-rated. Section 3.2.6 presents the concepts of using circulating currents to increase the capacity of the MMC without significantly

over-rating the components.

3.2.1 Inertia Provided by Onshore Wind Turbines

Renewable generation such as hydroelectric and thermal generation have historically been included in conventional power systems. Therefore, this work takes into consideration the following forms of renewable generation found in the modern power system: solar generation, wind generation and battery energy storage systems. Of these three, wind turbines possess moving parts in the form of the rotating blades, gearbox and electrical generators [32] which can participate in the contribution of stored kinetic energy to the network. This energy can be accessed and its inertia can be used in a similar fashion as the inertia from a synchronous machine. In order for the wind turbines to participate in cases where the frequency drops, it is imperative that the wind turbine is not operating at maximum capacity. The amount of energy stored is comparable to the average energy found in conventional power plants [32].

Wind turbines are connected to the grid either directly, as in the case of fixed speed inductions generators (FSIGs) or they are coupled (in some way) to the grid via converters, as seen in doubly fed induction generators (DFIGs). The FSIG behaves similarly to the synchronous machine when there is a sudden change in frequency. A frequency deceleration in the network causes the wind turbine to reduce in speed, releasing the stored kinetic energy of the FSIG. This kinetic energy is changed into electrical energy which is instantaneously injected into the network in the form of an active power surge. The inverse of this action is also true [33].

DFIGs such as variable wind speed turbines (VWSTs) make use of maximum power point tracking (MPPT). The pitch of the blades is controlled depending on the wind speed to ensure that the wind turbine generates the maximum power at that particular set point. In this case a control loop is required to change the power reference according to the need of inertia. Here, the derivative of frequency can be

monitored for inertia needs and the difference in frequency can be monitored for droop. The additional power required is sent to the MPPT controller, which updates the power reference, changing the pitch of the blades accordingly [34, 35].

In the case of FSIG, inertia is delivered to the network in the same fashion as synchronous machines, while VSWTs rely on a controller to request additional power, due to its decoupled nature. However, the intermittent nature of wind turbines create unreliable sources of inertia (whether actual or emulated), which during emergency situations needs to be readily available. Also, there is an economic cost of continuously operating wind turbines at less than the maximum power [33].

3.2.2 Import of Power from Offshore Wind Turbines

Offshore wind farms participate in inertia emulation using similar techniques as their onshore counterparts. However, due to the relative remoteness of where they exist, communication becomes the paramount bottleneck. There are two schemes commonly used to integrate offshore wind farms: a conventional scheme and a communication-less scheme. Both will be briefly described in the following section.

Conventional schemes rely on sufficiently fast and reliable communication to transfer the grid frequency required for participation in inertia emulation [36]. One such option is to use the already existing embedded fibre optic cables, found within a DC link [37]. Here, control can be implemented as a simple power-frequency controller.

Communication-less schemes ensure a proportional frequency variation from the onshore converter is transferred to the offshore converter without the use of communication as in [36]. In order to do this, a variation of DC link voltage is derived that is proportional to the frequency, using a frequency-voltage control. This voltage can be used by the offshore converter and, using a voltage-frequency controller, the frequency deviation can be utilized.

3.2.3 Stored Energy Provided from Capacitors of a VSC-HVDC link

As previously discussed, for a wind turbine system to provide inertial support, the units have to be run outside of the maximum power capacity. Also, only a fraction of that power is available for use. When the turbine reduces in speed, caution needs to be taken so that the turbine does not stall and that the turbine is able to recover to stable operation at its optimal operating point. As presented in [38] an alternative that tends to the inertia shortfall is to either use the stored energy in the DC link or to use the energy stored in the SM capacitors. As these topics have to do with either the DC link connecting to the inverter, SM capacitors of the MMC or a combination of both, this discussion expands to include photovoltaics, battery storage systems, and the aforementioned wind generation.

The capacitors of the MMC can be used to provide or absorb active power. In [38], a back-to-back MMC is considered that uses the energy stored in the virtual DC link to provide virtual inertia to the network in emergency situations. It is shown that an analogy can be made between the capacitor energy of the MMC and rotational energy of the synchronous machine. Therefore, an inertia constant H_{MMC} can be defined for the MMC ,that is analogous to the synchronous generator, as the stored potential energy over the base rating of the MMC. Which can be represented in equation form as,

$$H_{MMC} = \frac{CU_{\mathrm{dc}}^2}{S_B} \tag{3.6}$$

where C is the equivalent capacitance at of the generator-side of the MMC and the grid-side of the MMC, U_{dc} is the dc link voltage, and S_B is the base power of the MMC.

As seen in the above equation, H_{MMC} can be used to control the DC link voltage. This is accomplished through changing the reference values for the SM capacitors,

using techniques as seen in [39]. Since the DC side and AC side power controls are implemented separately, simply changing the energy storage of the SM capacitors does not necessarily translate to the desired amount of energy for frequency support. Therefore, the active power reference has to also change in accordance with the desired energy change.

In [40] the idea is expanded to include multi-terminal DC systems. When there are many renewable sources connected to the grid through MMCs, the requirements for the ancillary services, such as frequency support, can be distributed over many sources. This reduces the dependence on wind turbines, decreasing the mechanical stress and the probability of stalling. This allows them to operate closer to their maximum output (ensuring there is sufficient capacity to participate in the ancillary services). However, in the deregulated market this could pose economic issues that are not acceptable.

Virtual inertia can be delivered to the grid for frequency support via the energy stored in the MMC capacitors. Implementation is based on the analogous nature of energy stored in the capacitors of the MMC and the rotational energy of the synchronous machines. An active power controller has to be included to ensure the correct amount of power is delivered to the grid as DC and AC controls are not connected. MMCs have to be over-rated in design to ensure operation at higher voltage levels which introduces economic issues.

3.2.4 Storage Elements for Fast active Power Injection

The intermittent nature of renewable power generation often requires storage elements. These are used to store excess power generated during conditions of excess generation and deliver additional power in times of shortage. Storage elements come in many forms, such as battery energy storage systems (BESS) and ultracapacitors. Making use of the stored power for the purposes of mitigating large frequency distur-

bances has been researched.

Here, the frequency is monitored and when deviations outside a deadband are detected, active power from the battery is injected/absorbed [41]. This would happen in emergency scenarios. To use this method as a sole solution implies that large external batteries are required. Also, the converter would need to be designed for a larger rating in order to ensure that no damage was done during periods of extreme use. Since this is controlled by a control system, the power reference could be altered quickly and therefore, the reaction speed of the power injection is extremely fast.

3.2.5 MMC modelled as a Synchronous Machine

One way to ensure a safe level of inertia remains in the system, as synchronous machines are decommissioned, is to model the inverters (connecting the renewable generation) to behave as synchronous machines. The benefit of this logic is that the power system as a whole has very minimal changes and the theory that has existed for over 100 years does not have to be altered.

To mimic the behaviour of synchronous machines, synchronverters are governed by the following equations [8]:

$$T_e = M_f i_f \tag{3.7}$$

$$\boldsymbol{e} = \dot{\theta} M_f i_f \boldsymbol{sin\theta} \tag{3.8}$$

$$Q = -\dot{\theta} M_f i_f \tag{3.9}$$

where T_e is the electromagnetic torque, M_f is the magnitude of the mutual inductance between the field and stator coils, i_f is the field excitation current, θ is the angle between the rotor axis and one of the phases of the stator winding, e is the no load voltage and Q is the reactive power.

The above equations are used to generate the gating signals, e and θ, for the converter through the PWM. The controller is equipped with frequency and voltage

control loops that define $M_f I_f$, ω and θ with the moment of inertia, J, damping factors D_p and D_q and gain, $\frac{1}{K_v}$, being user defined. The current, i, and voltage, v, are feedback terms produced by the grid.

Simple versions of synchronverters require PLLs, but are prone to issues in weak grids. This brought on the development of self synchronized synchronverters. A consequence of using differential equations to generate the gating signals is the possibility of numerical instability. Also using a voltage-source implementation for synchronoverter's external protection may be required for safe operation as there is no protection form any type of severe disturbance.

The next section briefly introduces various methods of injecting active power into the AC network effectively emulating the characteristics of inertia.

3.2.6 Circulating Current Used to Operate MMC Outside of Rated Capacity

To provide additional active power via a HVDC link, using a MMC operating at its rated capacity, while not oversizing any components, the MMC must have a control system that allows it to operate outside of its rated capacity in a region defined as an overload region. To enter this overload region, this work focuses on reducing the peak of the arm current in the MMC. This reduction of the peaks can be achieved through techniques such as the one found in [7], where injecting judicious amounts of 2^{nd} harmonic current into the arms of the MMC is used to reduce the peak arm current to an acceptable level. A general example of how the 2^{nd} harmonic current is able to reduce the peak of the arm current is shown in Figure 3.2. Using this method an over-capacity of active power can be realized without a significant overrating of any individual components of the MMC.

In order to inject the correct amount of circulating current into the arms of the MMC, both the amplitude and phase of the circulating current are necessary. The

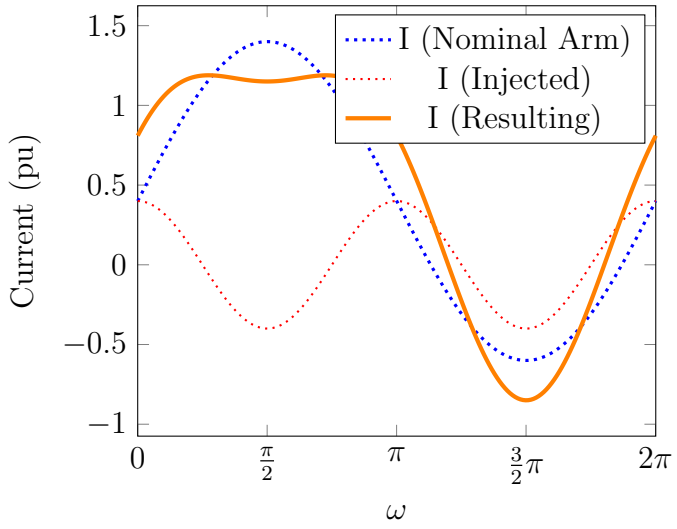

Figure 3.2: General method of reducing the peak of the arm current through injecting 2^{nd} harmonic current.

method chosen to obtain these two values was originally presented in [7]. Further discussion of this topic is provided in section 4.2, with the derivation of the circulating current's references, that create the flattening of the peaks of the arm current, in section 4.5.2.

3.3 Real World Implementation

FFR support can be used to quickly inject (or absorb) active power into the system to aid in the stabilization of frequency deviations in the system after a frequency event. Current technologies used in systems such as South Australia possess the ability to provide ancillary services within hundreds of milliseconds [42]. The nature of inverter-based generation allows for power to be quickly injected or reduced when compared to the governors found in synchronous machines. Therefore, ancillary services delivered in from FFR devices can be delivered much faster than traditional methods. However, this is dependent on quick and accurate frequency measurements [43].

Unlike synchronous machines, which are able to use the speed of the machine for frequency measurements, inverter-based generation must derive the frequency mea-

surement from observable quantities, such as voltage or current waveforms. This work utilizes a PLL for frequency measurements. In real-world applications, a common method for measurement of frequency is through the the use of a phasor measurement unit (PMU). Here, the assumption is that the signals of interest are sinusoidal. Frequency deviation from the nominal frequency manifests as the rate of change of the angle of the phasor measured by the PMU. This effectively means the frequency is the derivative of the signal. A consequence of this is that the recovered frequency signal will contain noise. Therefore, the measured frequency is unsuitable to be used instantaneously, and noise filtering is required. The RoCoF, being the derivative of the frequency, implies it can be recovered through taking the second derivative of the phasor angle, introducing additional noise that requires time to be filtered out. The reasons laid out often lead to measurement systems that are specifically built and tested to achieve desired results for specific applications [43].

3.4 Summary

This chapter briefly introduced various methods of delivering additional active power, which are used to emulate the benefits of the missing inertia. The next aspect, which is the main purpose of this research, is the ability of the converter to safely transfer this increased amount of active power to the network without causing damage to the components of the MMC. This is especially important as converters are often operated at (or near) their nominal power, and the adverse impacts of over-rating their components must be minimized. Therefore, a method that allows for the additional power transfer without violating the safe operating characteristics of the MMC has to be developed.

Chapter 4

Development of the Specialized Circulating Current Controller

This chapter provides information pertaining to the development of the circulating current controller that enables the MMC to deliver power during frequency events. The chapter begins with an introduction, providing context using the ideas developed in previous sections, moves on to implementation and concludes with verification results using the PSCAD/EMTDC simulator.

4.1 Introduction

With numerous generators connected to a power system, there needs to be some control that dictates the change in demand from each individual generator. In the case of the synchronous generation, this is initially through inertia and the response of a governor system. This allows a quick preliminary power response from the generator itself, which would be later followed by a change in the dispatch schedule by a control centre. In essence, the external controls for asynchronous generation are similar to its synchronous generation counterpart. The major difference exists in the additional complexities that internal controls have. Although asynchronous generation does not

possess large amounts of inertia, it possesses the advantage of being able to change its power reference relatively quickly (as compared to synchronous generation). This section goes through the controls involved in this process.

This controller is implemented in two sections. The first section is the external controller for the MMC. This controller is an active power/frequency controller. As the frequency falls, the active power injection increases and as the frequency rises, the active power injection decreases. The second section is the internal controller, which exists within the CCSC. As stated earlier, conventional CCSC forces the circulating current to zero. This is done to minimize losses within the arms of the MMC during steady state operation. However, the circulating current does not have to be forced to zero. This portion of the controller calculates the amount of circulating current (magnitude and phase) that is to be injected into the arms of the MMC for the desired manipulation of the arm current to ensure the safe operating area of the IGBTs are not violated.

The proposed controller requires a healthy system (stable dc source) for operation. If the DC link voltage is not stable or is operating under a voltage constraint, energy from the MMC is necessary to rectify this issue [44]. This would reduce (perhaps significantly) the amount of available active power to rectify the generation/load imbalance. It may also be required that a second harmonic current injection is needed to reduce an unacceptable voltage ripple on the SM capacitors [45]. As this second harmonic current injection to control the voltage ripple may be very different than the one that is required to minimize the peak arm current, it is not advised to use the hybrid controller in this situation. In practice this controller would be implemented at a connection point that is capable of producing a reliable and stable DC voltage.

4.2 P Overload Operating Range of the MMC

The MMC is designed to operate with high efficiency, near its rated values. However, to replace the effects of inertia that a synchronous machine provides during a frequency event, additional active power is required to pass through the MMC. To accomplish this without introducing a significant cost increase by over-rating the components in the converter, the converter must be able to safely operate in an overload region. In order to deliver the additional active power, either the current entering and exiting the MMC must increase or the the voltage across the MMC must increase. This defines the following four main limitations:

1. The peak arm current limit.
2. The peak SM voltage.
3. The arm voltage capability.
4. The modulation limit of the converter.

As stated, each of these limits can be increased by over-designing the components that make up the MMC. However, this introduces additional costs and may be undesired. For the purpose of increasing the active power capability, this work focuses on increasing the current delivered by the MMC. This increases the amount of current sent through each arm in the MMC and hence the limitation addressed is the peak arm current limit. The largest constraint to achieve this is found in the IGBT switches as they are sensitive to over-currents and must be operated in a physically imposed safe operating area (SOA). Pushing an IGBT outside the limits of its SOA runs the additional risk of thermal breakdown. Alternatively, an overload region can be reached, without significant increases in IGBT ratings, by manipulating the circulating current through the arms in such a way that the peak arm current is reduced to within the bounds of the SOA [5]. A graphical representation of this method is

provided in Figure 3.2. The circulating current resides internally in the MMC and does not leave the converter [4]. While it is true that injecting judicious amounts of circulating current continuously will increase the steady state losses, this controller will be used during frequency controlled ancillary services (FCAS) and the amount of losses during this time could be acceptable.

It also must be noted that the increase in current, associated with the additional active power capacity, creates an increase in the junction temperature of the IGBTs. A full overload capacity time period of two seconds was achieved in [6] before the dynamic temperature controls were applied, reducing the current to within the continuous thermal operating limits of the IGBTs. This controller utilizes the maximum additional active power capacity to reduce the RoCoF as well as the frequency nadir. After this is accomplished, the controller switches to a proportional operation, reducing the active power injection (assuming that the active power required to rectify the power imbalance within the network is less than the full additional active power capacity of the MMC). However, as IGBTs are sensitive to high thermal temperatures [5], either a temperature controller (ensuring the junction temperature remains at a safe operating level), or an improved cooling system would be recommended.

4.3 Hybrid Controller

The hybrid controller reacts to frequency events from within the system. Frequency can be measured using the PLL of the MMC, at a specific bus that lacks the traditional inertial support, or using the speed of a synchronous generator. The controls activate when the monitored frequency falls below a user-defined threshold. Once activated, the controller injects a maximum amount of active power, which reduces the extremity of the RoCoF. As stated above, the maximum power transfer, without damaging the MMC, is made possible through the ability of the MMC to operate in an overload

region. After the initial maximum active power transfer, the controller continues to provide additional active power in a proportional-droop mode, allowing for stable support for various active power/load imbalances. When the frequency returns within the limits of a user-defined threshold for an amount of time (which is also defined by the user), the controller returns to traditional CCSC operation. A high level overview of the controls is provided in Figure 4.1.

The next sections describe the theory behind the maximum power controller, the thought process that formed the basis of the proportional-droop controller and how they are implemented in the CCSC and the active power controller. The chapter concludes with model verification using a synchronous machine model connected to a MMC.

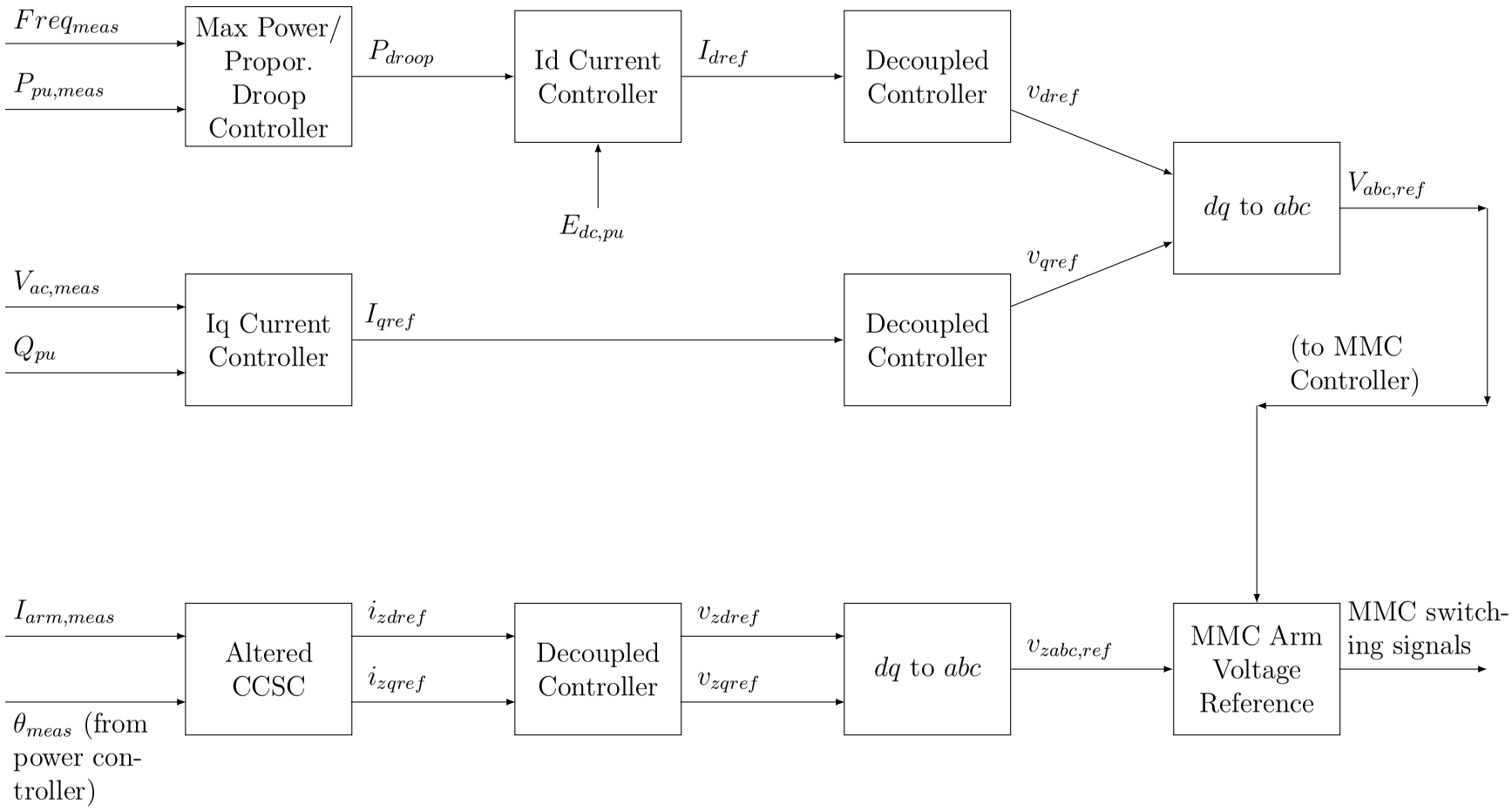

Figure 4.1: Overview of Controls

4.4 External Controls: Power Controller

The power controller is fed measurements from the system and creates a voltage reference that is used by the MMC controller to produce a desired result. As this work focuses on quick injection of active power, the path of interest resides in the active power loop. The reactive power loop is in ac voltage control with a reactive power droop and while it is included, it will not be covered in thorough detail. This work introduces a new variable, P_{droop}, in the power controller. P_{droop}, $V_{dc,meas}$, $V_{ac,meas}$ and Q are used to create current references in the dq frame. Making use of decoupled controllers, two voltages are recovered that, when sent through a dq to abc transformation, provide the voltage reference that corresponds to the desired operating condition. This section discusses each part.

4.4.1 Maximum Power/Proportional-Droop Control

The maximum power/proportional droop signal (P_{droop}) is produced by newly added controls (Figure 4.2). This loop receives an input of per unitized frequency (ω_{PLL}). This frequency can be measured at various points in the system, depending on specific needs. For example the PLL of the MMC, a weak bus in need of inertia, or to support synchronous machines. The total error signal, forced to zero by a PI controller, consists of the sum from the per unitized frequency error (with nominal frequency, ω_{nom}, being 1 pu) and an active power droop signal. Once the frequency falls below a user-defined threshold, a frequency event is detected. The detection of the frequency event sends a signal to the PI controller that resets the output of the integrator within it. The reset value of the integrator is set to the maximum output, corresponding to the maximum amount of additional power that can be sent through the MMC without violating the SOA of the IGBTs. This ensures that a fast response is achieved with the RoCoF (ideally) limited to values that do not pose a threat to

the generation within the network. The controller will stay in this mode until the frequency increases such that the error signal is sufficiently small. At this point the controller seamlessly switches to a proportional control, by unfreezing the integrator in the PI controller, which allows for adequate active power support for various active power/load imbalances. Therefore, this portion of the controller creates an active power reference (maximum power/proportional-droop signal, P_{droop}) which is initially set to the maximum power the MMC can safely provide and then naturally transitions into a proportional control once the frequency has recovered from the initial nadir.

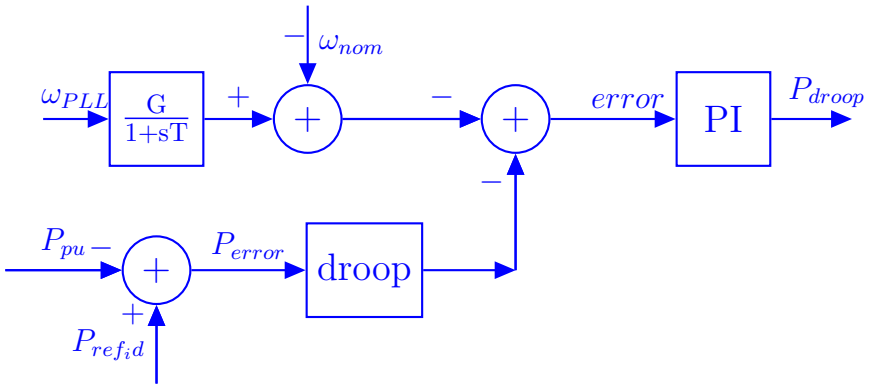

Figure 4.2: Proportional droop controller.

4.4.2 I_d and I_q Current Controllers

This loop produces the instantaneous current references required to increase the active power going through the MMC. Using a Park's Transformation, as presented in section 2.4.2, references for d and q components (I_{dref} and I_{qref}) of the internal currents are calculated. The d-axis reference (I_{dref}) is determined through the implementation of an active power controller with an additional control to ensure that a DC overvoltage is not experienced. The q-axis reference (I_{qref}) is determined through an ac voltage control with a reactive power droop. For completeness all reactive power block diagrams have been included, however, due to the fact that this research focuses on the active power controls, this is the depth the reactive power controls are covered.

Switching back to the active power controls, a maximum power/proportional-droop signal (P_{droop}) is added to the active power reference to produce a new reference that accounts for the additional active power required to mitigate the frequency event. Three signals, the new active power reference, the contribution to ensure there are no DC over-voltages and the measured active power are summed. The resulting error, from the summed terms, is driven to zero using a PI controller (Figures 4.4 and 4.5). The output of the PI controller, used to control the active power, is I_{dref} (Figure 4.4).

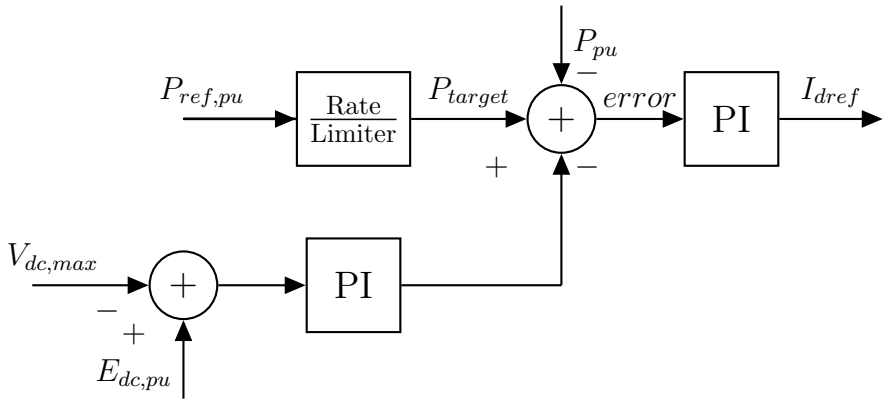

Figure 4.3: Original I_{dref} Internal Current Controller

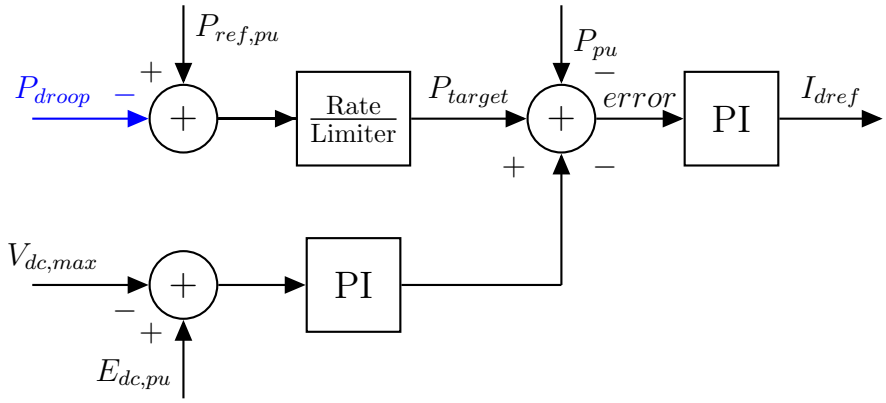

Figure 4.4: I_{dref} Internal Current Controller

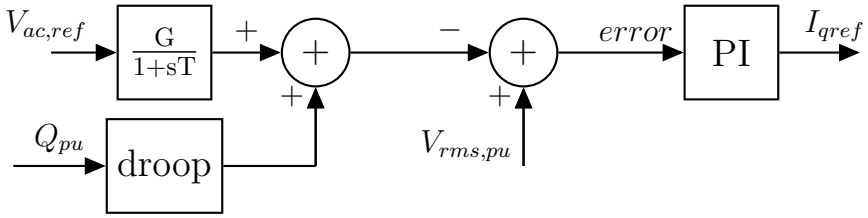

Figure 4.5: I_{qref} Internal Current Controller

4.4.3 Decoupled Controller

The two internal current references, I_{dref} and I_{qref}, are of little direct use for the MMC controls and have to be further manipulated. The errors between these reference currents and the actual measured values (I_{dpu} and I_{dpu}, derived by taking the Park's transformation of the per-unitized output AC current of the MMC) are passed through PI controllers and the resulting outputs are then added to v_{dpu} and v_{qpu} (derived by taking the Park's transformation of the high voltage side measurement of the MMC) and the respective decoupling term (as explained in Section 2.3.1). The result of these sums are the voltage signals v_{dref} and v_{qref} (Figures 4.6 and 4.7). These signals are then put back into a Park's transformation where the *abc* phase voltages are produced. The phase voltages are what is used by the MMC controls to construct the voltage waveform reference.

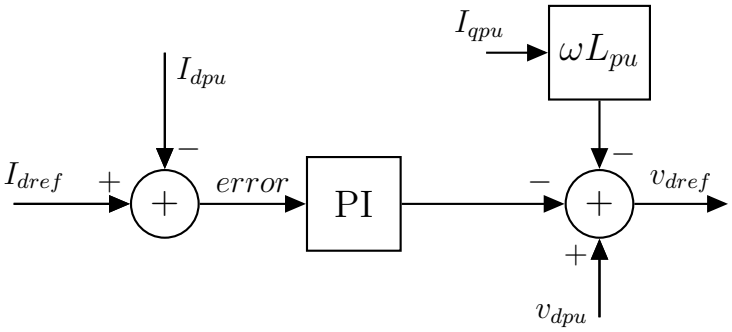

Figure 4.6: Internal Signal Conversion to v_{dref}

This section introduced the method of creating a new signal, P_{droop}, that is used to supply both the maximum amount of additional power the MMC is capable of

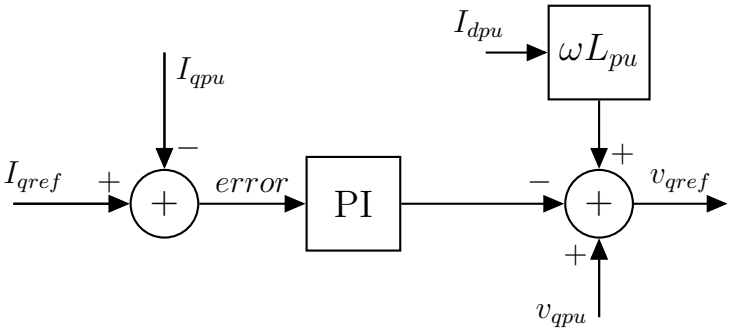

Figure 4.7: Internal Signal Conversion to v_{qref}

delivering as well as a proportional amount of power that allows adequate operation in a wide variety of network conditions. From this new variable and through decoupled control, a voltage reference is produced that will make the MMC deliver the desired amount of active power.

4.5 Internal Controls: MMC Controller

This section discusses the controls that allow the MMC to produce the desired active power from the control variables provided by the power controller described in the previous section.

The phase voltage references and phase angle are sent from the power controller to the MMC controls. The direct use of these will successfully produce the desired active power. However, the 2$^{\text{nd}}$ harmonic current, which remains solely in the arms of the MMC, requires further control. To achieve this, one additional signal, $v_{zabc,ref}$, is produced internally by the CCSC controller. $v_{zabc,ref}$ is typically produced in such a way that adding it to the phase voltage references eliminates the 2$^{\text{nd}}$ harmonic component of the arm current. As discussed in section 2.4.2, this was defined as traditional CCSC. The combination of these reference signals are used by the MMC controller to send the desired amount of active power with the desired amount of circulating current. This research manipulates the $v_{zabc,ref}$ component, such that

adding it to the voltage reference alters the arm current so it does not violate the SOA of the IGBTs.

4.5.1 Altered CCSC

In section 2.3.1 a decoupled CCSC was presented. The simple loop takes d and q components of the measured 2^{nd} harmonic currents and forces them to a defined reference signal. In the case of traditional CCSC the reference signal is zero. However, it does not have to be zero. This research alters the internal reference signals to specific values that achieve a desired effect on the arm current. There are three separate operational states of this altered CCSC:

- Traditional CCSC - where the $v_{zabc,ref}$ is calculated such that when it is added to the reference voltage wave, the circulating current component of the arm current is forced to zero.
- Maximum CCSC - where the $v_{zabc,ref}$ is calculated such that when it is added to the reference voltage wave, the circulating current component adds to the arm current such that the peaks of the arm current are flattened. This allows for the maximum amount of additional active power.
- Droop CCSC - where the $v_{zabc,ref}$ is calculated such that when it is added to the reference voltage wave, the circulating current component adds to the arm current such that the peaks of the arm current remain within the SOA of the transistor. This area of operation is between the minimum (Traditional CCSC) and maximum (Maximum CCSC). This represents the ability to support various active power/load imbalances in the systems after the RoCoF has been minimized.

Traditional CCSC is used when the network is in a steady state situation; it is achieved by setting the d and q components (of internal current references signals) to

zero. In this research, this situation happens before a disturbance is applied or after steady state is reached after a disturbance. The post-disturbance steady state could be determined by measuring the error signal of the frequency (from its nominal value). Once the frequency remains within certain thresholds for an allotted length of time the controls return to traditional CCSC. However, this can also be a manual change, after the generation in the system is re-dispatched to rectify the power imbalance.

The maximum CCSC mode is used when the frequency falls below a user-set threshold and is achieved by setting the d and q components (internal current reference signals) to the output from the maximum power controller. In this research, this situation typically happens shortly after the disturbance's inception. Here, maximum power is delivered through the MMC, without violating the SOA of the IGBTs, to directly address high RoCoFs. The controls remain in this state until the error between the measured frequency and reference frequency beomes zero. At this point, the controls switch to the final operating state, the proportional-droop CCSC.

The proportional-droop CCSC is used in the period after the the controller exits from the maximum CCSC and before it reverts back to the traditional CCSC. In this research, the proportional property, empirically discovered and presented in section 4.5.3, is exploited. An additional ratio signal is used to calculate the internal current references. The ratio signal, $ratio_{cc}$, is defined as,

$$ratio_{cc} = \frac{P_{ref,cc}}{P_{max,cc}} \tag{4.1}$$

where $P_{ref,cc}$ is the additional active power requested by the maximum power/proportional-droop controller and $P_{max,cc}$ is the maximum additional power that the MMC can safely transfer without violating the SOA of the transistors. This ratio signal is passed to the internal controls of the MMC. The proportional-droop signal, $droop_{signal}$ is then

calculated from the maximum signal, used in the maximum CCSC state as,

$$droop_{signal} = ratio_{cc} * max_{signal} \tag{4.2}$$

This signal is then used for the d and q internal current references.

As this controller is for use in inertia deficient systems the discussions in this chapter focused on a falling frequency. However, this system would also be able to participate in frequency swells. Once the frequency exceeds the upper limit of the user-defined deadband, the controller would enter proportional-droop operation (noting that maximum power operation is achieved only when a lower frequency threshold is crossed). In order to participate, it is required that a storage element with sufficient capacity is available.

This section presented the three operating states of the CCSC: traditional CCSC, maximum CCSC and proportional-droop CCSC. Traditional CCSC was presented in section 2.3.1. The next two sections will focus on maximum CCSC and proportional-droop CCSC.

4.5.2 Maximum CCSC

In order to inject the correct amount of circulating current into the arms of the MMC to achieve the maximum amount of active power transfer without violating the rating of the components of the MMC, both the amplitude and phase of the circulating current are necessary. The method chosen to recover these two values was originally presented in [7].

The general expression for the 2$^{\text{nd}}$ harmonic component of the circulating current is given in (4.3). The goal of this derivation is to recover the magnitude of the circulating current, I_{r2}, and the phase of the circulating current, $\psi^{'}$, such that when injected into the arm of the MMC it results in the minimum achievable peak of the

arm current.

$$i_{r2} = I_{r2}\sin(2\omega t^{'} + \psi^{'}) \tag{4.3}$$

The arm current through phase a at any given time can be generally represented as $\frac{1}{3}$ of the dc current (first term in (4.4)), $\frac{1}{2}$ of the ac current for that phase (second term in (4.4)) and the circulating current (third term in (4.4)). Mathematically, it is represented as follows,

$$i_{pa} = \frac{I_{dc}}{3} + \frac{I_{vm}}{2}\sin(\omega t^{'} + \gamma_{va} - \psi_{ac}) + I_{r2}\sin(2\omega t^{'} + \psi^{'}), \tag{4.4}$$

where ω is grid frequency, γ_{va} is the initial phase angle of the phase voltage, ψ_{ac} is the power factor angle measured at the connection point, and $\psi^{'}$ is the 2^{nd} harmonic phase shift.

Using the following substitutions

$$t = t^{'} + \frac{\gamma_{va} - \psi_{ac}}{\omega}, \tag{4.5}$$

$$\psi = \psi^{'} - 2(\gamma_{va} - \psi_{ac}), \tag{4.6}$$

$$k = \frac{I_{r2}}{\frac{I_{vm}}{2}}, \tag{4.7}$$

$$n = \frac{\frac{I_{dc}}{3}}{\frac{I_{vm}}{2}} \tag{4.8}$$

yields,

$$i_p = n + \sin(\omega t) + k\sin(2\omega t + \psi) \tag{4.9}$$

Equation (4.9) is used to derive the operating point for the 2^{nd} harmonic current in order to realize the maximum power controller at varying conditions. First, the extreme points are required to be found and then the proper substitutions need to be included to ensure the controller sufficiently reduces the peak. Taking the derivative

of (4.9) with respect to t is used to obtain the extrema of the arm current as follows:

$$\frac{d(i_p)}{dt} = \omega\cos(\omega t) + 2k\omega\cos(2\omega t + \psi) \tag{4.10}$$

The extreme points occur when the derivative is equal to 0; thus

$$\omega\cos(\omega t) + 2k\omega\cos(2\omega t + \psi) = 0 \tag{4.11}$$

Expanding (4.11) using trigonometric identities yields,

$$\omega\cos(\omega t) + 2k\omega\cos(\psi)\cos(2\omega t) - 2k\omega\sin(\psi)\sin(2\omega t) = 0 \tag{4.12}$$

Continuing to expand the double angle terms produces,

$$\omega\cos(\omega t) + 2k\omega\cos(\psi)[\cos^2(\omega t) - \sin^2(\omega t)] - 4k\omega\sin(\psi)\sin(\omega t)\cos(\omega t) = 0 \tag{4.13}$$

Making the substitution of $x = \cos(\omega t)$, dividing out the common ω term and rearranging the terms produces:

$$x + 2k\cos(\psi)[x^2 - (1 - x^2)] = 4k\sin(\psi)\sin(\omega t)x, \tag{4.14}$$

Further expanding (4.14) yields,

$$x + 4k\cos(\psi)x^2 - 2k\cos(\psi) = 4k\sin(\psi)\sin(\omega t)x, \tag{4.15}$$

Squaring both sides of (4.15) yields:

$$16k^2\cos^2(\psi)x^4 + 8k\cos(\psi)x^3 + [1 - 16k^2\cos^2(\psi)]x^2 - 4k\cos(\psi)x + 4k^2\cos^2(\psi) = 16k^2\sin^2(\psi)x^2[1 - x^2] \tag{4.16}$$

Trigonometric identities can be used on the right-hand side of (4.16) further reducing it to:

$$16k^2x^4 + 8k\cos(\psi)x^3 + [1 - 16k^2]x^2 - 4k\cos(\psi)x + 4k^2\cos^2(\psi) = 0 \tag{4.17}$$

which is,

$$x^4 + \frac{\cos(\psi)}{2k}x^3 + (\frac{1}{16k^2} - 1)x^2 - \frac{\cos(\psi)}{4k}x + \frac{\cos^2(\psi)}{4} = 0, (-1 \leq x \leq 1) \tag{4.18}$$

Returning to (4.9), for any n and k, $\psi = \frac{\pi}{2}$ yields the correct shift. Substituting $\psi = \frac{\pi}{2}$ into (4.18) yields:

$$x^4 + (\frac{1}{16k^2} - 1)x^2 = 0, (-1 \leq x \leq 1) \tag{4.19}$$

which can be written as follows:

$$x^2(x^2 + \frac{1}{16k^2} - 1) = 0, (-1 \leq x \leq 1) \tag{4.20}$$

In (4.20), under the condition that $0 \leq k < \frac{1}{4}$, the solutions is,

$$\begin{cases} x_1 = 0 \\ x_2 = 0 \end{cases}$$

Using these solutions, (4.9) produces the following extreme points:

$$\begin{cases} i_{p1_e x} = n + 1 - k, & (0 \leq k < \frac{1}{4}) \\ i_{p2_e x} = n - 1 - k, & (0 \leq k < \frac{1}{4}) \end{cases}$$

In (4.19), under the condition that $k \geq \frac{1}{4}$, the solutions is:

$$\begin{cases} x_1 = 0 \\ x_2 = 0 \\ x_3 = \sqrt{1 - \frac{1}{16k^2}} \\ x_4 = -\sqrt{1 - \frac{1}{16k^2}} \end{cases}$$

Using these solutions, (4.9) produces the following extreme points:

$$\begin{cases} i_{p1_{ex}} = n + 1 - k, & (k \geq \frac{1}{4}) \\ i_{p2_{ex}} = n - 1 - k, & (k \geq \frac{1}{4}) \\ i_{p3_{ex}} = n + k + \frac{1}{8k}, & (k \geq \frac{1}{4}) \\ i_{p4_{ex}} = n + k - \frac{3}{8k}, & (k \geq \frac{1}{4}) \end{cases}$$

Using the above, the maximum values can be obtained over specific intervals,

$$\begin{cases} \max(i_{p1_{ex}}) = n + 1 - k, & (0 \leq k \leq \frac{1}{4}, k < n) \\ \max(i_{p2_{ex}}) = -n + 1 + k, & (n \leq k < \frac{1}{4}) \\ \max(i_{p3_{ex}}) = -n + 1 + k, & (k \geq \frac{1}{8(1-2n)}, k \geq \frac{1}{4}) \\ \max(i_{p4_{ex}}) = n + k + \frac{1}{8k}, & (\frac{1}{4} \leq k < \frac{1}{8(1-2n)}) \end{cases}$$

Finally, the minimum of the maximum arm current can be derived as follows:

$$\min(\max(i_p(k, \psi, n))) = \begin{cases} 1 & : n < \frac{1}{4}, k = n, \psi = \frac{\pi}{2} \\ 1 - n + \frac{1}{8(1-2n)} & : \frac{1}{4} \leq n < \frac{1}{2} - \frac{\sqrt{2}}{8}, k = \frac{1}{8(1-2n)}, \psi = \frac{\pi}{2} \\ n + \frac{\sqrt{2}}{2} & : n \geq \frac{1}{2} - \frac{\sqrt{2}}{8}, k = \frac{\sqrt{2}}{4}, \psi = \frac{\pi}{2} \end{cases} \quad (4.21)$$

The following block diagram (Figure 4.8) displays the implementation a controller that allows the MMC to safely operate in an overload region.

This method determines the magnitude and phase angle of the 2$^{\text{nd}}$ harmonic cir-

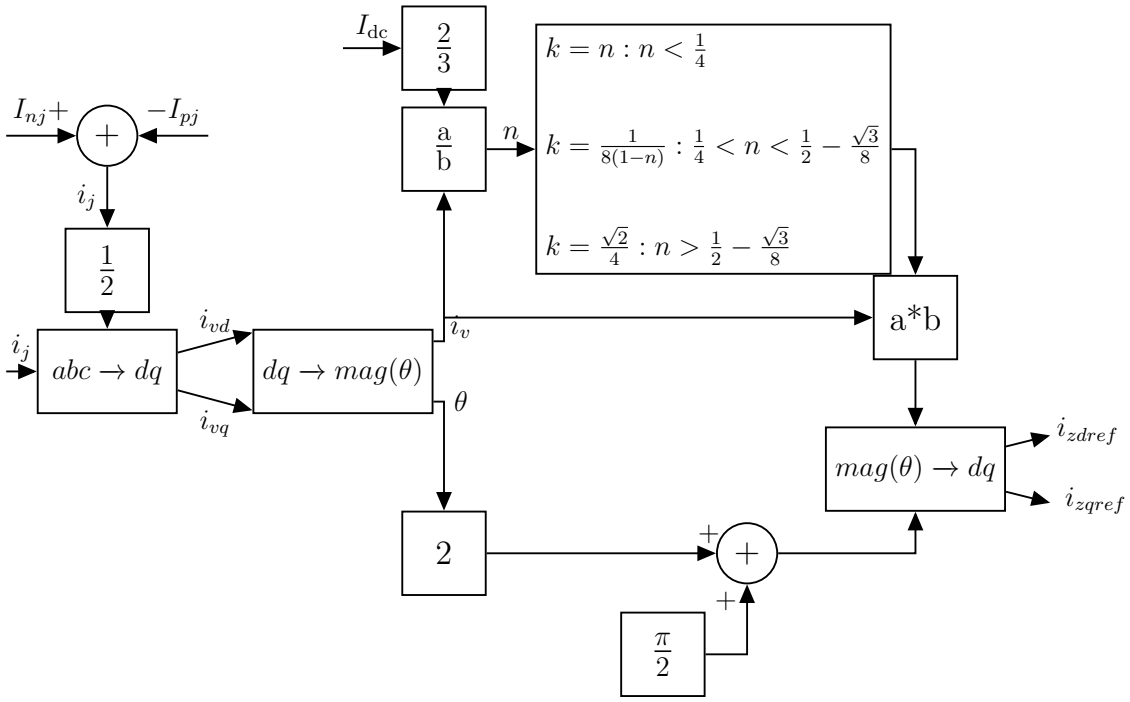

Figure 4.8: Block diagram of the maximum power control scheme.

culating current, such that injecting it into the arm current yields the minimum peak for the arm current. The implementation of this is found within the internal control system of the MMC. Therefore, the speed of realizing and producing the minimum arm current will be dependent on the ability of the control system and limited by the necessary requirements of stability of the connected network. This method is able to have a fast initial response and is used as the base for the proportional-droop CCSC, which is presented in the next section.

4.5.3 Proportional-Droop CCSC

After the inertial period where the RoCoF is minimized by the maximum power controller, the 2$^{\text{nd}}$ harmonic current injected into the arm is altered. Since the active power required from the inverter-based generation to resolve the power imbalance is reduced, there is no longer a need for judicious amounts of 2$^{\text{nd}}$ harmonic current to flatten the peaks of the arm current. Therefore, the 2$^{\text{nd}}$ harmonic current can also be

reduced in magnitude. The proportional nature of these controls allows for adequate performance for a variety of power imbalances. This is done until the power system's frequency controls are able to resolve the disturbance. The relationship between the amplitude of the injected 2nd harmonic current, the phase of the injected 2nd harmonic current and the peak of the arm current was recorded from simulations using a modulation index of 0.8 as presented in Figure 4.9. Figure 4.10 shows that if the phase of the injected 2nd harmonic current phase is kept constant (at -50 degrees) and the amplitude of the injected 2nd harmonic current is decreased, a linear relationship emerges. Through extensive simulations, this linearity is found to be consistent for different realistic modulating indices. Therefore, this relationship is used to implement a proportional droop controller. The proportion of active power required to maximum active power is sent to the circulating current controller as a ratio, called $ratio_{cc}$. This ratio is multiplied by the Maximum CCSC power magnitude, resulting in a new reference for the circulating current that allows for varying in-feed losses, while respecting the SOA of the IGBTs.

The proportional overload support ranges from a maximum of 27.5% above the rated power limit of the MMC, in line with the maximum power controller, to a minimum of rated power, that coincides with CCSC.

The proportional droop control's implementation is shown in Figure 4.11.

4.6 PSCAD/EMTDC Implementation and Verification

4.6.1 Test Network

Two tests were done to validate the operation of the controller on the test system presented in Figure 4.12. The test system specifications are provided in Table 4.1. A

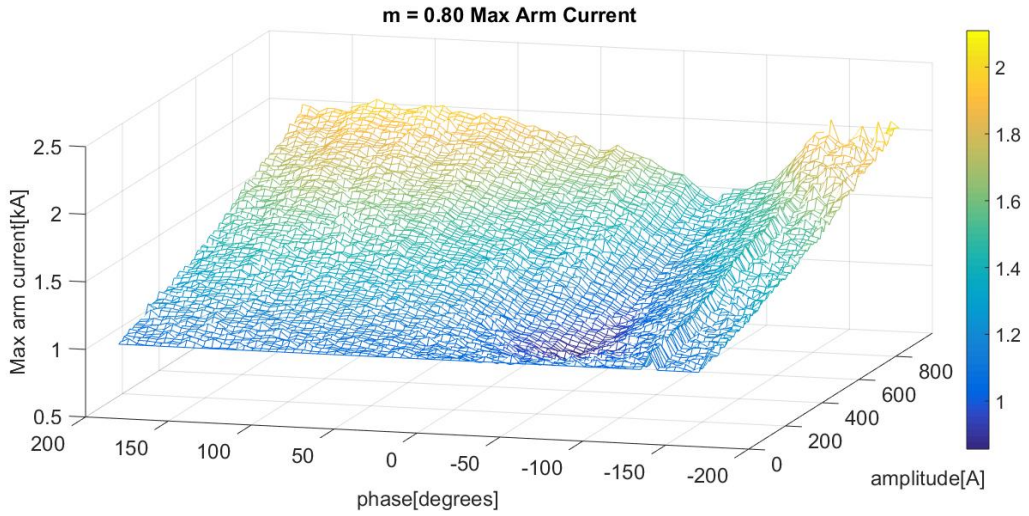

Figure 4.9: The behaviour of peak arm current as the phase and magnitude of the 2nd harmonic current is varied.

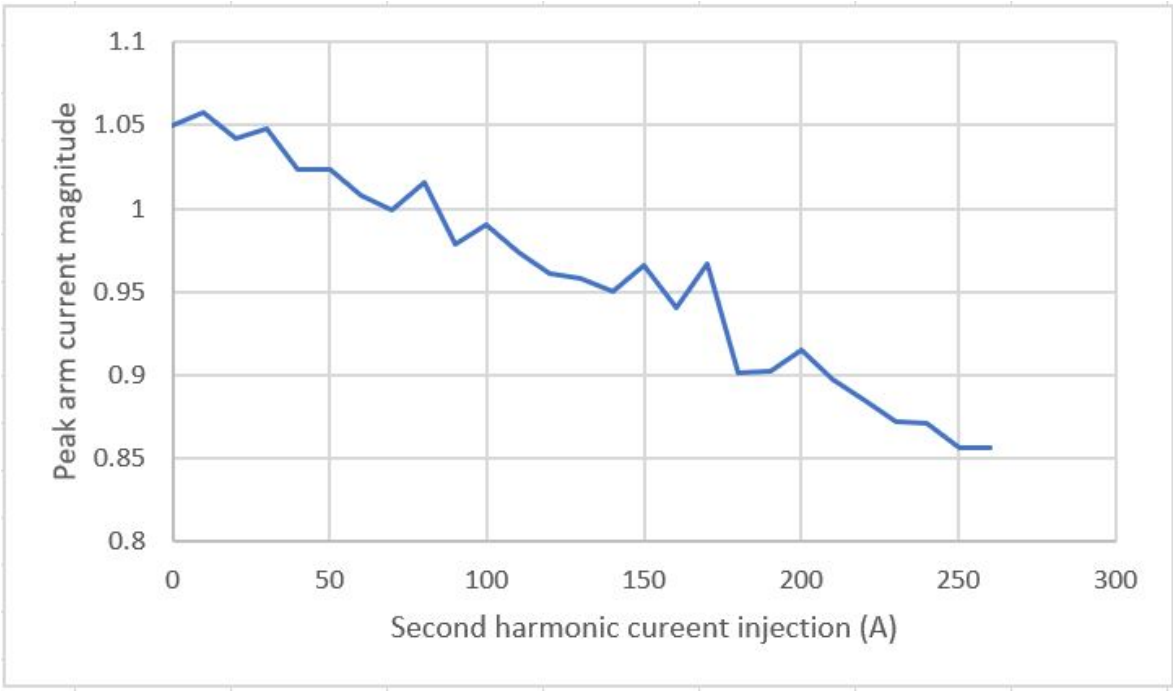

Figure 4.10: Peak arm current with the phase of the 2nd harmonic current kept constant while varying the magnitude of the 2nd harmonic current.

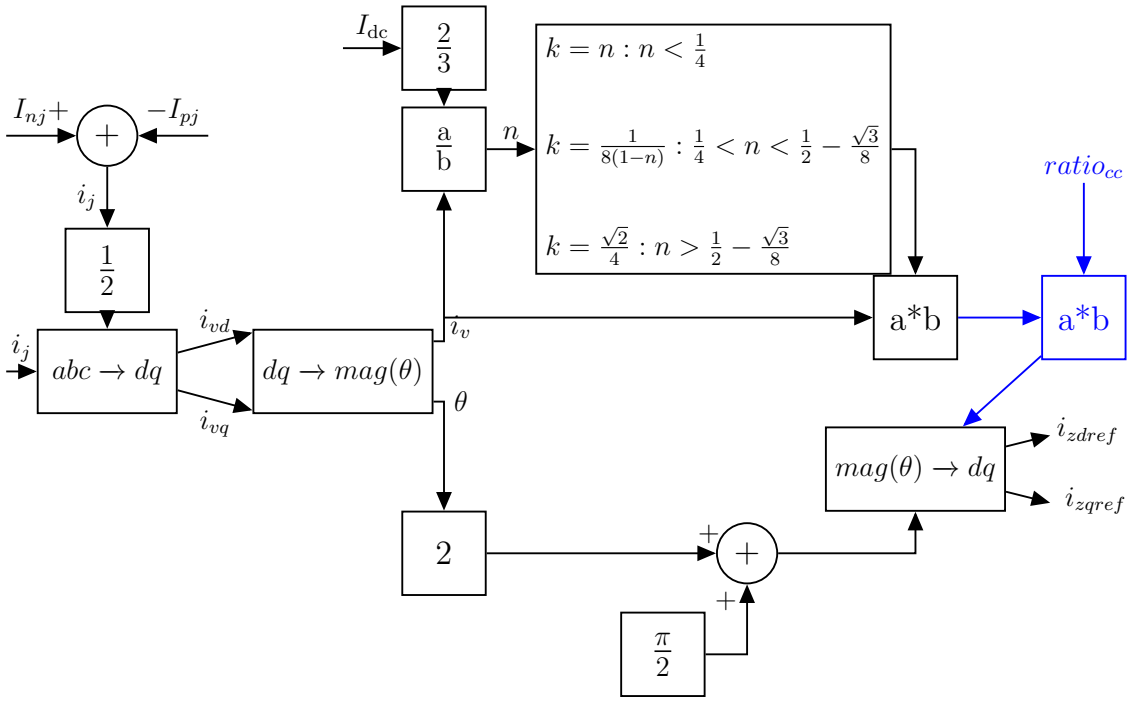

Figure 4.11: Block diagram of the proportional droop control scheme.

single-mass synchronous machine model is implemented in PSCAD-EMTDC for the purpose of simulating the inertial response and frequency control capabilities of the hybrid controller. The rotating masses of all the synchronous machines that link to conventional generation are lumped together as a single synchronous machine. The governor controls act solely on this single mass. In using this model, the frequency control dynamics are focused on, while other aspects of the power system, such as voltage variations and electromechanical oscillations can be neglected [46].

The MMC connects to an ideal DC voltage source. This simulates an HVDC interconnector where any amount of power can be delivered. This simulation does not take into account limitations such as HVDC link overload.

An active load of 120 MW is switched in at $t = 30$ s using a circuit breaker to create a controlled power imbalance. The inertia constant of the synchronous generator varies from 5.2 s to 1.2 s (in steps of 1 s) to simulate a progressively weaker system. This test system is provided in Figure 4.12.

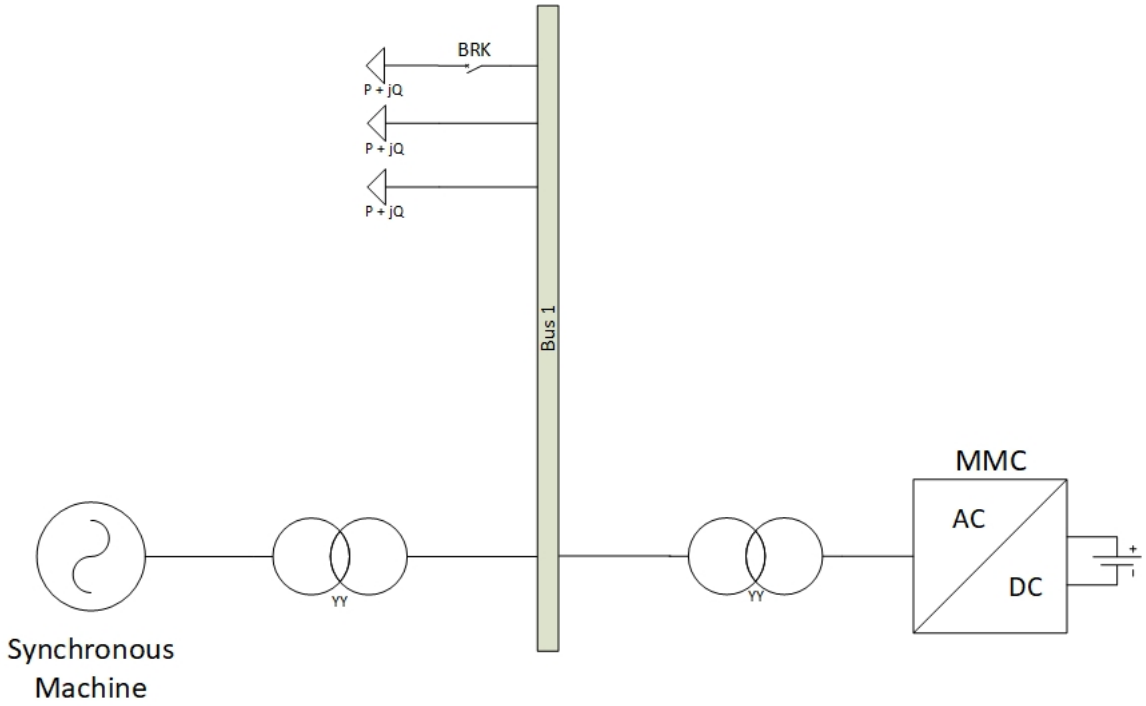

Figure 4.12: Test Network.

4.6.2 Simulation Results

To verify the effectiveness for the proposed controller two tests were simulated. In the first test the generator supplies the required amount of power to the grid, reacting to any frequency event and the MMC does not participate. In the second test, the power reference of the synchronous generator is held constant and the proposed controller in the MMC compensates for the power imbalance via the HVDC link. Five seconds after introducing the power imbalance, the power reference of the synchronous generator increases (simulating an updated dispatch) and the proposed MMC controls reduce the power delivered by the HVDC link in the same proportion that the synchronous generator increases its power. When the MMC is safely operating at the original set point, CCSC control takes over.

Table 4.1: System Parameters

Synchronous Machine Specifications		
Frequency: 60 Hz	Voltage: 18 kV	H: 1.2s - 5.2 s
Synchronous Machine Coupling Transformer		
Rating: 585 MVA, 18 kV/230 kV	$X_{leakage}$: 10%	
Converter Active Power Rating		
Nominal Rating: 400 MW	Overload Rating: 510 MW	
Converter Transformer Specifications		
Rating: 600MVA, 370kV/230kV	$X_{leakage}$: 10%	
Converter Specifications		
SMs/Arm: 76	C_{cell}: 2800μF	L_{arm}: 50 mH
System Specifications		
DC voltage = 640 kV	MMC POC SCR = 3	MMC X/R ratio = 5

Test 1: DC link power constant, power imbalance rectified by synchronous machine

Five simulations are done at different inertia constants to demonstrate the behaviour of the system with no specialized MMC control implemented. The synchronous generator alone reacts to correct the power imbalance that is introduced. The frequency response of the synchronous generator is displayed in Figure 4.13.

Decreasing the inertia constant in the synchronous machine reduces the ability of the generator to resist changes in frequency. This manifests as an increase in RoCoF, a more pronounced nadir, a faster reaction, and a decrease in stability. When the inertia constant is set to 1.2 s in this simulation, the generator becomes unstable.

Test 2: DC link power controlled by MMC, power imbalance rectified by synchronous machine after 35 s

Five simulations are done to show the behavior of the proposed MMC control. The inertia constant of the synchronous machine is changes for each simulation from 5.2

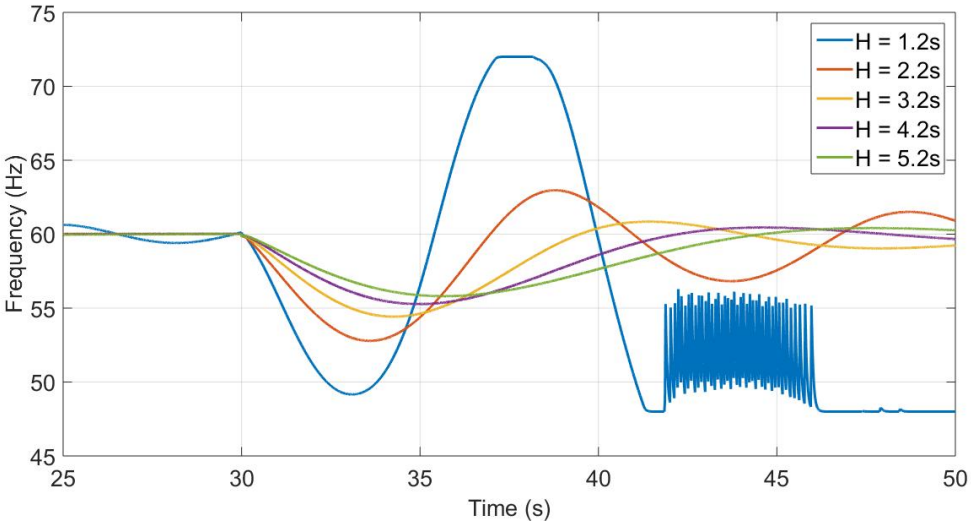

Figure 4.13: Frequency response of the synchronous generator with the proposed MMC controller disabled.

s to 1.2 s. The power imbalance is met with virtual inertia by means of the MMC-controlled HVDC link. In 2018 existing technologies were able to reliably provide ancillary services within hundreds of milliseconds [42]. This work assumes an active power injection time which is far lower (25 ms). To test the behaviour of the controls, a time of 170 ms was chosen. This time represents approximately what was reliably available in 2018 and serves as a worst-case scenario for this work. At $t = 35$ s the power reference of the synchronous machine increases to simulate the active power dispatch levels of machines in the area, being increased to resolve the power imbalance. The set point increases the synchronous generator's power such that it can correct the power imbalance. This allows the HVDC link power decrease to its pre-disturbance value. The frequency response is displayed in Figure 4.14.

As the inertia constant is decreased there is an increase in RoCoF and a lower nadir; however, the overall reaction time increases as compared to test 1, as does the stability. The use of the proposed controller ensures that even low inertia constants, such as 1.2 s, are stable.

Looking closer at the worst-case scenario ($H = 1.2$ s) in Figures 4.15 and 4.16 the

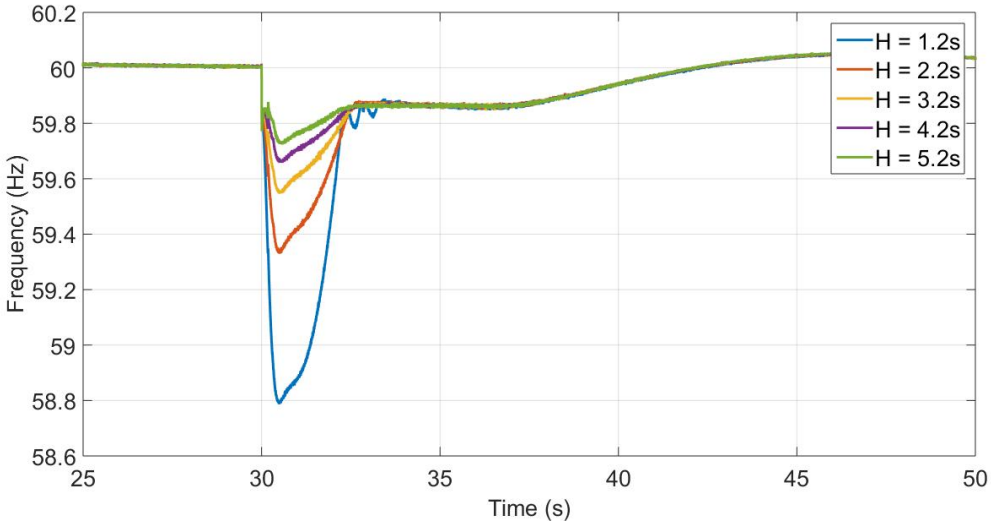

Figure 4.14: Frequency response of the synchronous generator with the proposed MMC controller enabled.

power imbalance that causes a decrease in the synchronous machine frequency is not initially corrected by the inertia stored in the synchronous machine; rather, it is met with an increase in power delivered from the HVDC link (Figure 4.15). In this scenario, a ripple, caused by switching between maximum power and proportional-droop operation was observed. To rectify this issue, once the maximum power operation sufficiently reduced the RoCoF and the error between the measured frequency and reference frequency was zero, the controller was switched to proportional-droop operation. It then remained solely in this state (with no option to return to the quick injection of maximum power) until a condition was met where traditional CCSC was appropriate. This improvement is implemented in the final version of the controller, with testing presented in Chapter 5. To ensure that IGBT switches operate in the SOA, a judicious amount of circulating current is injected into the MMC (Figure 4.16).

The upper and lower arm currents of a single-phase leg of the MMC are shown in Figures 4.17 and 4.18. Prior to the power imbalance, the MMC operates in CCSC control. The arm current, prior to $t = 30.17$ s, in the top graph of Figure 4.17 shows

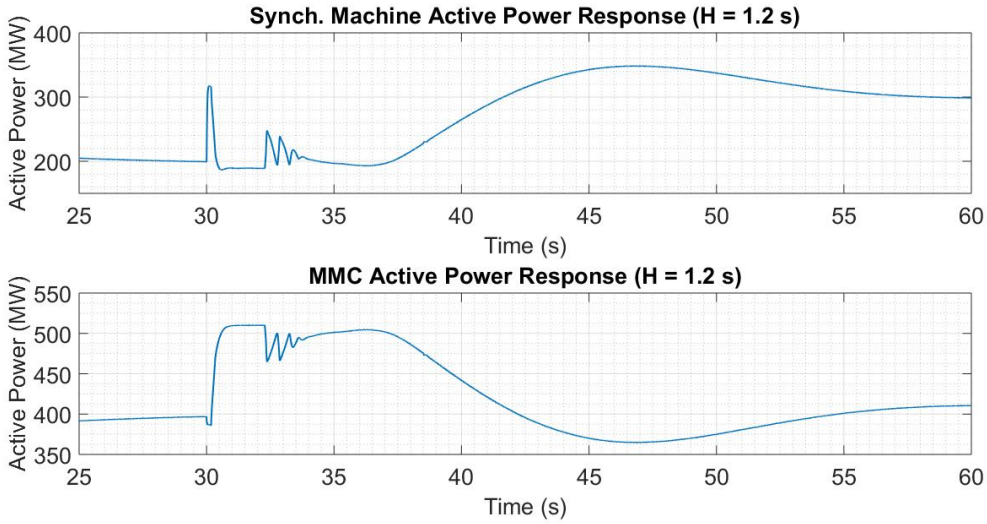

Figure 4.15: System response with proposed controller enabled, $H = 1.2$ s, (top) active power delivered from synchronous generator, (bottom) active power delivered via HVDC link.

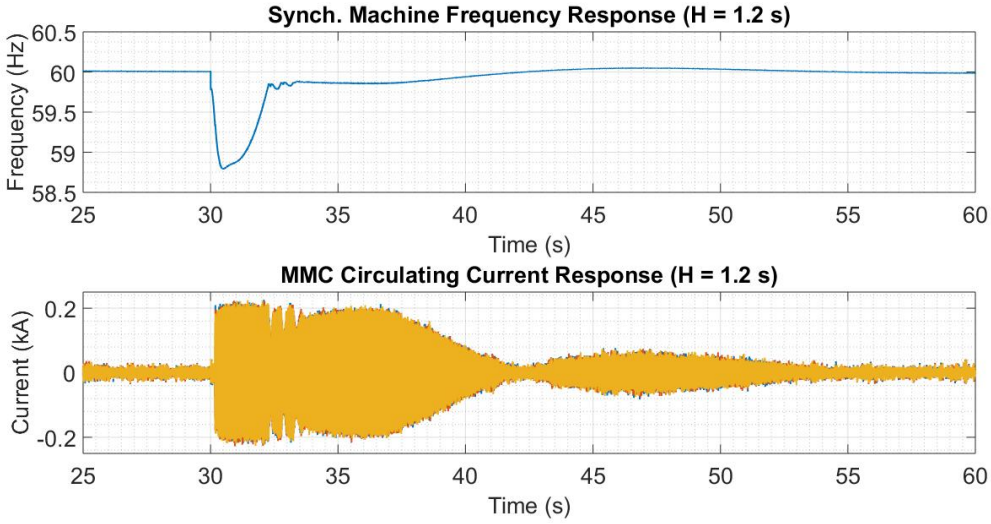

Figure 4.16: System response with proposed controller enabled, $H = 1.2$ s, (top) frequency of synchronous generator, (bottom) three phase circulating current.

that the circulating current is close to zero. CCSC control is used until a frequency deviation is detected. A delay time of 170 ms is used to register the detection at which point the maximum power controller is enabled. This transition from CCSC to maximum power control is seen in the top image of Figure 4.17. In this control mode the MMC delivers the maximum amount of additional power while obeying

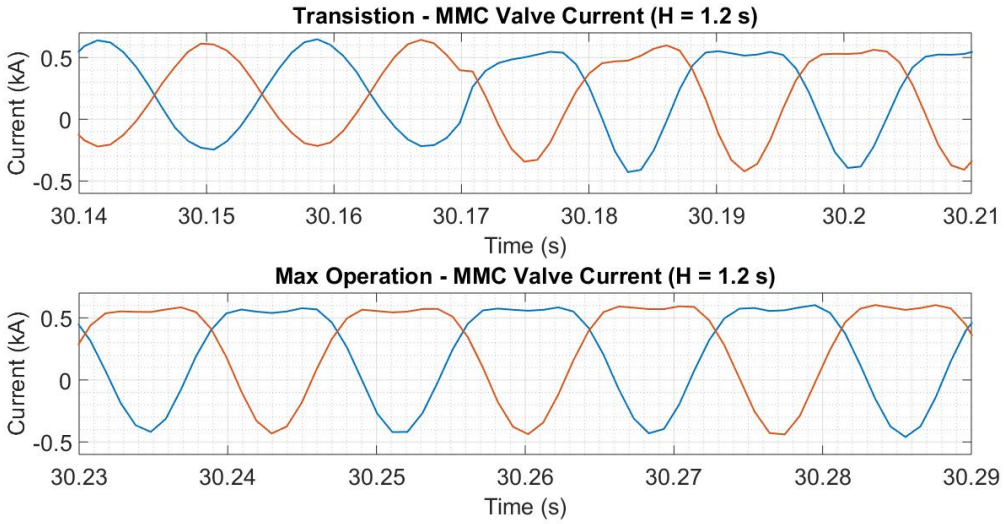

Figure 4.17: Phase A, top and bottom arm current of the MMC with proposed controller enabled, $H = 1.2$ s.

the SOA of the IGBTs. In order for this to happen, judicious amounts of circulating current are injected into each arm of the MMC as seen in the bottom image of Figure 4.16. This reduces the peak of the arm current such that the SOA of the IGBTs is satisfied, as seen in the bottom graph of Figure 4.17. As the synchronous machine begins to increase the active power set-point to another operating point, the power delivered by the DC link, controlled by the MMC, begins reducing. At this point the controller switches to the proportional droop control. The amount of circulating current required to safely operate at this point reduces and the arm current takes a form unlike pure CCSC or maximum power (as seen starting in the top image of Figure 4.18. Finally, the HVDC link returns to its rated power output and the controller switches back to CCSC control as seen in the bottom graph of Figure 4.18.

4.7 Summary

Emulation of inertia was achieved by quickly supplying active power into the system. To ensure the SOAs of the IGBTs in the MMC were not violated, circulating current

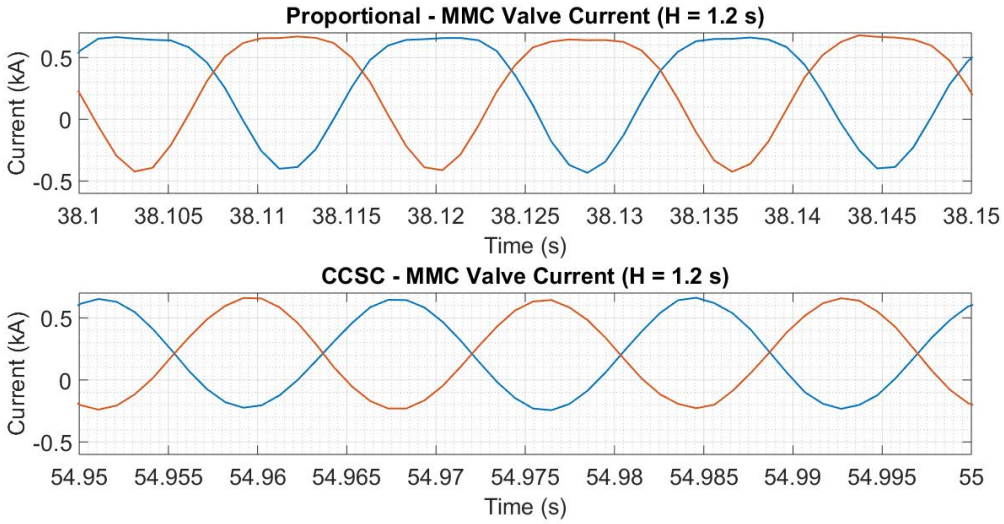

Figure 4.18: Phase A, top and bottom arm current of the MMC with proposed controller enabled, $H = 1.2$ s.

was injected into the arms of the MMC. The maximum power controller is able to meet a power imbalance significantly reducing the nadir of the frequency. The linear relationship that exists when the amplitude of the of the 2$^{\text{nd}}$ harmonic current is reduced while keeping the phase of the 2$^{\text{nd}}$ harmonic current constant, allows the controller to react effectively to different active power/load imbalances. This section validated the proposed MMC controller performance through extensive electromagnetic transient simulation studies of a test system and showed that there is significant improvement in frequency response in terms of nadir, RoCoF and stability (Figure 4.19), especially in scenarios of very lower synchronous machine inertia.

This section discussed the internal controls of the maximum power/proportional-droop controller. It describes how the variables produced by the maximum power/droop controls (I_{dref} and I_{qref}) are manipulated until they are useful phase voltage signals, ready for use by the MMC controls. This section concluded with verification of the proposed controller using a synchronous machine (with varying inertia constants) connected to a MMC (that has access to reliable active power via the dc link). The next section implements the proposed controller in a more complex system.

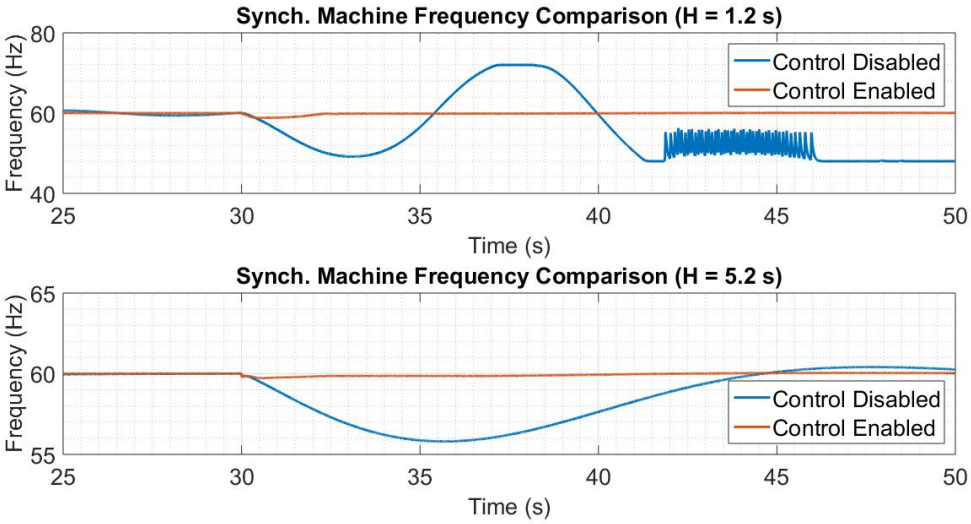

Figure 4.19: Comparison of frequency responses at different H constants.

Chapter 5

PSCAD/EMTDC Testing of the Hybrid Controller Using the IEEE 9-Bus Network

5.1 Overview of Test System

The proposed controller was validated on a test system using a basic network, consisting of only a synchronous machine and a MMC in the last section, for the purposes of ensuring proper controller operation. This section increases the complexity of the test network by testing the controller using the IEEE 9-bus system. The IEEE 9-bus system was chosen as the test system for the proposed controller, as it would be better suited if the controller was only tasked to respond to power imbalances within it's direct vicinity. The controller responding to far imbalances risks the possibility of adverse controller interactions. If the controller was to respond to distant disturbances, this could result in adverse controller interactions between renewable plants. Therefore, the controller should be solely used locally. All simulations were done using PSCAD/EMTDC version 4.6.3.

Two new connections are introduced into the IEEE 9-bus system. One of the 9 buses connects to a synchronous machine through a generic transmission line, and another bus connects to a MMC. The DC side of the MMC is connected to an ideal DC source. This is done under the assumption that active power is readily available, either through plants in the area that have a surplus of active power capacity (not delivering peak power) or some sort of storage system that has available capacity. A 40 MVAr capacitor was connected to the same bus that the synchronous machine is connected to. This was done to strengthen the voltage of that bus to an acceptable level. Lastly, loads were added to balance the additional power injection introduced by the synchronous machine and the MMC.

To further validate the controller a series of tests were completed that use a controlled power imbalance. In order to create a controlled power imbalance, the voltage source (strong source) is disconnected from the system via a breaker once the system is able to reach a steady state condition. Removing the strong source creates a situation where the active power in the system is insufficient to maintain the synchronous frequency and hence the frequency within the system begins to decrease.

Using this test system three sets of simulations were completed. The tests differ in where the frequency measurement is taken from. The first test measures the inverter frequency. This measurement is an internal measurement of the MMC with the frequency measured from the internal PLL. The second test measures the frequency of a bus within the network. A PMU is used to measure a bus frequency in the network and the frequency signal is delivered to the MMC via a fibre optic cable (i.e., a fast delivery system). The last test remotely measures the synchronous speed of the synchronous machine. This is to validate the use of this controller in addressing low inertia buses.

From a design perspective, the communication delay would be very fast when using the frequency measurement of an internal PLL. In this case 5 ms was used.

However, as the measurement moves external to the MMC (as in the case of a synchronous machine) the assumed delivery method would be via a fibre optic cable with a communication delay time of 25 ms. This time was chosen to represent the required measurement time of a single 60 Hz cycle (16.67 ms) as well as the time delay of the fibre optic cable itself (1.3 ms for a 127.5 km fiber optic link [47]). The remaining time was included to serve as a worst case scenario. The fiber-optic cable is necessary to simulate the fast communication time required to tend to the system in a similar manner as inertia would (which happens instantaneously). Below is a description of the test system. The remainder of this chapter will present the results from these three tests and provide visual comparisons of the results.

5.1.1 Overview of IEEE Transmission Network

IEEE benchmark systems are provided to investigate new research ideas. The IEEE 9 bus system used in this research is depicted in Figure 5.1. As mentioned above, a voltage source was kept in the model to represent a strong source. The other two voltage sources, originally found in the IEEE 9-bus system, were replaced with a synchronous machine model and a MMC model.

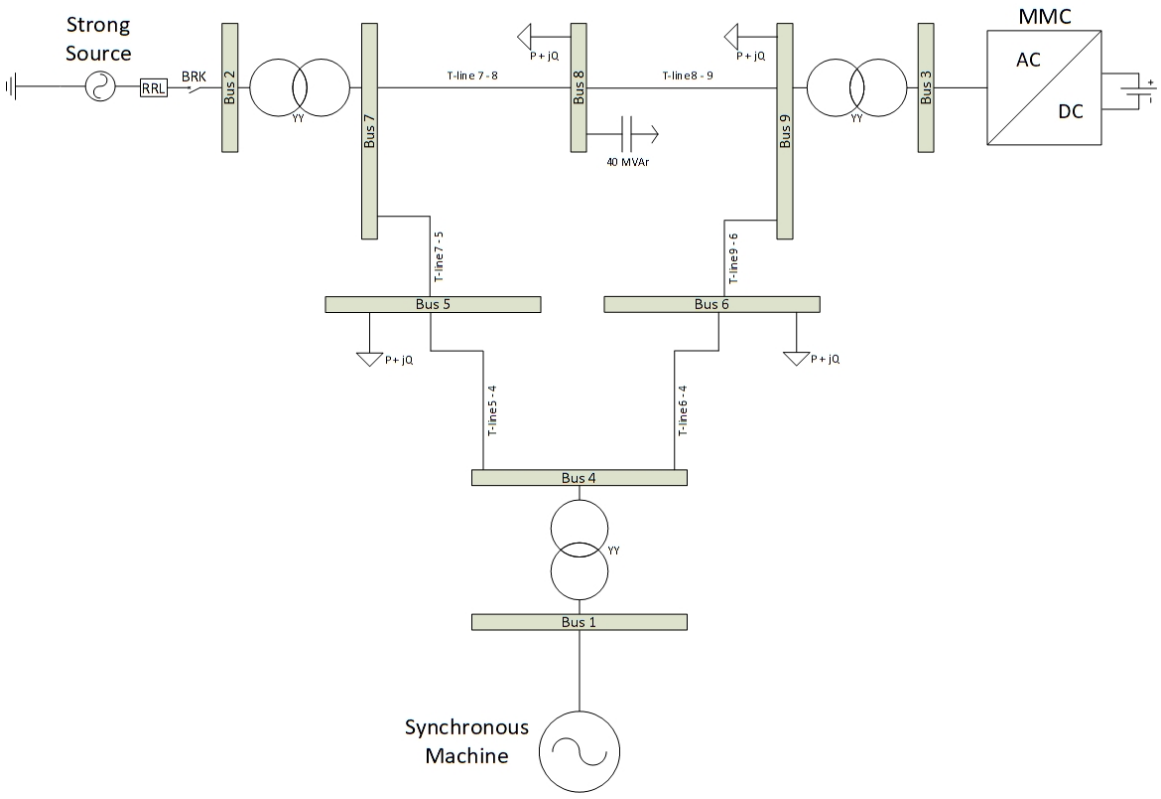

Figure 5.1: The modifies IEEE 9-bus system model in PSCAD/EMTDC.

5.1.2 Overview of the Synchronous Machine Model

A generic synchronous machine model was used to introduce dynamic behaviour as well as simulate different inertia constants. Two different control methods of the synchronous machine are used. One method keeps the angular frequency reference, fed to the governor, at a constant 1.0 pu. This simulates the synchronous machine controlling the frequency disturbance introduced by creating a power imbalance through the opening of the breaker, disconnecting the strong source.

The other control mode uses a PI controller to produce two specific active power references (representing secondary frequency control). The purpose of this setup is to simulate a situation where the MMC is tasked to attend to the frequency disturbance introduced by disconnecting the strong source. Prior to the disturbance the active

power is set to a dispatch level that produces a stable pre-disturbance response. When the strong source is disconnected the MMC initially responds to the disturbance. After 5 s, the active power of the synchronous machine is dispatched to a higher value to attend to the frequency disturbance. This is set up to simulate the manual correction to a more suitable dispatch level in a network.

5.1.3 Overview of MMC

The MMC selected for this simulation was the half bridge topology, due to its widespread prevalence. The operation of the proposed hybrid controller is initiated by an adverse frequency event. When the frequency falls below a user-defined threshold the altered CCSC controller is activated. Initially the output is set to the maximum output. When the frequency error crosses zero, the reset applied to the integrator in the PI controller is removed making a proportional response. This proportional response is applied for a time limit of 30 s. This value was chosen to represent a long enough period of time. In practice the switch back to pure CCSC would be initiated when the frequency event has been fully corrected by changing the dispatch levels within the generating system.

5.2 Control Tests

To adequately evaluate the effectiveness of the proposed controller, two additional simulations were conducted. The first tasked the synchronous machine to attend to the frequency disturbance with the MMC providing constant active power and remaining in traditional CCSC operation. The second one was to allow the MMC to inject additional active power to rectify the frequency disturbance with the internal controls of the MMC remaining in traditional CCSC operation. These two tests will be discussed in the remainder of this section.

5.2.1 Only Synchronous Machine Responding to the Frequency Event

This test was conducted to identify adverse behaviours when a frequency event is applied to this test network without sufficient inertial energy available to attend to it. To perform this simulation the MMC active power/frequency control loop is disabled, which entails that it will not be participating in providing active power to help rectify the power imbalance. Also, traditional CCSC in the MMC remains in place; therefore, the MMC will force the circulating current to be zero (ideally).

When the disturbance (strong voltage source disconnected) is applied to the network at $t = 30$ s, the synchronous machine begins to increase its active power output to attend to the power imbalance. This is seen in Figure 5.2. Since the active power/frequency controls are disabled in the MMC, it does not increase its active power output and remains constant at ∼400 MW, as depicted in Figure 5.3.

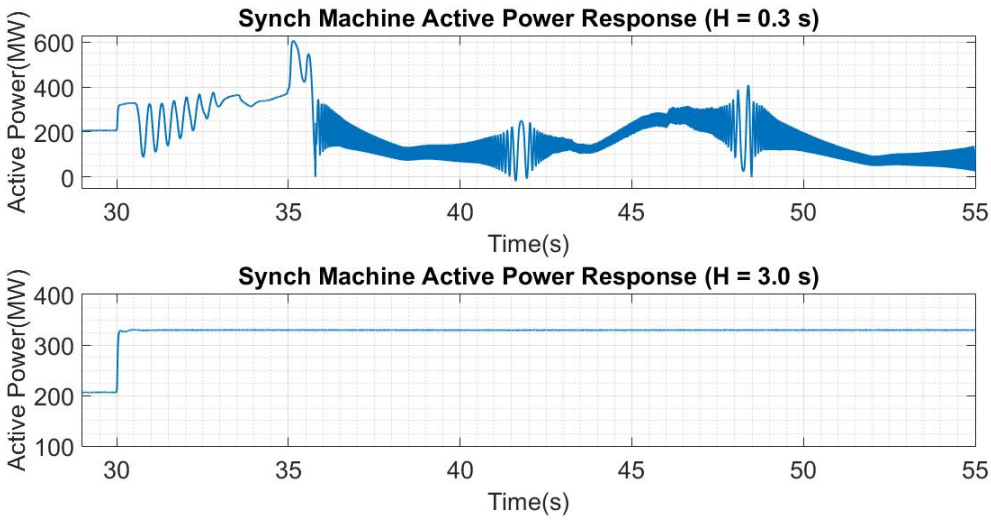

Figure 5.2: Active power response measured at the synchronous machine POC when the synchronous machine responds to the power imbalance.

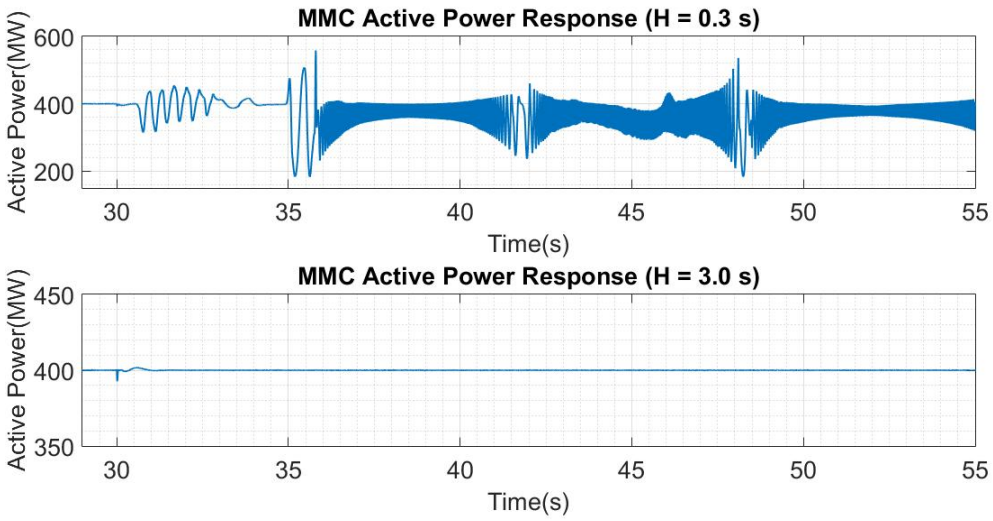

Figure 5.3: Active power response measured at the MMC POC when the synchronous machine responds to the power imbalance.

It is worthwhile noting that when using very low inertia constants, large fluctuations are observed in the active power of both the synchronous machine and the MMC. This happens because without sufficient inertial energy from the synchronous machine, the frequency nadir reaches a level where a stable operating point cannot be achieved. This behaviour is not realistic in practice, as the synchronous machine's over frequency protections would trip the generator from the system. However, it is included to demonstrate the hybrid controller's ability to positively contribute to the overall stability of the system. Figure 5.4 displays the frequency behaviour measured at the synchronous machine and Figure 5.5 presents the frequency measured at the MMC POC. Lastly, it can be seen that as the inertia constant increases, the frequency nadir, caused by the frequency event, decreases. The inertia constant increase, meaning the size of the synchronous machine is physically larger, also increases the amount of time it takes to rectify the initial frequency nadir and reduces any overshoot. This is expected because as the machine increases in size it takes longer for its frequency to change.

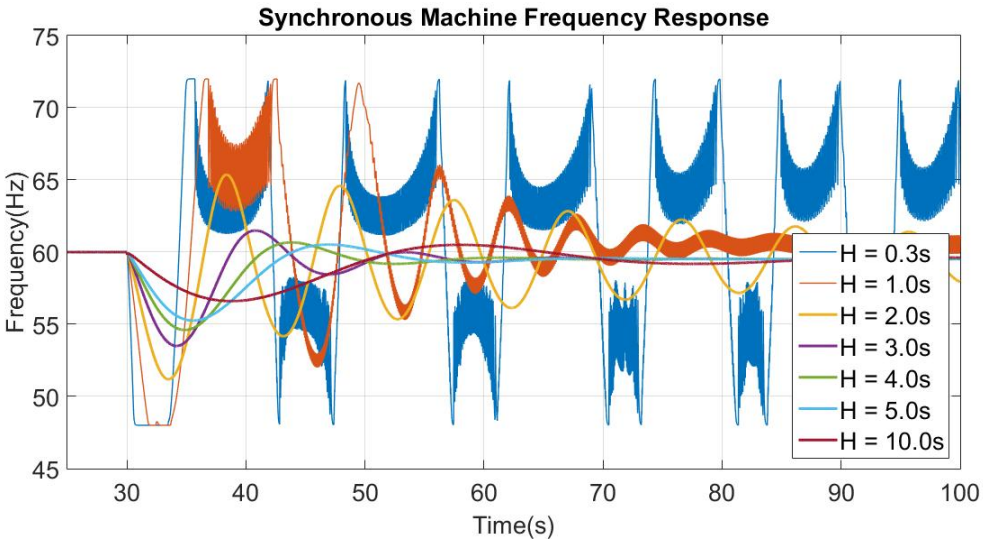

Figure 5.4: Frequency response measured at the synchronous machine POC when the synchronous machine responds to the power imbalance.

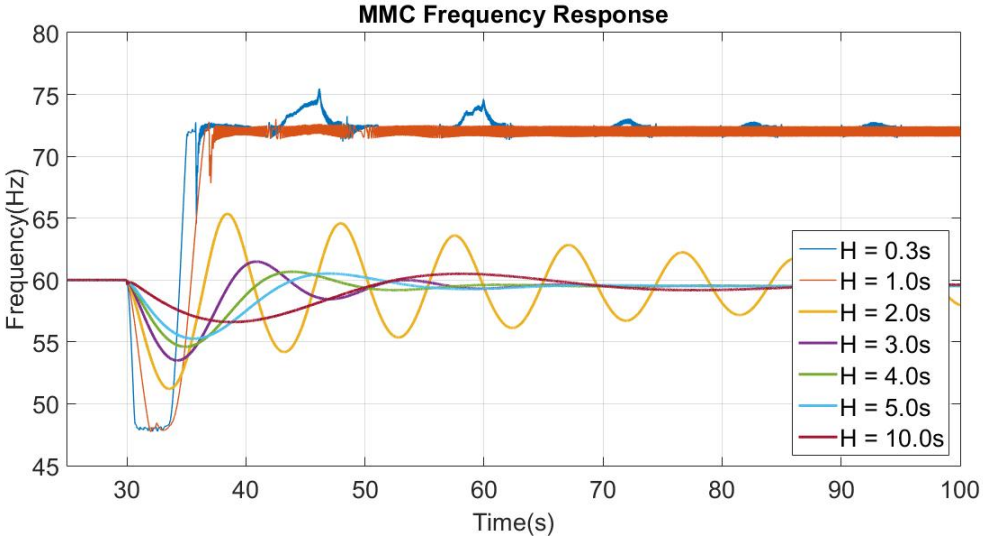

Figure 5.5: Frequency response measured at the MMC POC when the synchronous machine responds to the power imbalance.

Due to the MMC being in a CCSC operation it is expected that very little circulating current will be present in the MMC. When H = 0.3 s, there appears to be some circulating current injected in the system. As mentioned earlier, the CCSC

produces a voltage that when added to the voltage reference waveform, suppresses the circulating current. However, if the voltage required is unable to be produced (in times of an unstable system) the CCSC will not be able to completely suppress the circulating current. This is shown to be the case in Figure 5.6.

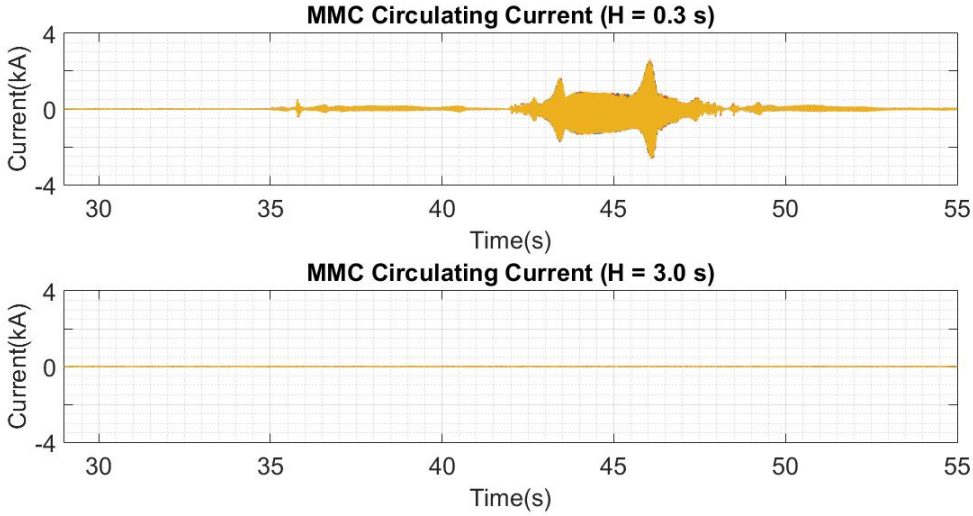

Figure 5.6: Circulating Current of the MMC when the only synchronous machine responds to the power imbalance.

In the control case of the synchronous generator solely responding to the frequency event, the network becomes unstable at very low inertia constants and the frequency nadir decreases as the inertia constant of the synchronous machine increases. Key measurements are summarized in Table 5.1.

Table 5.1: Frequency Response of the synchronous machine when the synchronous machine responds to the power imbalance

H **Constant (s)**	**Freq. Nadir (Hz)**	**Freq. Overshoot (Hz)**	**stable/unstable**
0.3	48	72	Unstable
1.0	48	72	Unstable
2.0	51.2	65.4	Stable
3.0	53.5	61.5	Stable
4.0	54.6	60.7	Stable
5.0	55.3	60.5	Stable
10.0	56.6	60.5	Stable

5.2.2 Only MMC Responding to the Frequency Event

This test was conducted to show the excessive arm currents when a frequency event is applied to a system and the MMC provides additional active power while remaining in CCSC operation. To perform this simulation the MMC's active power/frequency control loop is enabled, which entails that it will be participating in providing active power to deal with the power imbalance. The traditional CCSC in the MMC remains in place, meaning the MMC will force the circulating current to be zero (ideally). Three tests were conducted. The tests differed in where the frequency measurement was taken from as explained in the Overview of the Test System. These three tests produced generally the same response and therefore only the third test, using the speed of the synchronous machine as the frequency measurement will be presented.

Synchronous Machine Frequency Measurement

The frequency measurement in this case is provided by the speed of the synchronous machine. To ensure that the measurement is delivered to the MMC. A high level

location of where the measurement originates is shown in Figure 5.7.

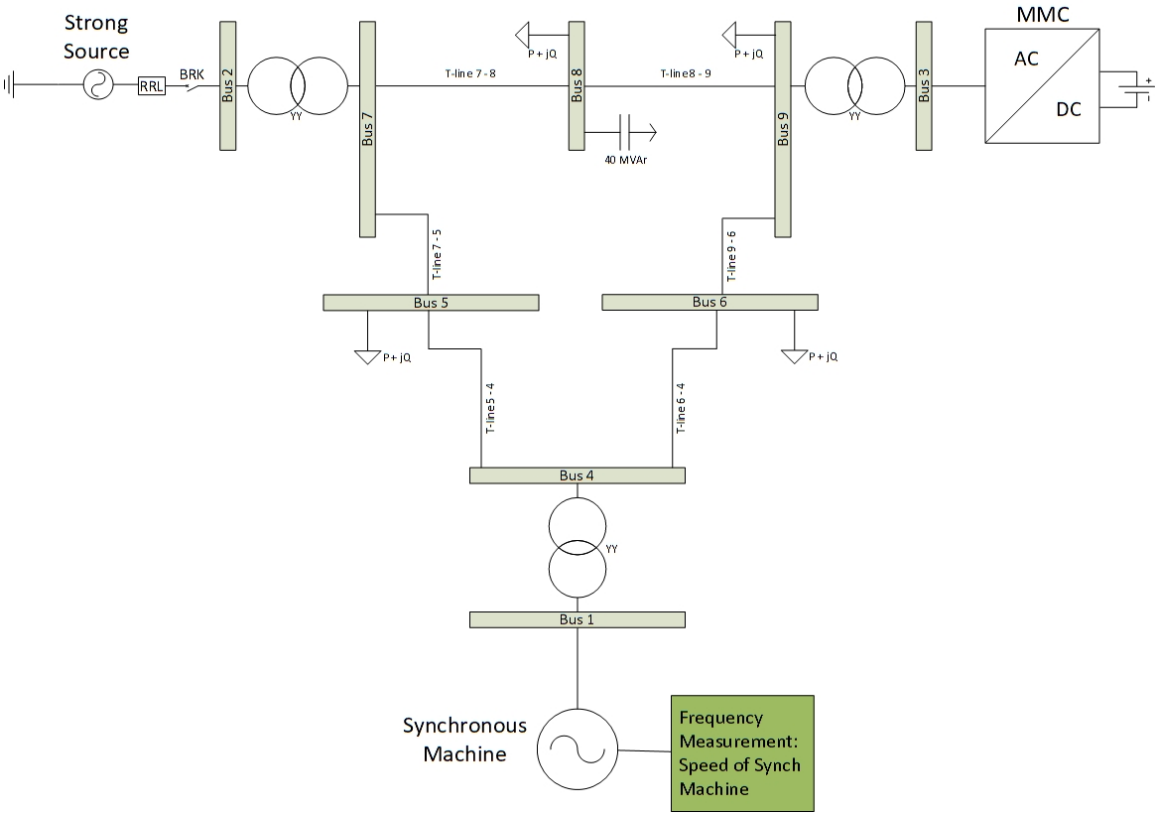

Figure 5.7: Frequency measurement using the speed of the synchronous machine.

When the disturbance (strong voltage source disconnected) is applied to the network at $t = 30$ s, the synchronous machine begins to increases its active power output momentarily before staying near its dispatched level. At $t = 35$ s the active power reference point is increased to resolve the power imbalance. This is seen in Figure 5.8. The MMC begins to increases its active power output (which is dictated by the active power/frequency control loop) and attends to the power imbalance, as provided in Figure 5.9. After the synchronous machine's active power reference is increased to rectify the power imbalance, the MMC reduces its active power output to pre-contingent levels. As stated earlier, it is assumed that the MMC has a reliable source of excess active power available.

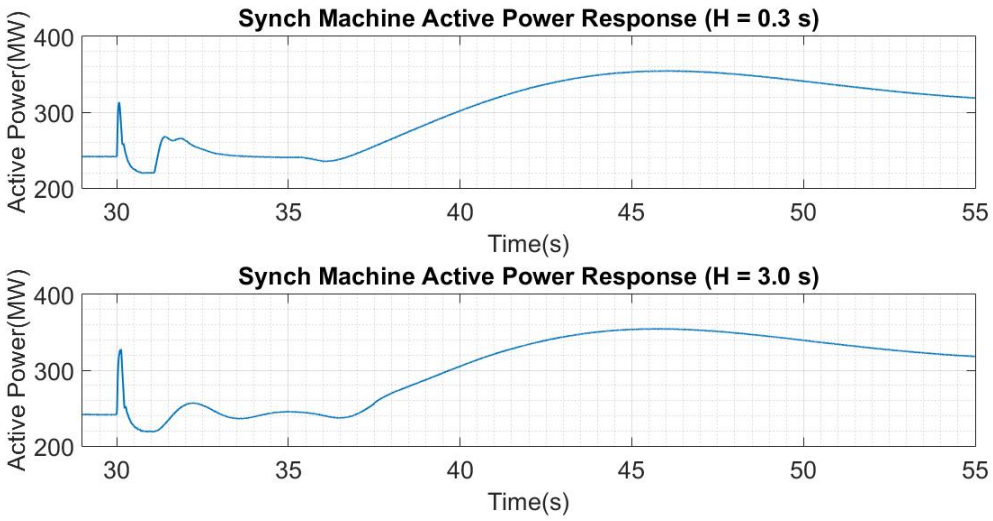

Figure 5.8: Synchronous machine active power response - MMC in traditional CCSC (freq. measurement: speed of the synchronous machine).

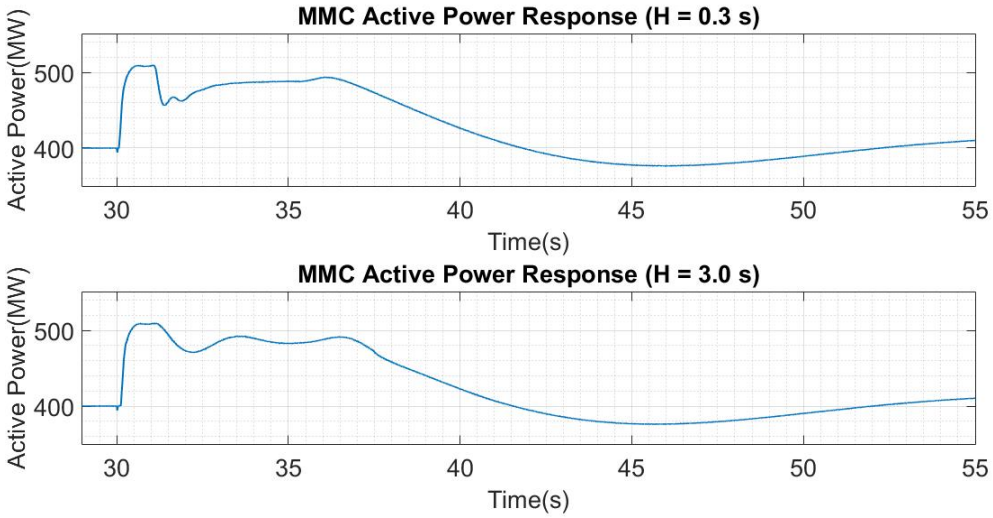

Figure 5.9: MMC active power response - MMC in traditional CCSC (freq. measurement: speed of the synchronous machine).

The quick additional active power that the MMC injects greatly improves the frequency response when compared to having only the synchronous machine respond as seen in Figures 5.10 and 5.11. Again, it can be seen that as the inertia constant

increases, the frequency nadir, caused by the frequency event, decreases. However, more importantly, it is observed that the network remains stable even in the case of a very low inertia constant ($H = 0.3$ s).

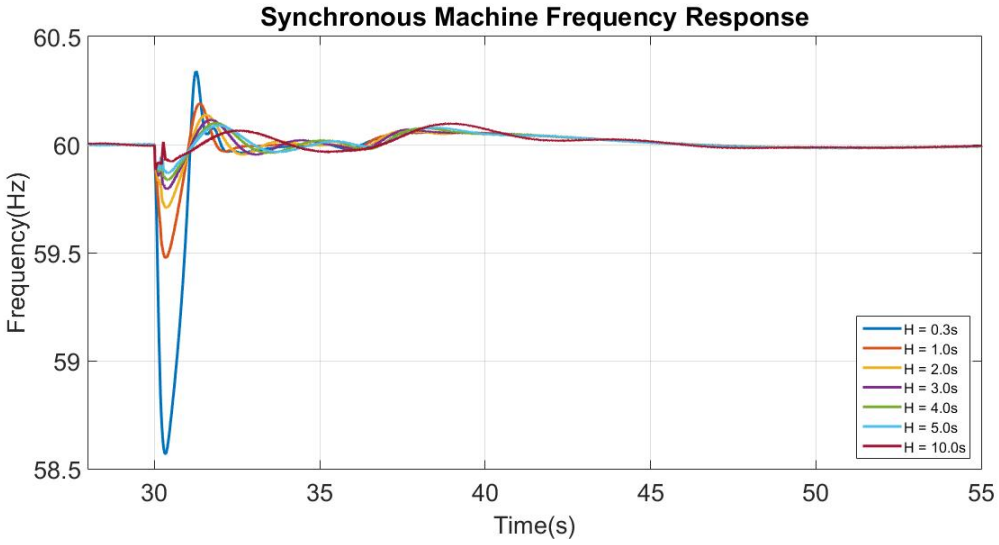

Figure 5.10: Synchronous machine frequency response - MMC in traditional CCSC (freq. measurement: speed of the synchronous machine).

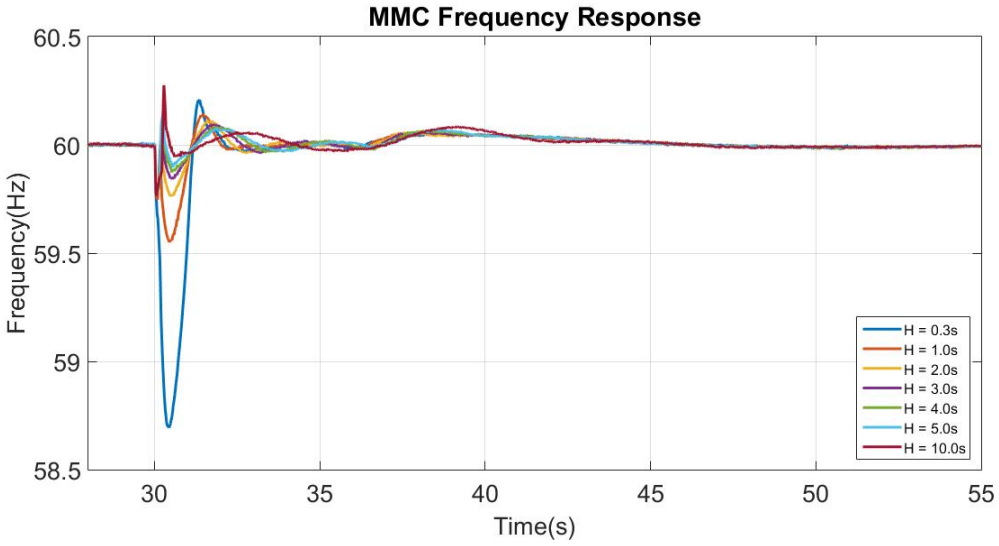

Figure 5.11: MMC frequency response - MMC in traditional CCSC (freq. measurement: speed of the synchronous machine)..

The MMC remains in the traditional CCSC operation and as expected very little circulating current is present in the MMC as seen in Figure 5.12.

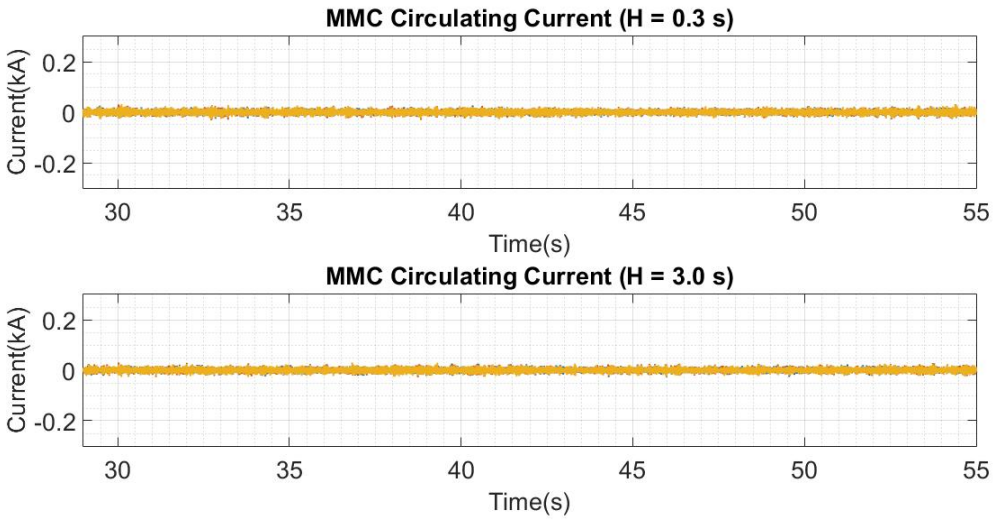

Figure 5.12: Circulating Current of the MMC - MMC in traditional CCSC (freq. measurement: speed of the synchronous machine).

The active power increase provided by the MMC is accompanied by an increase of the upper and lower arm current of the MMC. This rise in magnitude from pre-contingent current levels to post-contingent current levels is displayed in Figure 5.13. It is observed that regardless of the time taken for the current measurement, a waveform dominated by the first harmonic is produced. This is expected because the circulating current (which is of 2^{nd} harmonic) is forced to zero. Also, the additional active power transfer is accompanied by an increase in arm current. Without any manipulation of this arm current, it is shown that the peaks of the arm currents reach levels higher than the pre-contingent levels.

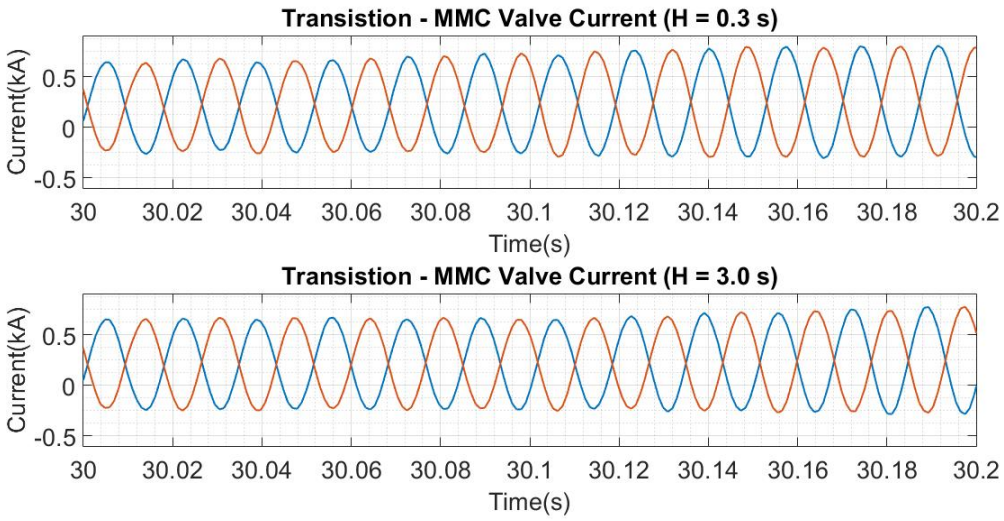

Figure 5.13: Phase A arm Currents - MMC in traditional CCSC (freq. measurement: speed of the synchronous machine).

In the control case of the MMC responding to the frequency event (measured internally using the PLL of the MMC), the network remains stable at all inertia constants, the frequency nadir decreases as the inertia constant of the synchronous machine increases and as the active power provided by the MMC increases, so does the arm currents of the MMC. It was noted that due to the fact that the circulating current is suppressed nearly to zero, the arm currents are dominated by the first harmonic and reach levels greater than pre-contingent levels. The key measurements are summarized in Table 5.2.

Table 5.2: Frequency Response - MMC in traditional CCSC (freq. measurement: speed of the synchronous machine).

H **Constant (s)**	**Freq. Nadir (Hz)**	**Freq. Overshoot (Hz)**	**Peak Arm I (kA)**
0.3	58.57	60.34	0.84
1.0	59.48	60.19	0.85
2.0	59.71	60.14	0.85
3.0	59.80	60.11	0.84
4.0	59.84	60.10	0.85
5.0	59.87	60.08	0.85
10.0	59.89	60.07	0.85

Regardless where the frequency measurement is taken the following observations are made:

- The MMC active power injection reduces the frequency nadir (as compared to the synchronous machine control).
- As the inertia constant increases, the frequency nadir increases.
- As the MMC provides more power, the arm current peak is much higher than the pre-contingent arm current.

The next three section present the same disturbance, with the frequency measured using the locations referred to in the overview of the test system, using the proposed hybrid controller.

5.3 Test 1: PLL Frequency Measurement

This test uses of the internal PLL measurement of frequency for the power/frequency controller (Figure 5.14).

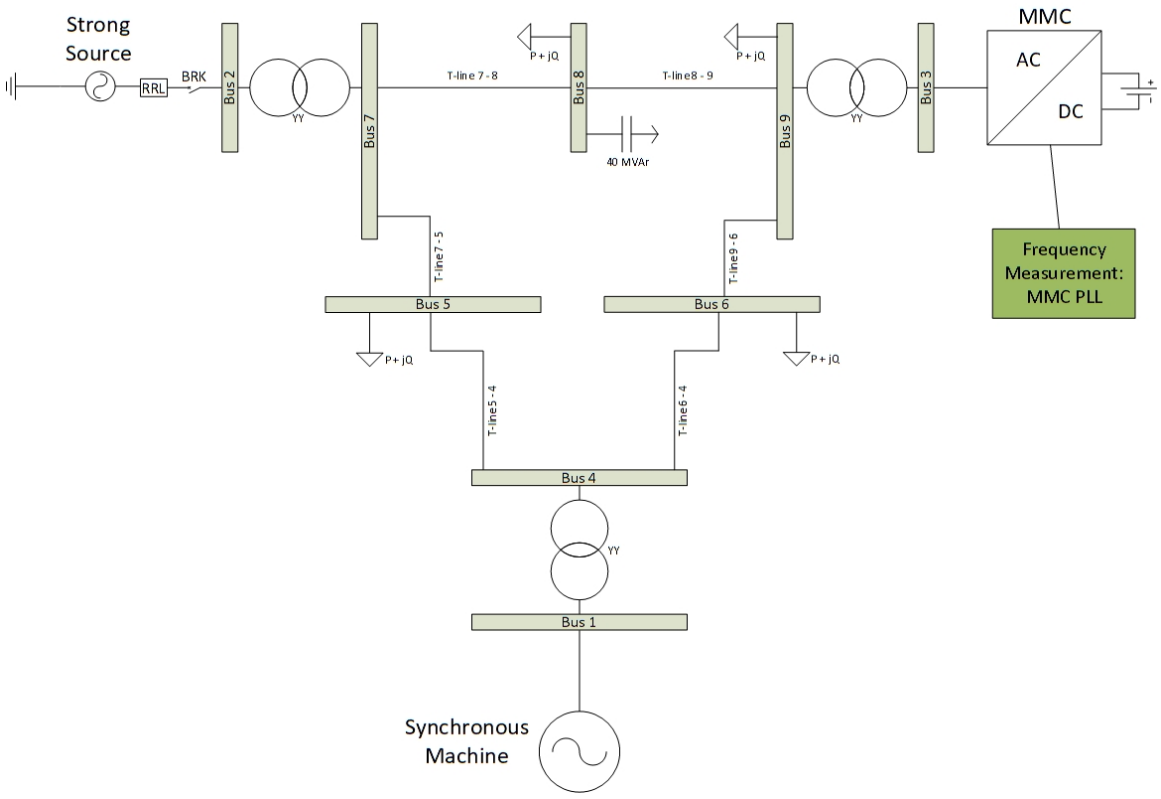

Figure 5.14: Frequency measurement using the MMC's PLL.

The active power response of both the synchronous machine and the MMC is generally the same as in the case when the MMC's power/frequency control is enabled with the MMC operating in traditional CCSC mode. The active power responses are presented in Figures 5.15 and 5.16.

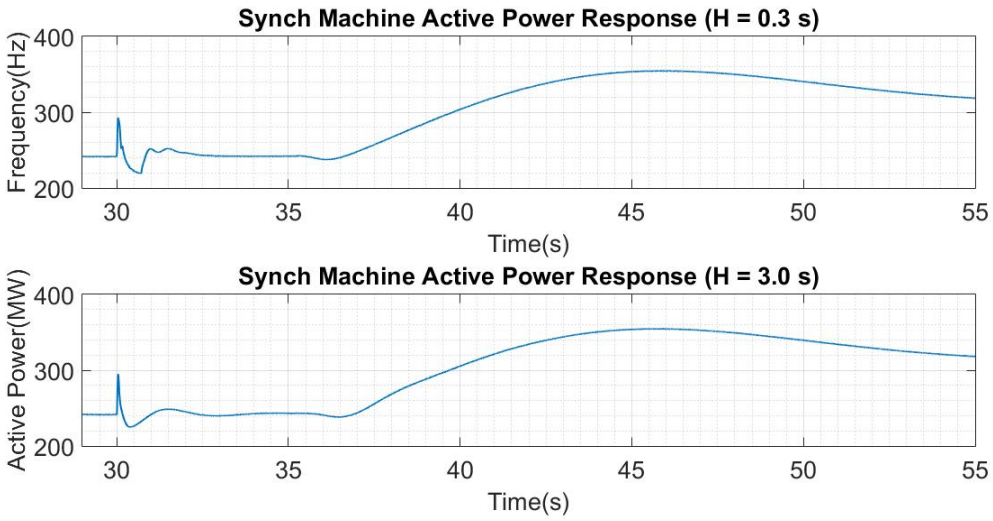

Figure 5.15: Synchronous machine active power response - Hybrid controller (freq. measurement: MMC PLL.)

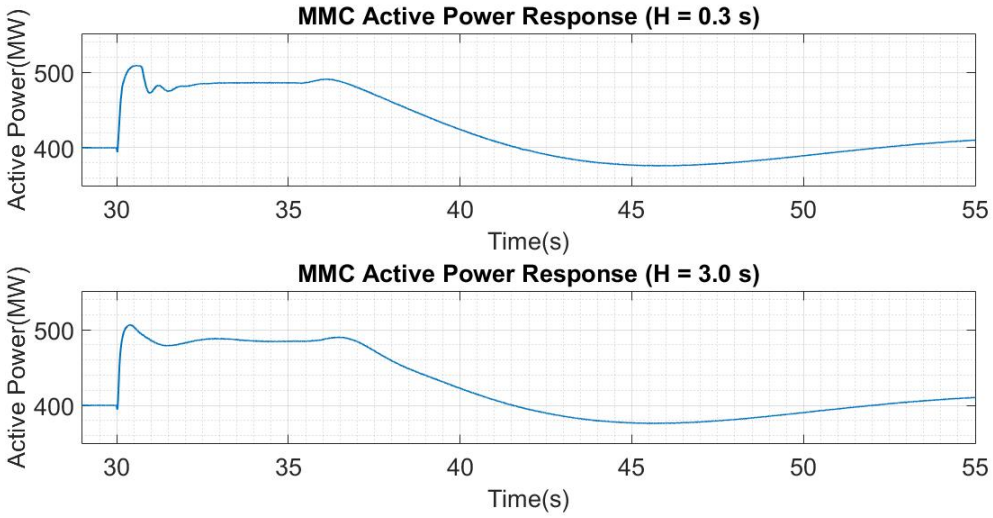

Figure 5.16: MMC active power response - Hybrid controller (freq. measurement: MMC PLL.)

The frequency also shares the same improvements as the PLL Frequency Measurement Case (when the power/frequency controls are enabled and the CCSC is disabled) and is provided below in Figures 5.17 and 5.18.

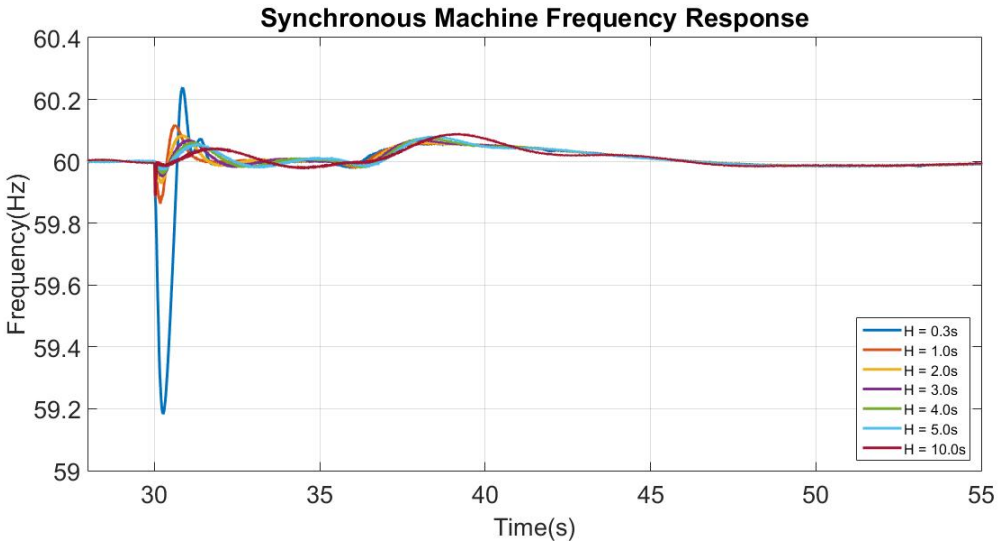

Figure 5.17: Synchronous machine frequency response - Hybrid controller (freq. measurement: MMC PLL.)

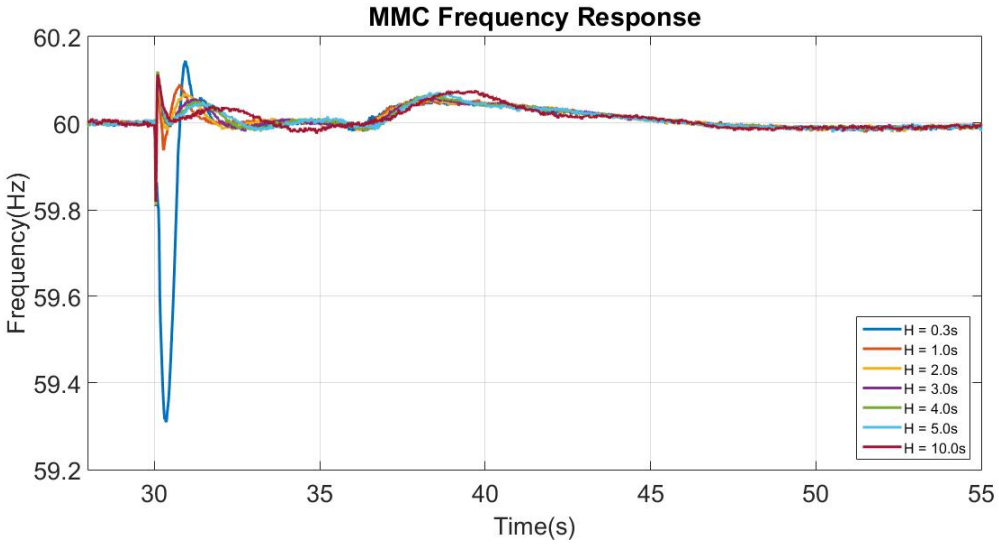

Figure 5.18: MMC frequency response - Hybrid controller (freq. measurement: MMC PLL.)

Now, with the 2nd harmonic controls also enabled there is an expectation to observe judicious amounts of circulating current in the MMC. This is indeed the case and is presented in Figure 5.19.

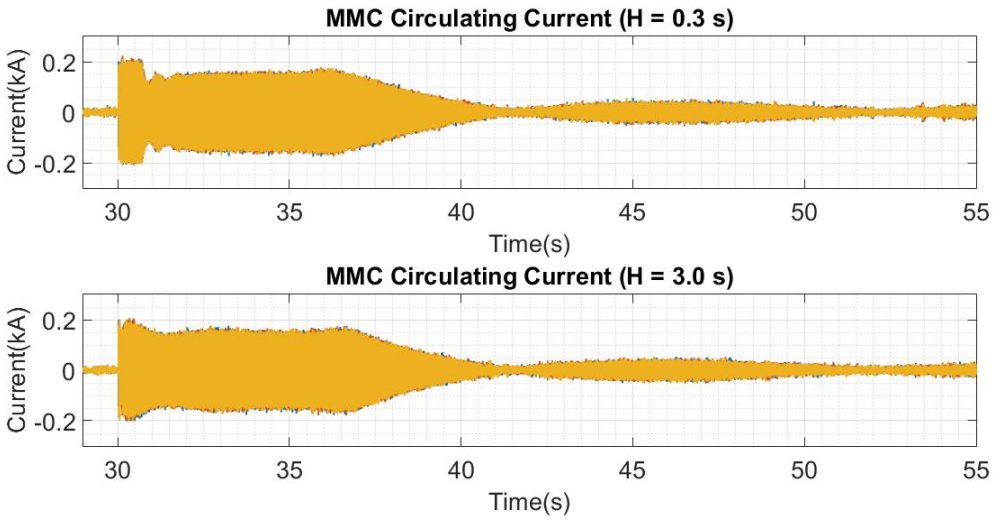

Figure 5.19: Circulating Current of the MMC - Hybrid controller (freq. measurement: MMC PLL.)

This circulating current is used to alter the peaks of the arm current in the MMC. The active power increase provided by the MMC is accompanied by an increase of the upper and lower arm current of the MMC, much like in the previous case where the MMC was responding to the power imbalance with the MMC operating with traditional CCSC. However, in this case the power rise is accompanied by an injection of 2^{nd} harmonic current into the arm currents. This begins to flatten the peaks of the arm current. This transition from pre-contingent CCSC operation and the controller commencing operation (flattening peaks) is displayed in Figure 5.20.

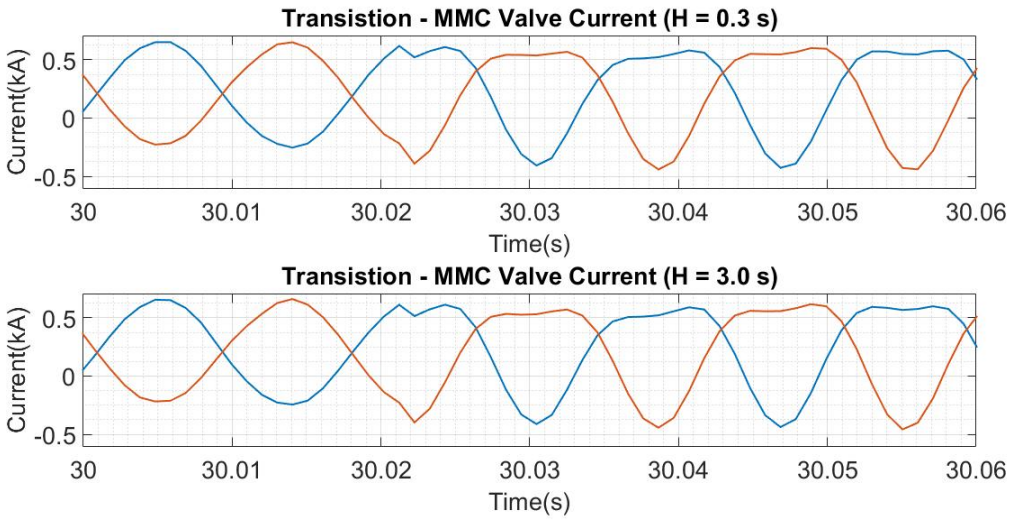

Figure 5.20: Phase A arm Currents (Transition) - Hybrid controller (freq. measurement: MMC PLL.)

After the commencement of the controller, it enters its maximum operation mode. In this mode the maximum amount of power is transferred via the MMC to the network. However, 2^{nd} harmonic current is injected into the arm creating a flattened peak. This flattened peak is due to the 2^{nd} harmonic now present in the arm current. At this time the maximum amount of active power is injected to the network while the SOAs of the IGBTs in the MMC are respected. This portion of the operation is presented in Figure 5.21.

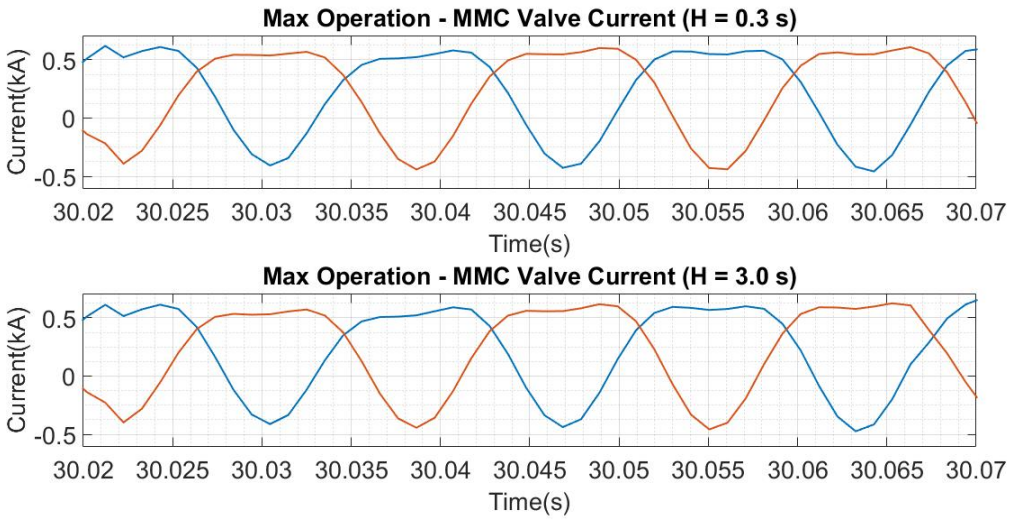

Figure 5.21: Phase A arm Currents of the MMC (Max Power Transfer) - Hybrid controller (freq. measurement: MMC PLL.)

As the frequency recovers and the synchronous machine begins injecting more active power (due to the switch in dispatch levels), less active power is required from the MMC. With the MMC injecting less active power, it is no longer mandatory to flatten the peaks of the arm current. This means that less circulating current is required to ensure the current operation remains within the SOA of the IGBTs in the MMC. This section remains within the SOA and is characterized in Figure 5.22 with rounded peaks.

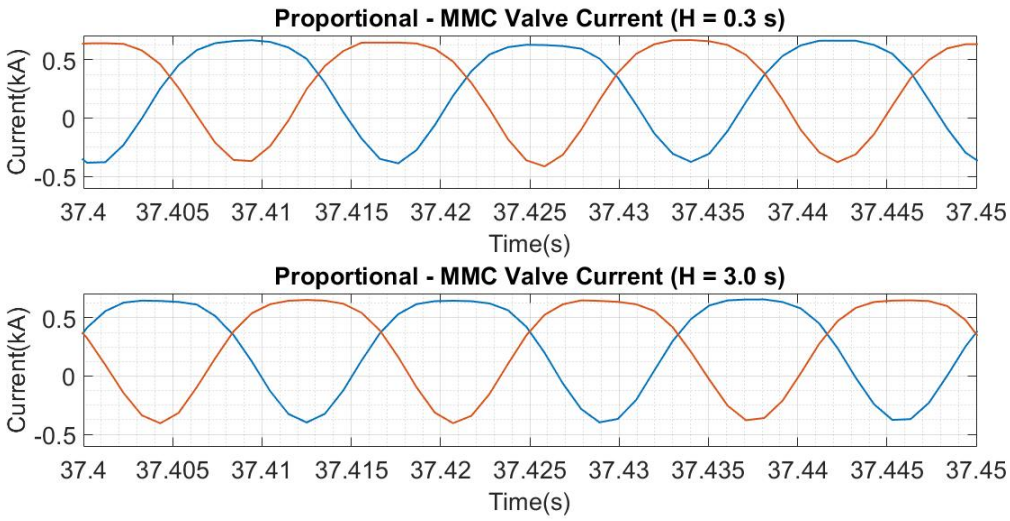

Figure 5.22: Phase A arm Currents of the MMC (Proportional Response) - Hybrid controller (freq. measurement: MMC PLL.)

Finally, as the synchronous machine injects sufficient active power to address the power imbalance, the MMC reduces it's active power injection to pre-contingent levels. This allows the circulating current to further reduce to traditional CCSC levels, as seen in Figure 5.23.

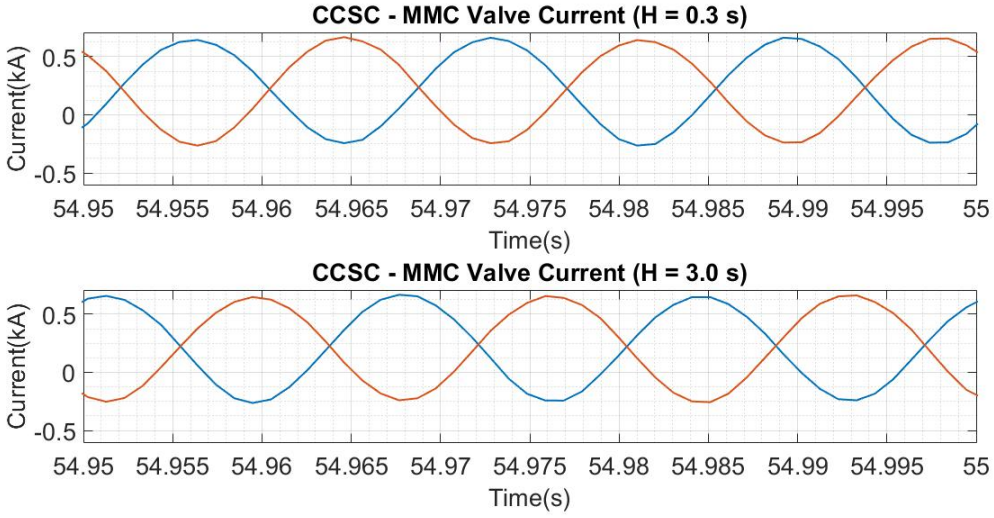

Figure 5.23: Phase A arm Currents of the MMC (Steady State) - Hybrid controller CCSC (freq. measurement: MMC PLL.)

In this first test case of the MMC responding to the frequency event (measured internally using the PLL of the MMC), the network remains stable at all inertia constants, the frequency nadir decreases as the inertia constant of the synchronous machine increases and as the active power provided by the MMC increases, the circulating current increases, which aids in limiting the peaks of the MMC arm currents to acceptable values. The key measurements are summarized in Table 5.3.

Table 5.3: Frequency Response - Hybrid controller (freq. measurement: MMC PLL.)

H **Constant (s)**	**Freq. Nadir (Hz)**	**Freq. Overshoot (Hz)**	**Peak Arm I (kA)**
0.3	59.18	60.24	0.68
1.0	59.87	60.12	0.69
2.0	59.89	60.08	0.69
3.0	59.89	60.07	0.69
4.0	59.89	60.06	0.69
5.0	59.89	60.05	0.68
10.0	59.89	60.04	0.69

The next two sections will provide data for the other two frequency measurements; A bus frequency measurement and the speed of the synchronous machine.

5.4 Test 2: Bus Frequency Measurement

This test uses the frequency measured by a PMU installed at the bus of interest. Its high level location is shown in Figure 5.24.

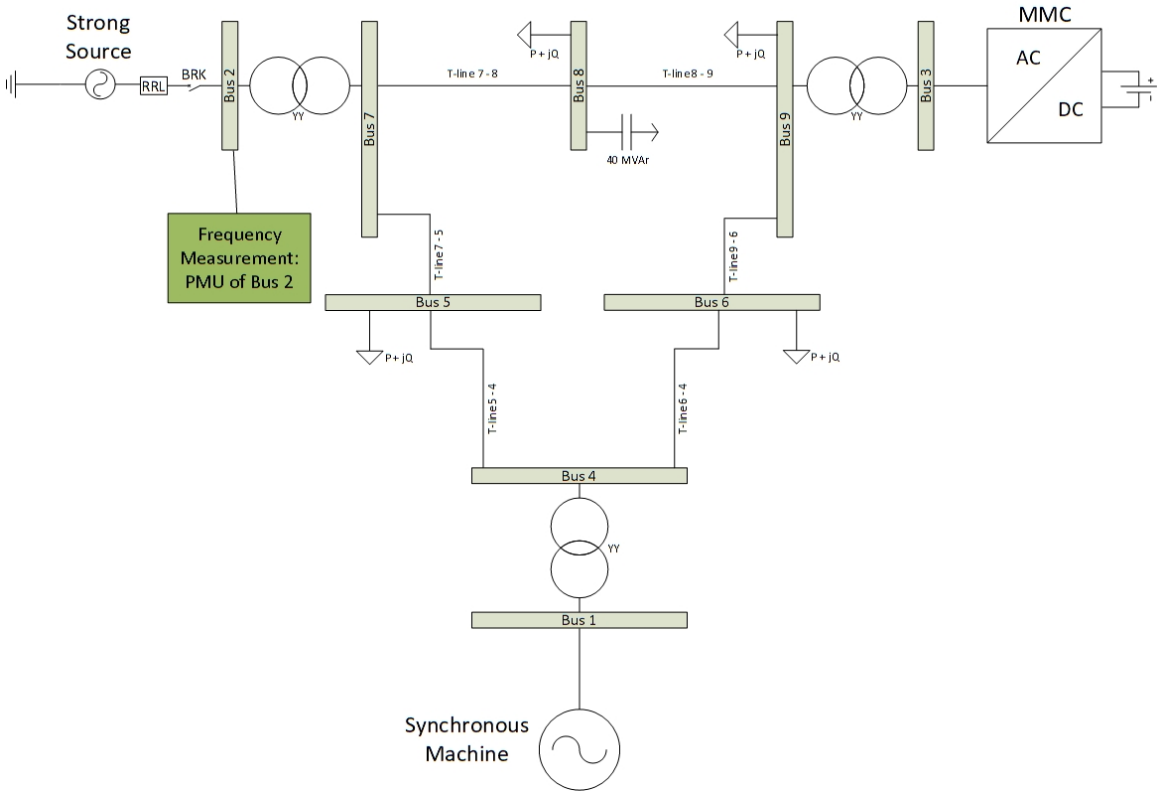

Figure 5.24: Frequency Measurement using a Bus in the network.

The active power behaviour is generally the same as Test 1. The active power response from the synchronous machine and the MMC is provided below in Figures 5.25 and 5.26.

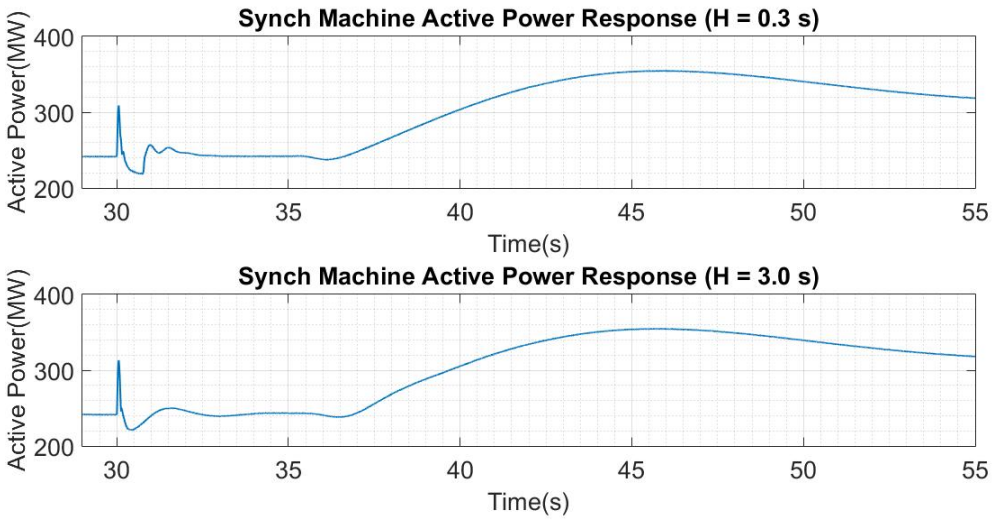

Figure 5.25: Synchronous machine active power response - Hybrid controller (freq. measurement: Network Bus.)

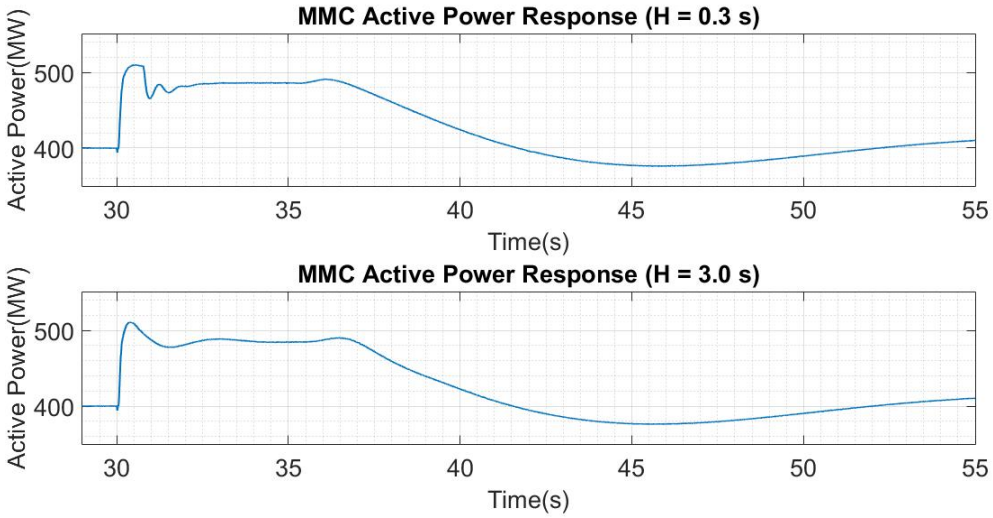

Figure 5.26: MMC active power response - Hybrid controller (freq. measurement: Network Bus.)

The frequency shares generally the same improvements as observed in Test 1 and are provided below in Figures 5.27 and 5.28.

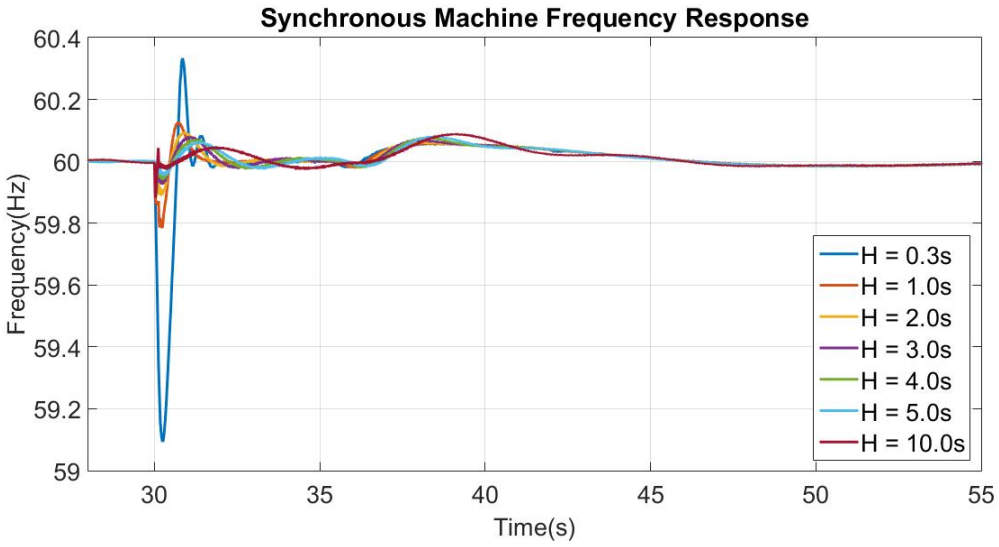

Figure 5.27: Synchronous machine frequency response - Hybrid controller (freq. measurement: Network Bus.).

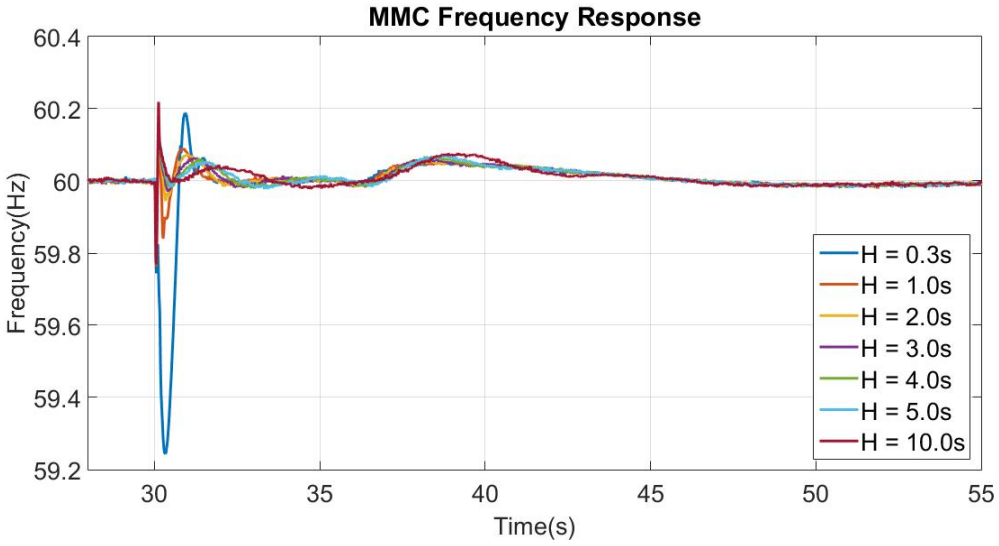

Figure 5.28: MMC frequency response - Hybrid controller (freq. measurement: Network Bus.)

As in Test 1, the MMC (now in an altered CCSC control) injects judicious amounts of circulating current into the arms, as seen in Figure 5.29.

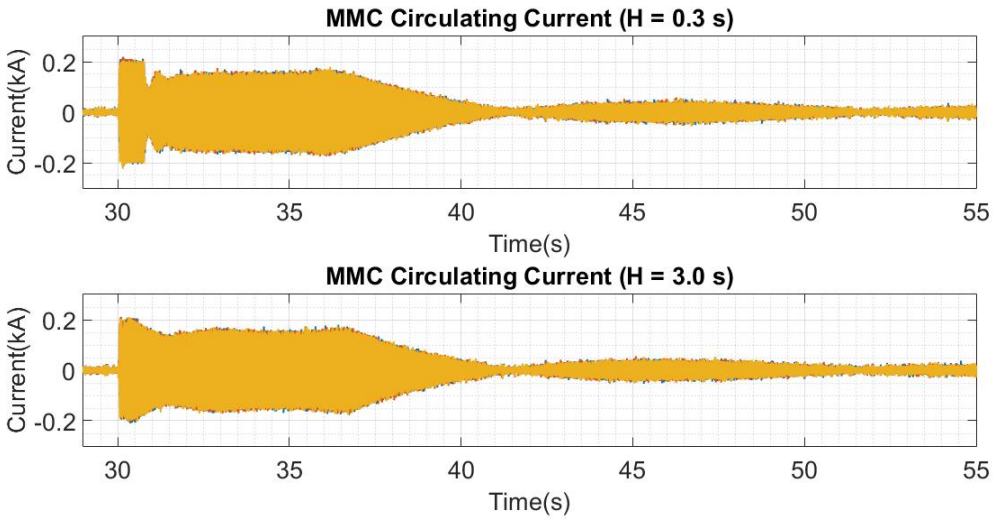

Figure 5.29: Circulating Current of the MMC - Hybrid controller (freq. measurement: Network Bus.)

This test also shares a similar arm current behaviour to Test 1. After the commencement period, the controller injects maximum power, which in turn injects maximum circulating current, flattening the peaks of the arm current to acceptable levels (Figure 5.30).

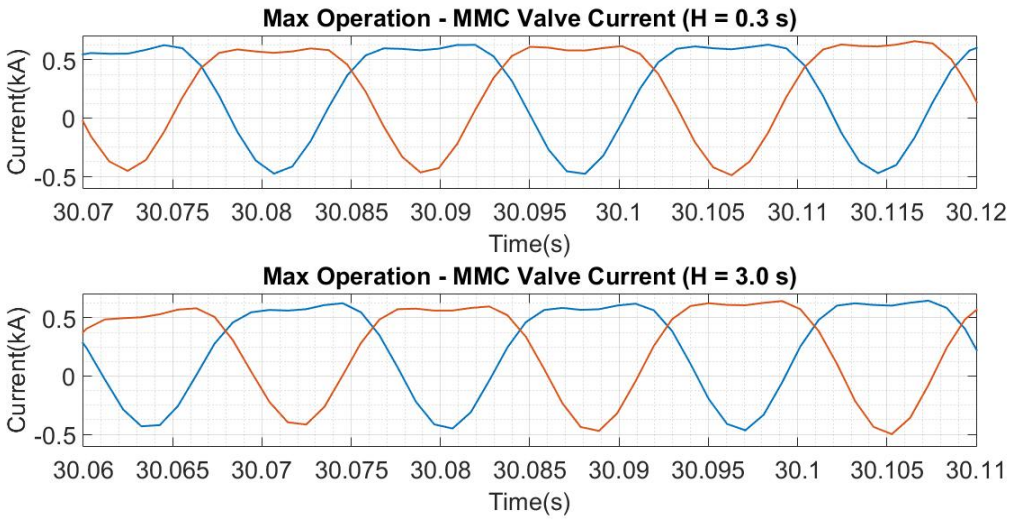

Figure 5.30: Phase A arm Currents of the MMC (Max Power Transfer) - Hybrid controller (freq. measurement: Network Bus.)

As the frequency returns to its nominal value and the synchronous machine has its active power dispatch level increased, the controller enters a proportional period, reducing the circulating current injection and is characterized by rounded peaks (Figure 5.31).

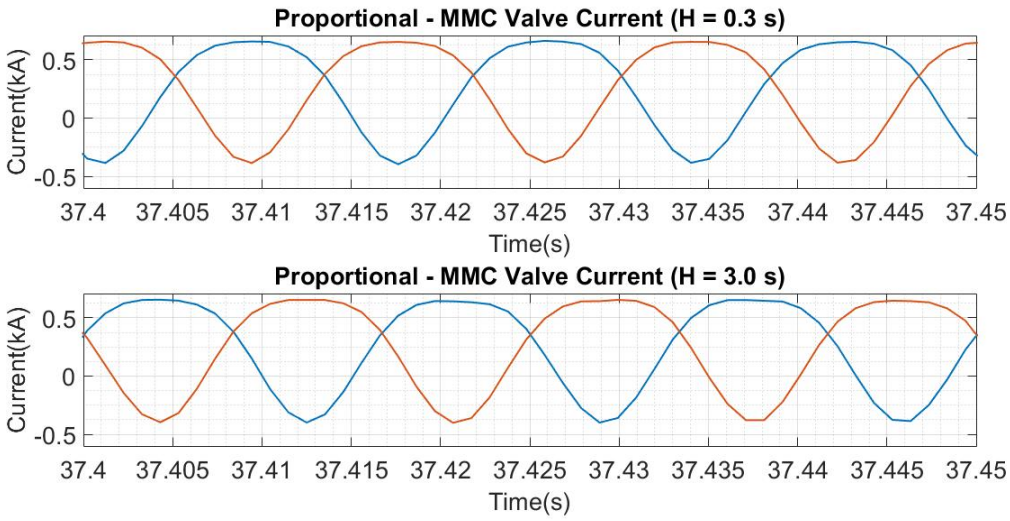

Figure 5.31: Phase A arm Currents of the MMC (Proportional Response) - Hybrid controller (freq. measurement: Network Bus.)

Finally, as in Test 1, once the synchronous machine is able to provide sufficient power to address the power imbalance, the controller begins to return to a traditional CCSC control.

In the control case of the MMC responding to the frequency event (measured externally using a PMU at a bus), the network remains stable at all inertia constants, the frequency nadir decreases as the inertia constant of the synchronous machine increases. As the active power provided by the MMC increases, so does the circulating current of the MMC, which help to limit the peaks of the arm currents. The key measurements are summarized in Table 5.4.

5.5 Test 3: Synchronous Machine Frequency Measurement

This test uses the speed of the synchronous machine for its frequency measurement. Its high level location is shown in Figure 5.7.

Table 5.4: Frequency Response - Hybrid controller (freq. measurement: Network Bus.)

H **Constant (s)**	**Freq. Nadir (Hz)**	**Freq. Overshoot (Hz)**	**Peak Arm I (kA)**
0.3	58.50	60.16	0.70
1.0	59.79	60.13	0.77
2.0	59.89	60.09	0.74
3.0	59.89	60.08	0.77
4.0	59.89	60.07	0.78
5.0	59.89	60.06	0.77
10.0	59.89	60.04	0.80

The active power behaviour is generally the same as Tests 1 and 2. The active power response from the synchronous machine and the MMC are provided below in Figures 5.32 and 5.33.

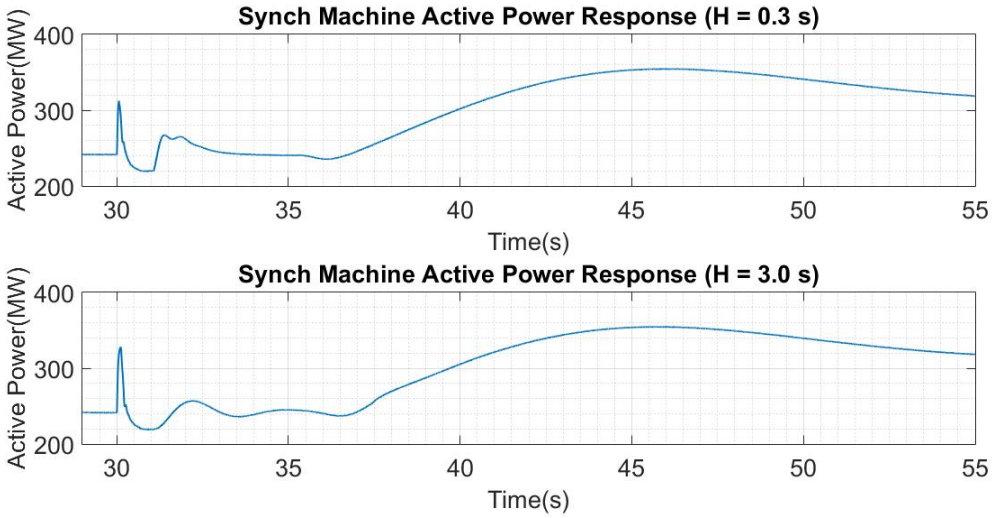

Figure 5.32: Synchronous machine active power - Hybrid controller (freq. measurement: Synch. machine)

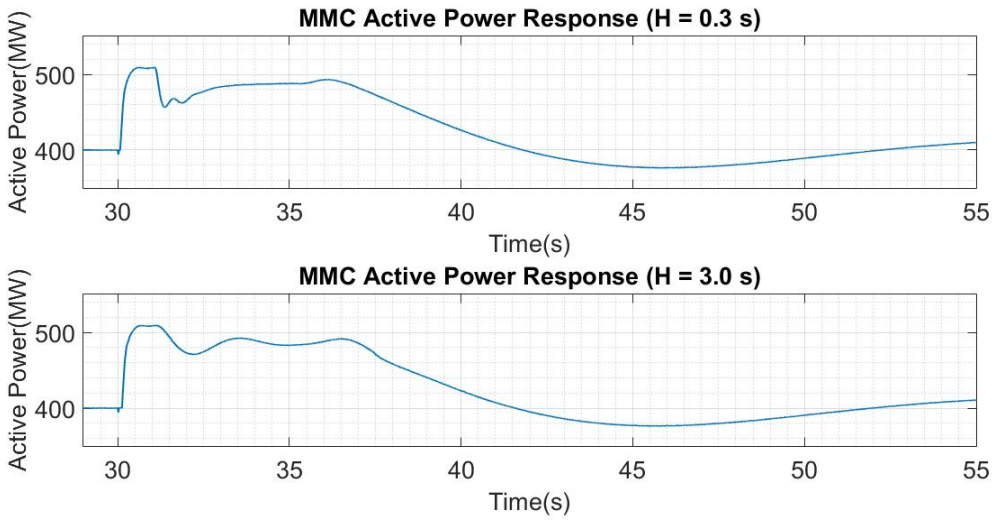

Figure 5.33: MMC active power response - Hybrid controller (freq. measurement: Synch. machine)

The frequency shares generally the same improvements observed in Tests 1 and 2 and are provided below in Figures 5.34 and 5.35.

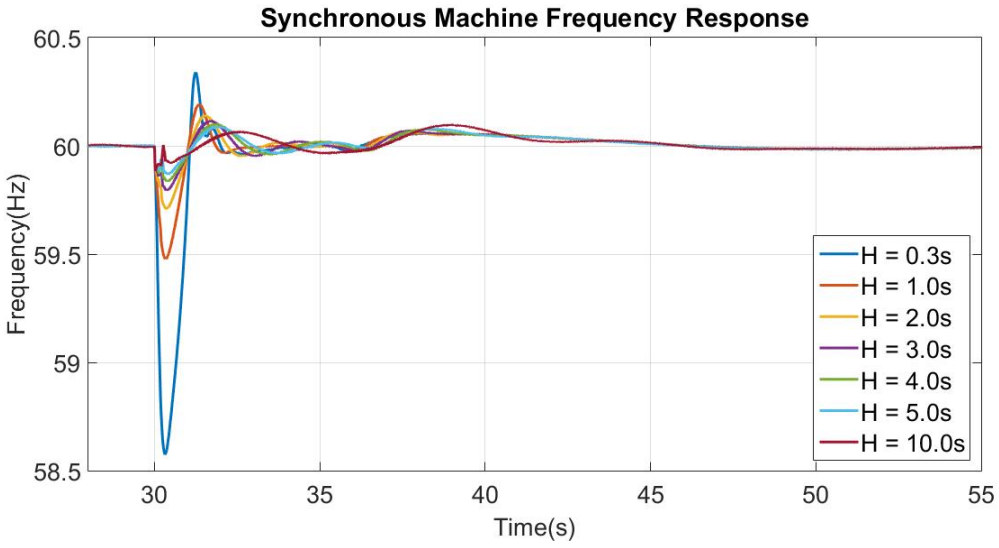

Figure 5.34: Synchronous machine frequency response - Hybrid controller (freq. measurement: Synch. machine)

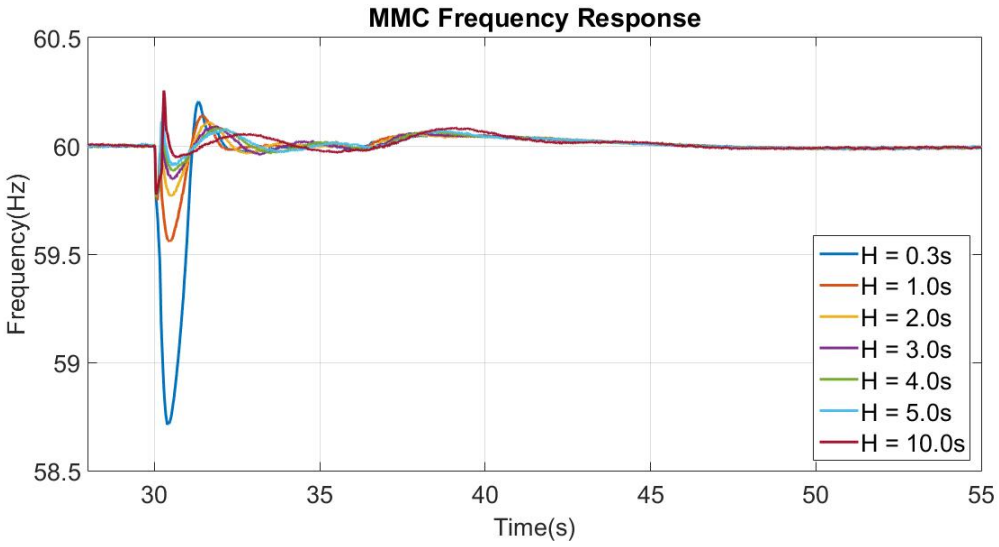

Figure 5.35: MMC frequency response - Hybrid controller (freq. measurement: Synch. machine)

As in Tests 1 and 2, the MMC (in an altered CCSC control) injects judicious amounts of circulating current into the arms, as seen in Figure 5.36.

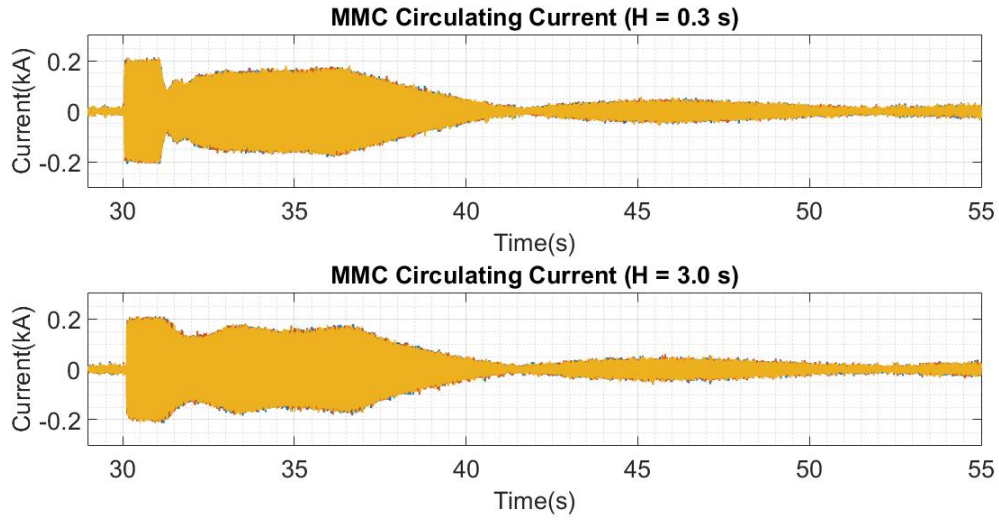

Figure 5.36: Circulating Current of the MMC - Hybrid controller (freq. measurement: Synch. machine)

The arm current operation shares a similar behaviour to Test 1 and Test 2.The

controller injects maximum power, flattening the peaks of the arm current to acceptable levels (Figure 5.37).

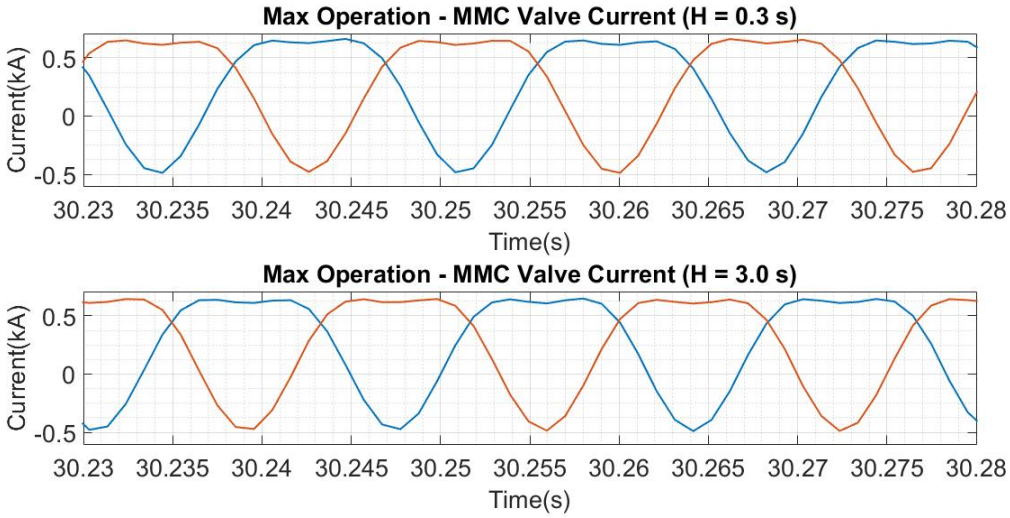

Figure 5.37: Phase A arm Currents of the MMC (Max Power Transfer) - Hybrid controller (freq. measurement: Synch. machine)

The controller enters a proportional period, as the synchronous machine's dispatch level increases (Figure 5.38). Finally, the controller returns to a traditional CCSC control.

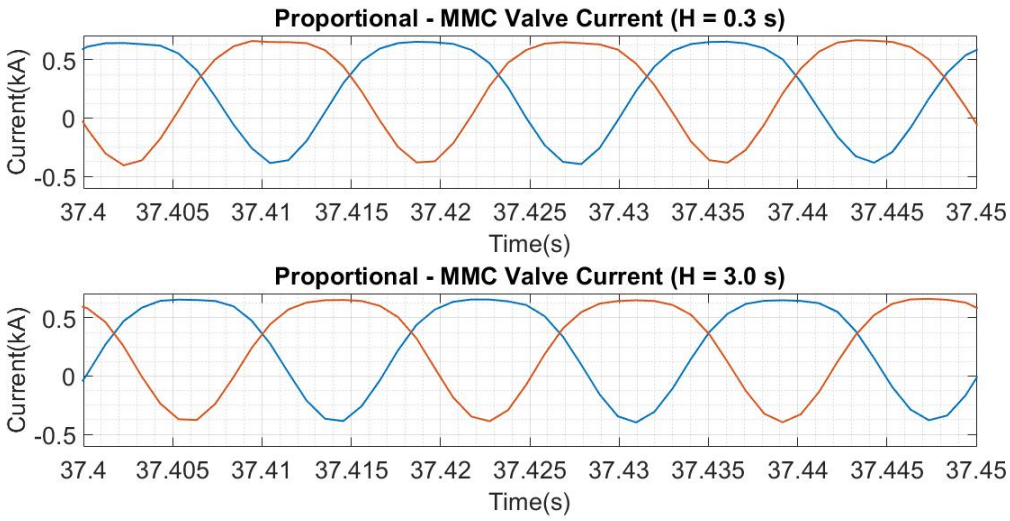

Figure 5.38: Phase A arm Currents of the MMC (Proportional Response) - Hybrid controller (freq. measurement: Synch. machine)

In the control case of the MMC responding to the speed of the synchronous machine, the network remains stable at all inertia constants, the frequency nadir decreases as the inertia constant of the synchronous machine increases. As the active power provided by the MMC increases, so does the circulating current of the MMC, which the injection aids in limiting the peaks of the arm current. The key measurements are summarized in Table 5.5.

Table 5.5: Frequency Response - Hybrid controller (freq. measurement: Synch. machine)

H **Constant (s)**	**Freq. Nadir (Hz)**	**Freq. Overshoot (Hz)**	**Peak Arm I (kA)**
0.3	58.58	60.34	0.69
1.0	59.48	60.19	0.68
2.0	59.71	60.14	0.68
3.0	59.80	60.11	0.68
4.0	59.84	60.10	0.70
5.0	59.87	60.09	0.69
10.0	59.89	60.06	0.69

The next section provides comparisons, clearly showing the existence of improvements in the network when using the proposed controller.

5.6 Comparisons

The frequency nadir, from the power imbalance, is significantly reduced when the MMC is allowed to participate in the contingency, and inject active power. When the active power is increased, while remaining in traditional CCSC operation, the arm current increases to unacceptable levels. The altered CCSC, with the injection of circulating current, manipulates the arms current in such a way that the arm current remains in an acceptable level, while increasing the power output. This section will present these two improvements. Since the results from the three frequency measurements generally produce the same results, only the case where the frequency measurement is obtained from the synchronous machine will be presented in detail.

As presented in Figure 5.39, the frequency response is observed to have a significant improvement when the MMC is also tasked to inject active power into the network. This conclusion derives from the observation that the frequency nadir decreases by a relatively large factor when compared with only the synchronous generator attending to the power imbalance, regardless of the inertia constant used. This is expected as the the MMC has the advantage of speed. As long as additional power is readily available, it can easily change its power reference, with the expected results from that change happening quite fast. As the inertia constant of the synchronous machine is increased the overall effect is the frequency becomes more difficult to change. The result of this effect is a smaller frequency change, but also a frequency that takes longer to reach a nadir.

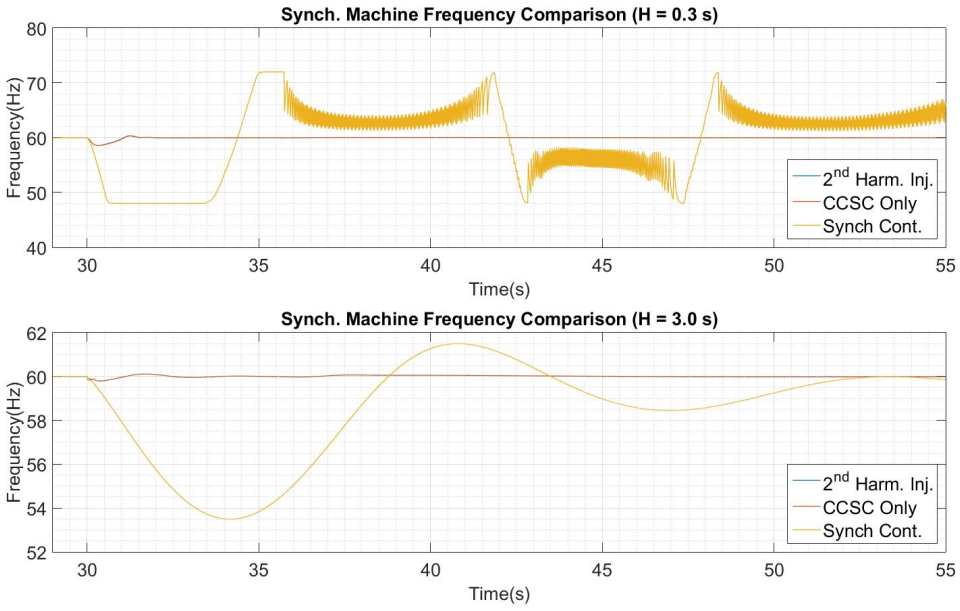

Figure 5.39: Comparison of the synchronous machine frequency response (freq. measurement: speed of the synchronous machine)

The MMC generally injects the same amount of active power into the network regardless of the CCSC (traditional or altered) method used. One difference arises when measuring the circulating current. As seen in Figure 5.40, there is a judicious amount of circulating current injected in the arm current when the active power is at a high level. This circulating current is also seen to manipulate the arm current such that the peaks begin to flatten. The end result is additional active power is available with the peak of the arm current remaining at generally the same magnitude as its pre-contingent magnitude.

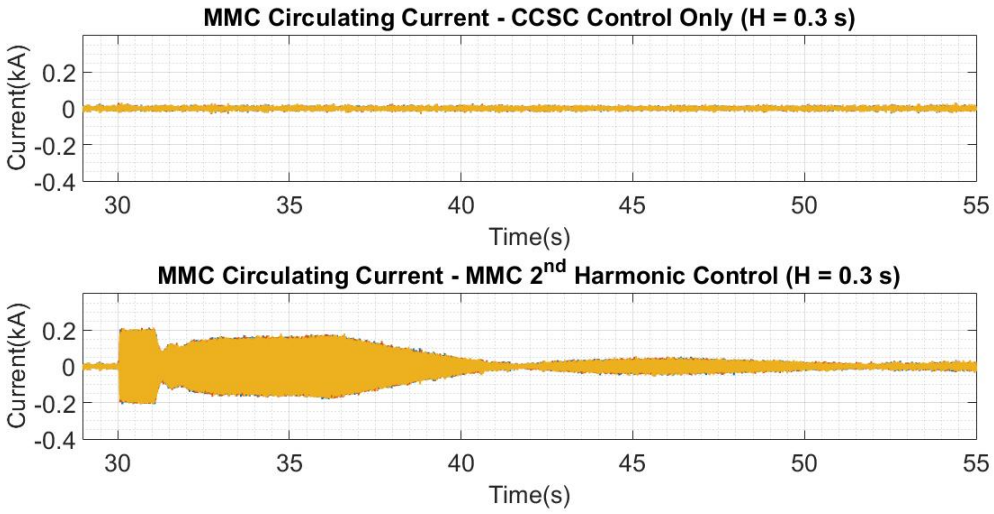

Figure 5.40: Comparison between circulating current injection (freq. measurement: speed of the synchronous machine)

The arm current is manipulated in two major ways. First, when the MMC is transferring the maximum amount of power (Figure 5.41). This behaviour is characterized by flattened peaks.

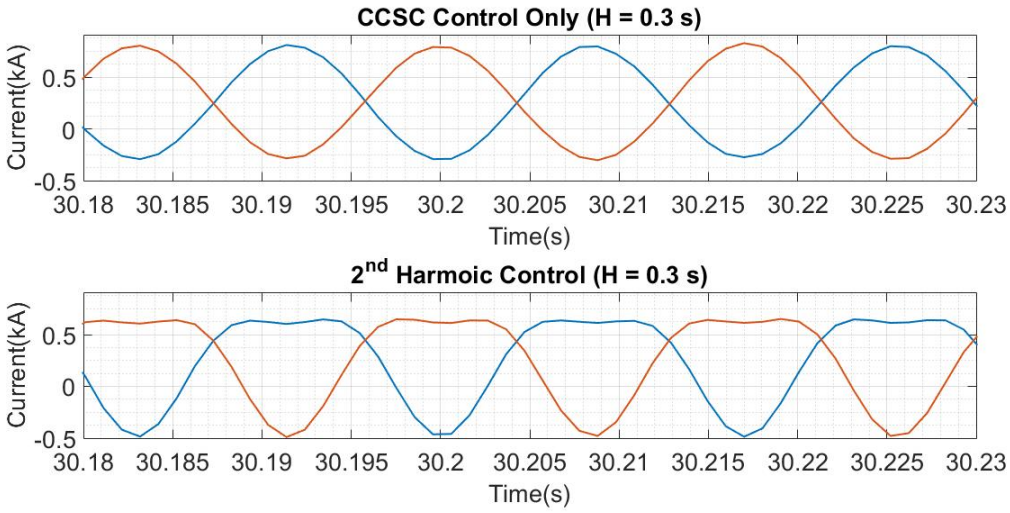

Figure 5.41: Comparison of Phase A arm currents - maximum active power transfer (freq. measurement: speed of the synchronous machine).

Second, when the synchronous machine increases its active power output and the MMC is transferring a proportional amount of active power (Figure 5.42). This behaviour is characterized by rounded peaks.

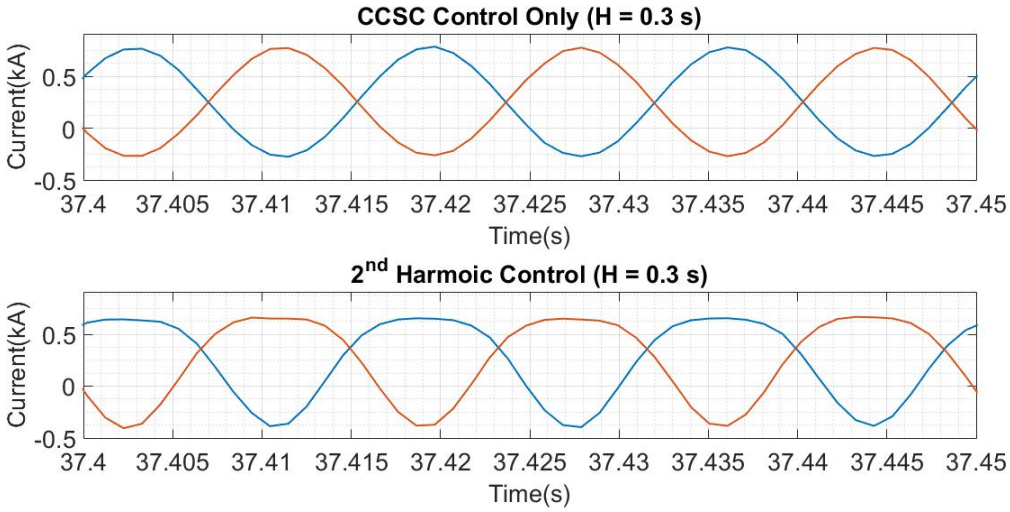

Figure 5.42: Comparison of Phase A arm currents - proportional active power transfer (freq. measurement: speed of the synchronous machine).

Regardless of where the frequency measurement originates from, there are advantages to the proposed controller:

- The circulating current injected manipulates the arm current to acceptable levels when additional active power is injected by the MMC.
- The frequency response of the network is improved when the MMC is allowed to inject active power.

5.7 Analysis

This section provides a numerical view of the benefits the proposed controller add to the system. The labels for the table are provided below:

- 1: Synchronous machine attends to the frequency disturbance. MMC, in traditional CCSC, holds the active power at a constant 400 MW.
- 2: MMC, in traditional CCSC, attends to the frequency disturbance. Synchronous machine is dispatched, 5 s after the disturbance, to fully correct it. (Frequency measurement: MMC PLL)
- 3: MMC, in traditional CCSC, attends to the frequency disturbance. Synchronous machine is dispatched, 5 s after the disturbance, to fully correct it. (Frequency measurement: Bus in the network)
- 4: MMC, in traditional CCSC, attends to the frequency disturbance. Synchronous machine is dispatched, 5 s after the disturbance, to fully correct it. (Frequency measurement: speed of synchronous machine)
- 5: MMC, using proposed controller, attends to the frequency disturbance. Synchronous machine is dispatched, 5 s after the disturbance, to fully correct it. (Frequency measurement: MMC PLL)
- 6: MMC, using proposed controller, attends to the frequency disturbance. Synchronous machine is dispatched, 5 s after the disturbance, to fully correct it. (Frequency measurement: Bus in the network)
- 7: MMC, using proposed controller, attends to the frequency disturbance. Synchronous machine is dispatched, 5 s after the disturbance, to fully correct it. (Frequency measurement: speed of synchronous machine)

The data presented in Table 5.6 clearly shows that if a MMC is tasked with the responsibility of adding additional active power to a system during an extreme power imbalance there is a significant improvement in frequency behaviour (with the frequency measurement taken from the angular frequency of the synchronous machine),

Table 5.6: Frequency Nadir Comparisons.

H **Constant (s)**	**1 (Hz)**	**2 (Hz)**	**3 (Hz)**	**4 (Hz)**	**5 (Hz)**	**6 (Hz)**	**7 (Hz)**
0.3	48.00	59.12	59.01	58.57	59.18	58.50	58.58
1.0	48.00	59.86	59.76	59.48	59.87	59.79	59.48
2.0	51.20	59.89	59.88	59.71	59.89	59.88	59.71
3.0	53.50	59.89	59.87	59.80	59.89	59.89	59.80
4.0	54.60	59.89	59.89	59.84	59.89	59.89	59.84
5.0	55.30	59.89	59.89	59.87	59.89	59.89	59.87
10.0	56.60	59.89	59.89	59.89	59.89	59.89	59.89

especially when considering a low inertia system. This benefit is observed regardless if the MMC is operated in traditional CCSC or with the proposed controller.

Table 5.7: MMC Peak Arm Current Comparisons.

H **Constant (s)**	**1 (kA)**	**2 (kA)**	**3 (kA)**	**4 (kA)**	**5 (kA)**	**6 (kA)**	**7 (kA)**
0.3	unstable	0.84	0.85	0.84	0.68	0.70	0.69
1.0	unstable	0.86	0.89	0.85	0.69	0.77	0.68
2.0	0.69	0.85	0.85	0.85	0.69	0.74	0.68
3.0	0.69	0.84	0.85	0.84	0.69	0.77	0.68
4.0	0.69	0.84	0.85	0.85	0.69	0.78	0.70
5.0	0.69	0.84	0.84	0.85	0.68	0.77	0.69
10.0	0.68	0.84	0.84	0.85	0.69	0.80	0.69

The data presented in Table 5.7 shows that the injection of judicious amounts of circulating current into the arm of the MMC can successfully limit the peak arm current to pre-contingent levels. Therefore, if the MMC is operating at a high efficiency level, an overload region can be successfully entered and exited, providing ancillary services, without risk to the IGBTs. It is to be noted that when the proposed controller is used at a bus in the network, there was a current spike that exceeded acceptable limits (the peak of the spike is recorded in column **6 (kA)** in Table 5.7). It is believed that this unwanted occurrence can be rectified with controller tuning. However, aggressive controller tuning is outside of the scope of this work.

5.8 Summary

This chapter presented a more complex test system for the proposed MMC hybrid controller. The IEEE 9-bus system was the chosen starting point because this controller would be best served in a local area, minimizing the chance of negative controller interactions with other asynchronous plants. The IEEE 9-bus system was modified with one synchronous machine (that could be used at various inertia levels), one Thevenin equivalent (that serves as a strong source and is disconnected to create the power imbalance) and the MMC (connected to a reliable source of active power). To create metrics for evaluating the proposed controller, two control tests were done on this modified IEEE 9-bus system; (1) only the synchronous machine responds with the MMC in CCSC and (2) the MMC responds with the MMC in CCSC (this test was conducted using three different frequency measurements). Testing was repeated with the proposed hybrid controller enabled. Using the control tests, comparisons were made with the proposed hybrid controller, highlighting the observed improvements. The MMC participating in the power imbalance greatly improved the frequency response in the system. This was true regardless if traditional CCSC was used or the controls within the proposed hybrid controller were used. However, if traditional CCSC was used then the arm current's peak reached unacceptable magnitudes, this was rectified by the manipulation that the proposed hybrid controller provides in two of the cases. Namely, when the frequency was measured internally by the MMC PLL and when the frequency measurement came from the speed of the synchronous machine. In the remaining case, where the frequency measurement came from a bus in the network, a spike was observed that reached unacceptable levels. It is believed that this can be rectified by more aggressive controller tuning (this is outside of the scope of this work).

Chapter 6

Contributions, Conclusions, and Future Work

6.1 Contributions

- Identified that the magnitude of circulating current has a linear relationship to the peak of the arm current in a MMC, with phase remaining constant.
- Used the above point to implement a proportional-droop controller, based off a maximum power controller, to address varying in-feed losses.
- Created a hybrid controller model in the PSCAD/EMTDC environment that addressed high RoCoFs as well as varying in-feed losses without violating the SOA of the IGBTs.
- Implemented the control system through freezing the integrator in the PI controller at the maximum output power and releasing it when the frequency error between the measured frequency and reference frequency reached zero .
- Validated the hybrid controller, in PSCAD/EMTDC, using the IEEE 9-bus system (this was chosen due to the recommendation that these controls should

be used locally) using a synchronous machine model and a strong source (which was switched out to model a power imbalance) at various inertia constants.

- Verified that a fast injection of circulating current into the arm current of a MMC can positively benefit frequency nadirs and frequency overshoots while keeping the peaks of the arm currents in the MMC consistent with the precontingent levels.

6.2 Conclusions

The modern power system is on a path that will continually increase renewable penetration. As the non-renewable synchronous plants are decommissioned, the ancillary services lost, traditionally provided by these large machines and necessary for secure and stable operation, require modern replacements.

Inertia has been the historical method used to balance the mechanical and electric torques during a frequency event. The large rotating masses are difficult to speed up or slow down and because of this, additional active power can be extracted. The rotating mass will continue to spin, under its own weight, near its synchronous frequency even though the electrical load requirement has surpassed the mechanical load requirement.

This thesis presented and validated one method of replacing the inertia that is lost in the system when large amounts of synchronous machines are rendered offline, using MMCs. To minimize steady state losses, the circulating currents in a MMC are traditionally filtered out. However, they can manipulated and injected into the arms of the MMCs for different purposes. One such purpose is the limiting of the peak arm current in the MMC, to respect SOA of the transistors. This allows the MMC to enter an overload region where additional active power can be transferred into the network without damaging the MMC. If this transfer is performed is a sufficiently small amount of time, this is one potential solution to the reducing network inertia

problem.

Two approaches were successfully combined to create this controller. One approach (maximum power transfer) calculates the magnitude and phase of the circulating current required to flatten the arm current to levels below the SOA of the transistors. The other approach (proportional support) makes use of the fact that reducing the magnitude of the current calculated above, while keeping the phase constant, results in a linear relationship. This controller was capable of providing maximum capacity (reducing the RoCoF and frequency nadirs) as well as proportional support (minimizing overall losses) in a sufficiently small amount of time.

The modern power system will require a variety of methods to replace the ancillary services lost, as synchronous generation is disconnected from the network. This thesis presented one of those modern replacements for inertia.

6.3 Future Work

- Verify proper control using hardware-in-loop real-time simulations.
- Investigate and identify possible controller interactions when the hybrid controller responds to far disturbances, using a more complex IEEE bus system, with a greater amount of asynchronous generation connected.
- Create high level controller that monitors the available additional power locally, and only dispatches the MMCs connected to plants (or batteries) that have sufficient available active power storage.
- Implement active power and reactive power priority. Create a controller that has the option to provide additional reactive power. Test this controller in a network that requires both active and reactive power after a disturbance. The requirement of active power during a frequency event does run the risk that a

sufficient capacity of reactive power would not be available to support the bus voltage, possibly causing a voltage collapse in the area. Insight on sizing of the MMC, for worst case scenarios, would be beneficial information.

- Create controls for fault ride-through. Many controllers are frozen during a fault. Taking this into account, as well as, the time required to sync the PLL, one cycle for a frequency measurement, and communications delays, is the time still sufficiently small that the MMC can reasonably participate in inertia emulation.

Bibliography

[1] M. Guarnieri, "The beginning of electric energy transmission: Part one [historical]," *IEEE Industrial Electronics Magazine*, vol. 7, no. 1, pp. 50–52, 2013.

[2] S. Lee, S. Cui, and S. K. Sul, "Control of hybrid hvdc transmission systems with lcc and fb-mmc," *in 2014 IEEE Energy Conversion Congress and Exposition (ECCE)*, pp. 475–482, 2014.

[3] A. Lesnicar and R. Marquardt, "An innovative modular multilevel converter topology suitable for a wide power range," *2003 IEEE Bologna Power Tech Conference Proceedings*, vol. 3, p. 6, 2003.

[4] K. Sharifabadi, L. Harnefors, H. P. Nee, S. Norrga, and R. Teodorescu, *Design, control and application of modular multilevel converters for HVDC transmission systems*. John Wiley and Sons, Incorporated, 2016.

[5] I. M. Sanz, P. D. Judge, C. E. Spallarossa, B. Chaudhuri, and T. C. Green, "Dynamic overload capability of vsc hvdc interconnections for frequency support," *IEEE Transactions on Energy Conversion*, vol. 32, no. 4, pp. 1544–1553, 2017.

[6] P. D. Judge and T. C. Green, "Dynamic thermal rating of a modular multilevel converter hvdc link with overload capacity," *2015 IEEE Eindhoven PowerTech*, 2015.

[7] Z. Lianghe, S. Chao, L. Qifu, L. Pandian, Z. Hongqi, and H. Tao, "Research on new circulating current control strategy for increasing the power transmission capacity of modular multilevel converter," *2018 International Conference on Power System Technology (POWERCON)*, 2018.

[8] U. Tamrakar, D. Shrestha, M. Maharjan, B. Bhattarai, T. Hansen, and R. Tonkoski, "Virtual inertia: Current trends and future directions," *Applied sciences*, vol. 7, no. 7, p. 654, 2017.

[9] Q. Tu and Z. Xu, "Impact of sampling frequency on harmonic distorion for modular multilevel converter," *IEEE Transactions on Power Delivery*, vol. 26, no. 1, pp. 298–306, 2011.

[10] Q.-C. Zhong and G. Weiss, "Synchronverters: Inverters that mimic synchronous generators," *IEEE Transactions on Industrial Electronics*, vol. 58, no. 4, pp. 1259–1267, 2011.

[11] G. Delille, B. François, and G. Malarange, "Dynamic frequency control support by energy storage to reduce the impact of wind and solar generation on isolated power system's inertia," *IEEE Transactions on Sustainable Energy*, vol. 3, no. 4, pp. 931–939, 2012.

[12] Y. Luo, P. Yi, X. Xiaofu, W. Jiang, and S. Yonghui, "Dc fault ride-through method for full-bridge mmc-based mtdc systems," *Journal of engineering (Stevenage, England)*, vol. 2019 (16), pp. 3175–3179, 2019.

[13] R. Vidal-Albalate and J. Forner, "Modeling and enhanced control of hybrid full bridge-half bridge mmcs for hvdc grid studies," *Energies (Basel)s*, vol. 13 (1), p. 180, 2020.

[14] X. He, J. Peng, P. Han, Z. Liu, S. Gao, and P. Wang, "A novel advanced traction power supply system based on modular multilevel converter," *IEEE Access*, vol. 7, pp. 165018–165028, 2019.

[15] A. The, B. Freudenberg, S. Dieckerhoff, V. Vahrenholt, W. Fischer, R. Stornowski, and M. Wildmann, "Operation range of hvdc-mmc with circulating current suppression and energy balancing control," *2015 17th European Conference on Power Electronics and Applications (EPE'15 ECCE-Europe)*, pp. 1–9, 2015.

[16] D. G. Holmes and T. A. Lipo, *Pule Width Modulation for Power Converters: Principles and Practice*. Wiley-IEEE Press, 2003.

[17] A. K. Gupta and A. M. Khambadkone, "A space vector pwm scheme for multilevel inverters based on two-level space vector pwm," *IEEE Transactions on Industrial Electronics*, vol. 53, no. 5, pp. 1631–1639, 2006.

[18] Y. Deng, K. H. Teo, C. Duan, T. G. Habetler, and R. G. Hartley, "A fast and generalized space vector modulation scheme for multilevel converters," *IEEE Transactions on Power Electronics*, vol. 29, no. 10, pp. 5204–5217, 2014.

[19] M. H. Nguyen and S. Kwak, "Nearest-level control method with improved output quality for modular multilevel converters," *IEEE Access*, vol. 8, pp. 110237–110250, 2020.

[20] P. M. Meshram and V. B. Borghate, "A novel voltage balancing method applied to direct control strategy of mmc-hvdc system," *IEEE - International Conference On Advances In Engineering, Science And Management (ICAESM - 2012)*, pp. 448–452, 2012.

[21] R. H. Park, "Two-reaction theory of synchronous machines generalized method of analysis-part i," *Transactions of the American Institute of Electrical Engineers*, vol. 48, no. 3, pp. 716–727, 1929.

[22] H. Akagi, Y. Kanazawa, and A. Nabae, "Instantaneous reactive power compensators comprising switching devices without energy storage components," *IEEE Transactions on Industry Applications*, vol. IA-20, no. 3, pp. 625–630, 1984.

[23] P. C. Krause, O. Wasynczuk, and S. D. Sudhoff, *Analysis of Electric Machinery and Drive Systems*. Wiley-IEEE Press, 2002.

[24] S. Zhou, J. Liu, L. Zhou, and Y. Zhang, "Dq current control of voltage source converters with a decoupling method based on preprocessed reference current feedforward," *IEEE Transactions on Power Electronics*, vol. 32, no. 11, pp. 8904–8921, 2017.

[25] P. Kundur, *Power System Stability and Control*. McGraw-Hill, Inc., 1994.

[26] C. P. Steinmetz, "Power control and stability of electric generating stations," *Transactions of the American Institute of Electrical Engineers*, vol. XXXIX, no. 2, pp. 1215–1287, 1920.

[27] P. Kundur, J. Paserba, V. Ajjarapu, G. Andersson, A. Bose, C. Canizares, N. Hatziargyriou, D. Hill, A. Stankovic, C. Taylor, T. V. Cutsem, and V. Vittal, "Definition and classification of power system stability," *IEEE Transactions on Power Systems*, vol. 19, no. 2, pp. 1387–1401, 2004.

[28] P. Tielens and D. V. Hertem, "The relevance of inertia in power systems," *Renewable and Sustainable Energy Reviews*, vol. 55, pp. 999–1009, 2016.

[29] H. Gu, R. Yan, and T. Saha, "Review of system strength and inertia requirements for the national electricity market of australia," *CSEE Journal of Power and Energy Systems*, vol. 5, no. 3, pp. 295–305, 2019.

[30] DNV KEMA Energy and Sustainability, "Rocof an independent analysis on the ability of generators to ride through rate of change of frequency values up to 2hz/s," 2013. `http://www.eirgridgroup.com/site-files/library/EirGrid/DNV-KEMA_Report_RoCoF_20130208final_.pdf`, Last accessed on 2022-07-31.

[31] "Australian, Energy, Market, and Operator", "Fast frequency response in the nem," 2017. `https://aemo.com.au/-/media/files/electricity/nem/security_and_reliability/reports/2017/ffr-working-paper.pdf` Last accessed on 2022-06-28.

[32] J. Morren, J. Pierik, and S. W. H. de Haan, "Inertial response of variable speed wind turbines," *Electric Power Systems Research*, vol. 76, pp. 980–987, 2006.

[33] L. Holdsworth, J. B. Ekanayake, and N. Jenkins, "Power system frequency response from fixed speed and doubly fed induction generator-based wind turbines," *Wind Energy*, vol. 7, pp. 21–35, 2004.

[34] J. Jallad, S. Mekhilef, and H. Mokhlis, "Frequency regulation strategies in grid integrated offshore wind turbines vis vsc-hvdc technology: A review," *Energies*, vol. 10, no. 1244, pp. 1–29, 2017.

[35] L. Zeni, A. J. Rudolph, J. Munster-Swendsen, I. Margaris, A. D. Hansen, and P. Sorensen, "Virtual inertia for variable speed wind turbines," *Wind Energy*, vol. 16, pp. 1225–1239, 2013.

[36] Y. Pipelzadeh, B. Chaudhuri, and T. C. Green, "Inertial response from remote offshore wind farms connected through vsc-hvdc links: A communication-less scheme," *2012 IEEE Power and Energy Society General Meeting*, pp. 1–6, 2012.

[37] I. M. Sanz, B. Chaudhuri, and G. Strbac, "Inertial response from offshore wind farms connected through dc grids," *IEEE Transactions on Power Systems*, vol. 30, no. 3, pp. 1518–1527, 2015.

[38] V. N. abd Abhijit Kshirsagar and N. Mohan, "Utility scale interface for renewables and storage using a power electronic transformer with back-to-back mmcs: A novel proposal and control scheme for virtual inertia," *2018 IEEE Energy Conversion Congress and Exposition (ECCE)*, 2018.

[39] S. Yang, J. Fang, Y. Tang, H. Qiu, C. Dong, and P. Wang, "Modular multilevel converter synthetic inertia-based frequency support for medium-voltage microgrids," *IEEE Transactions on Industrial Electronics*, vol. 66, no. 11, pp. 8992–9002, 2019.

[40] A. E. Leon, "Short-term frequency regulation and inertia emulation using an mmc-based mtdc system," *IEEE Transactions on Power Systems*, vol. 33, no. 3, pp. 2854–2863, 2018.

[41] A. P. Asensio, F. Gonzalez-Longatt, S. Arnaltes, and J. L. Rodriguez-Amendo, "Analysis of the converter synchronizing method fot the contribution of battery energy storage systems to inertia emulation," *Energies*, vol. 13, no. 1478, pp. 1–18, 2020.

[42] Operational Analysis and Engineering, AEMO, "Inertia requirements methodology inertia requirements and shortfalls," 2018. `http://www.aemo.com.au/-/media/Files/Electricity/NEM/Security_and_Reliability/System-Security-Market-Frameworks-Review/2018/`

Inertia_Requirements_Methodology_PUBLISHED.pdf, Last accessed on 2022-06-26.

[43] N. Miller, D. Lew, R. Piwko, L. Hannett, S. Achilles, J. MacDowell, M. Richwine, D. Wilson, and M. Adamiak, "Technology capabilities for fast frequency response," tech. rep., GE Energy Consulting, 2017.

[44] M. Lopez, F. Briz, A. Zapico, D. Diaz-Reigosa, and J. M. Guerrero, "Operation of modular multilevel converters under voltage constraints," *IEEE Energy Conversion Congress and Exposition (ECCE)*, pp. 3550–3556, 2015.

[45] G. V. Bharath and P. T. Balsara, "Optimum injection of second harmonic circulating current for reduction in submodule capacitor voltage ripple in overmodulated mmc," *IEEE Energy Conversion Congress and Exposition (ECCE)*, pp. 2684–2689, 2021.

[46] A. Adamczyk, M. Altin, Ömer Göksu, R. Teodorescu, and F. Iov, "Generic 12-bus test system for wind power integration studies," *2013 15th European Conference on Power Electronics and Applications (EPE)*, 2013.

[47] Y. Serizawa, M. Myoujin, S. Miyazaki, and K. Kitamura, "Transmission delay variations in opgw and overhead fiber-optic cable links," *IEEE Transactions on Power Delivery*, vol. 12, no. 4, pp. 1415–1421, 1997.